DISSERTATION

ALTERATIONS IN LUMBAR SPINE MECHANICS DUE TO DEGENERATIVE DISC DISEASE

Submitted by

Ugur Murat Ayturk

Department of Mechanical Engineering

In partial fulfillment of the requirements for the degree of

Doctor of Philosophy

Colorado State University

Fort Collins, Colorado

Fall 2010

Doctoral Committee:

Department Head: Susan James

Advisor: Christian M. Puttlitz

Susan James
Xianghong Qian
Paul Heyliger

ABSTRACT

ALTERATIONS IN LUMBAR SPINE MECHANICS DUE TO DEGENERATIVE DISC DISEASE

Degenerative disc disease is a major source of low back pain. It is hypothesized to significantly alter the biomechanics of the lumbar spine both at the tissue and motion segment (multi-vertebral) levels. However, explicit correlations between the former and the latter has not been established, and this critical link is only possible through modeling the intervertebral disc tissue behavior within a constitutive framework and implementing it in a finite element model of the lumbar spine.

In order to develop a better appreciation of the biomechanics of disc degeneration, the main objectives of this dissertation work were to investigate the degenerative disease related mechanical alterations on lumbar spine through finite element modeling and experimentation, and evaluate the contemporary treatment strategies. To meet this objective, a finite element model of the healthy human lumbar spine was generated based on computed tomography (CT) imagery. Mesh convergence was verified based on strain energy density predictions. Kinematic and mechanical predictions of clinical interest, including range of motion and intradiscal nuclear pressure, were validated under pure moment loading.

The mechanical properties of healthy and degenerated annulus fibrosus tissue were quantified using an orthotropic continuum model, with empirical determination of the requisite material coefficients derived from biaxial and uniaxial tension tests. The resultant material

models were implemented into the validated finite element model in order to simulate disc degeneration at the L3-L4 level. At the tissue level, degeneration was found to significantly increase the dispersion in the collagen fiber orientation and the nonlinearity of the fiber mechanical behavior. At the motion segment level, degeneration increased the mobility of the spine, with concomitant increases in the local stress predictions in the annulus and facet force transmission. Our results were in good agreement with the clinical findings of instability and injury to the intervertebral disc due to degeneration.

Total disc replacement was also considered as a treatment option within the aforementioned finite element framework. The model predictions indicated that single and two-level disc replacement restored motion at the treated levels, while linearizing the kinematic response and increasing the facet force transmission. The data reflect that the successful surgical outcome is most likely obtained when maximum preservation of native disc tissue is achieved during implantation of the prosthetic device.

Ugur M. Ayturk
Department of Mechanical Engineering
Colorado State University
Fort Collins, CO
Fall 2010

ACKNOWLEDGMENTS

I know by experience that this is the hardest part of a thesis to write. I also know that a couple of months are enough to develop the cynicism to look back and harshly criticize your work. This is probably the very reason for my hesitation in writing these pages: glorifying your own work while it is fresh (and possibly immature). Nevertheless, these will be my own ever-evolving self perception and opinions, and should not stop me from giving the well-deserved credit to certain people who have contributed to this work. Here goes:

Dr. Christian Puttlitz: The wise man, the graduate advisor, the good friend, and the mentor who failed at teaching me how to use the word “the” appropriately. Other than that, I think he has done a pretty good job. All kidding aside, his guidance (six years and counting) has been the foundation of all that I have learned and done in the field of orthopaedic biomechanics. Thank you for everything. Stay thirsty my friend.

My committee members: Dr. Susan James, Dr. Xianghong Qian and Dr. Paul Heyliger not only improved this dissertation with their constructive criticism, but also made a huge impact on my professional development by teaching many graduate-level courses I had the fortune to attend.

Dr. Jose J Garcia from Universidad del Valle, Cali, Colombia kindly shared his expertise in soft tissue mechanics, and has helped me tremendously especially during the model development and experimental design stages. He also acted as a co-author for part of the work presented here, which was published as a peer-reviewed journal article.

The suggestions of Dr. Vikas Patel from University of Colorado-Denver were very helpful in CT image analysis and geometry reconstruction. I would like to thank him for evaluating the MR images of several intervertebral disc specimens and thus laying the groundwork for the remainder of the experimental work. Dr. Patel is the co-author of numerous abstracts (as part of the numerical and experimental findings reported in this dissertation) I have presented in scientific meetings over the years.

I would also like to thank Mr. Jim zumBrunnen from CASE, Colorado State University, who has been very helpful with the statistical analysis of experimental data.

Members of the Orthopaedic Bioengineering Research Laboratory: Cecily Broomfield handled the specimen orders, made sure I was paid on a regular basis and could travel to a number of conferences, and kept everything in the lab in order. Ben Gadomski improved many aspects of the computational model I have developed, and made it much better than I imagined it would be. Devin Leahy helped with the machining of several parts during the fixturing of the experimental setup without a single complaint. As a sign of great empathy, he bought me a "Bozo the Clown" to blow off some steam when things get tough. Kirk McGilvray built the biaxial testing machine and not only made the biomechanical tests possible, but also reduced the time I had to spend on them significantly with his helpful suggestions and incredible troubleshooting skills. Brandon Santoni is another gifted researcher whose help and mentorship on designing and executing biomechanical experiments were invaluable. Amy Lyons-Santoni patiently showed me how to read histology slides under the microscope, took care of a ridiculous amount of paperwork, and never got tired of buying me wodka (yes that's a "w") shots. Dieter Schuldt eagerly evaluated the geometry of the specimens, which required a lot of dissection and coding. His results constituted an integral part of the findings of this work. In addition to being a great

colleague/officemate, Snehal Shetye also bore my constant presence as a roommate over the last year. I'll make sure I buy him some IPA the next time we see each other. Kevin Troyer helped with the experimental design at different stages of the project, and it was a pleasure to have this humorous and incredibly modest person around. Wes Womack took on modeling challenges very similar to mine. Without his help, the model development process would be much longer and more painful than it was.

I have the best parents in the world. Their encouragement and love made me survive many tough challenges during the course of my tenure at CSU. My younger sister appeared to be (naively) influenced by my interest in biomechanical engineering for a while, but fortunately this did not last long. I keep saying that she's the smarter sibling for a reason. I love you all, and I will continue to do my best to be worthy of your support.

DEDICATION

This dissertation is dedicated to my beautiful fiancée, Dr. Didem Goz. She has walked down the same path with me over the last five years, and made this work possible with her never ending support. At the same time, she has managed become a very successful, yet down to earth scientist.

I love you, and I am proud of you.

TABLE OF CONTENTS

LIST OF FIGURES

LIST OF TABLES

CHAPTER 1:

Background

1.1 FUNCTIONAL ANATOMY OF HUMAN LUMBAR SPINE

The human lumbar spine is a load bearing structure that carries and transfers the weight of the upper body to the lower extremities through the sacrum and the pelvis. Its mechanical function is not only limited to resisting multi-dimensional loads, but it also confers a certain range of mobility to the upper body via tissue deformation.

The lumbar spine consists of 5 bony vertebral elements connected to each other through avascular intervertebral discs (semi-joints) anteriorly and articulating facet joints (full-joints) posteriorly both at the inferior and superior ends. This repeating pattern comes to an end at the inferior aspect of L5 (lumbosacral junction), where this vertebra is also connected to the sacrum through an intervertebral disc and two articulating facet joints.

The combination of the physiologic loads and moments on this multi-joint complex yield different ranges of segmental motion (ROM) at each level (Figure 1.1). However, this load-displacement relationship is commonly nonlinear. Furthermore, relatively small loads generate large displacements due to low tension in the ligaments and the intervertebral disc, resulting in an initially compliant kinetic response known as the neutral zone. The neutral zone (NZ) is regarded as a measure of the joint laxity, and its magnitude can be significantly altered as a result of injuries to the disc such as degeneration or herniation (Mimura, et al., 1994). Excessive changes in the extent of the NZ have been theorized to be predictors of spinal instability, and therefore, it is an important diagnostic parameter in detecting the aforementioned injuries and diseases.

There is an increasing trend of range of motion in the inferior direction from L1 to S1; however no significant differences are reported except between the lumbosacral level and all of the intra-lumbar levels (Guan, et al., 2007).

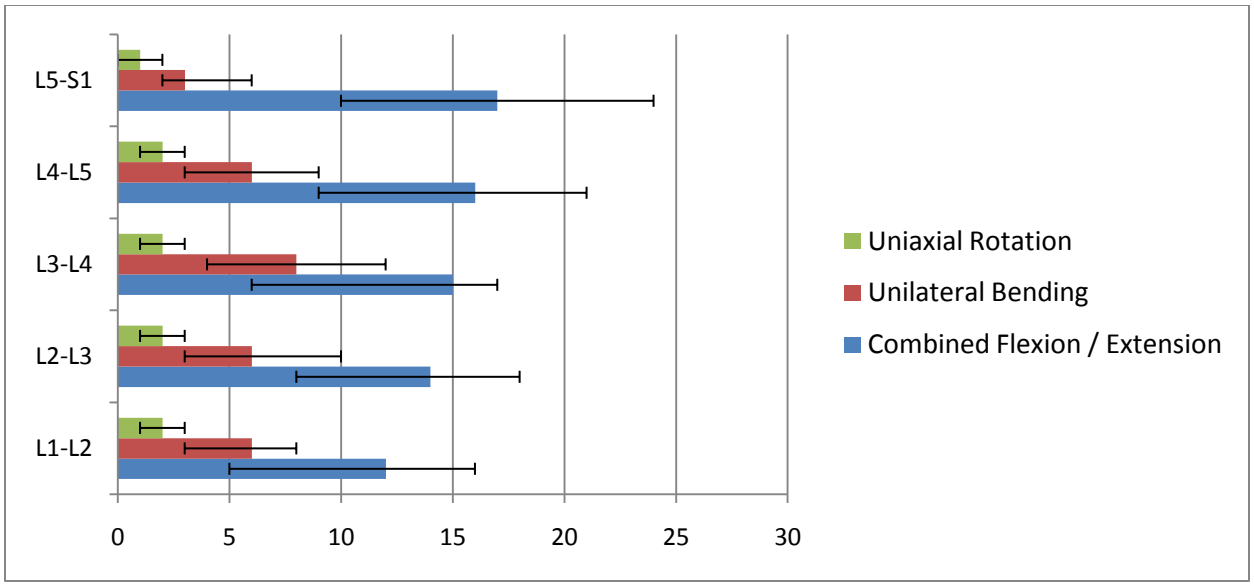

Figure 1.1: Average physiological ROM (in degrees) of lumbar motion segments in principal loading axes. Error bars indicate the normal physiologic limits (Panjabi, et al., 1990).

1.1.1 Bony Vertebrae

The two major components of the vertebrae are the cortical and trabecular bone. While the former is significantly stiffer and denser, the latter has a sponge-like porous structure which produces a globally more compliant behavior. Several studies have shown that aging leads to different levels of reduction in the solid volume fraction in trabecular bone, and, in severe cases, this leads to osteoporosis (Adams, et al., 2002). Moreover, physiological loading is known to affect the bone remodeling process, with the major trabecular orientation coincident with the principal loading directions (Freiberg, 1902).

In the anterior column, a stiff cortical shell encloses a trabecular core, and this structural feature becomes especially advantageous under compressive loads. The cortical endplate distributes the load almost uniformly over the trabecular bone, providing additional support at the radial extrema. The posterior elements have an extremely complex geometry, and the "spinal canal" encompasses the volume between these elements and the vertebral bodies (Figure 1.2). This provides a physical, protective environment for the spinal cord. A total of four facets in the inferior and superior regions form the zygapophyseal joints through articulation with superior and inferior adjacent vertebral levels. Bilateral transverse processes and the pedicles at the posterior extremities serve as ligament insertion sites, transmitting force between each level and improving stability.

The reduction in the bone quality in many cases is followed by endplate fractures or critical damage on the vertebral bodies, preventing the vertebra from carrying out its primary load-carrying function (Bogduk, 1999). Bone cement injection and vertebroplasty are current techniques of surgical intervention which seek to provide immediate stability to the spine.

The aforementioned types of bone tissue are known to undergo infinitesimal deformations *in vivo* during the activities of daily living. Therefore, a simplistic approach such as linear elasticity is sufficient for describing the physiological mechanical response of these tissues (Crawford, et al., 2003). Orthotropic and fully isotropic constitutive relationships have been proposed, and a large range of elastic moduli values are reported in the literature.

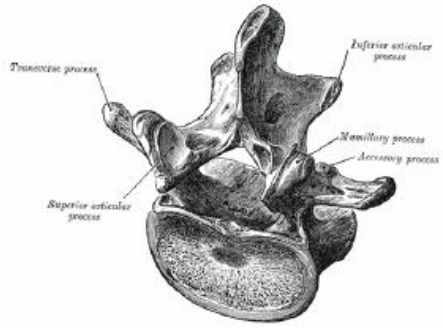

Figure 1.2: A lumbar vertebra with its extremities (Mosby, 2004)

1.1.2 Intervertebral Discs

The intervertebral discs are bound to the vertebral bodies inferiorly and superiorly through cartilaginous endplates (Figure 1.3). Nutrients are transported to the avascular discs through these hyaline cartilage tissues via diffusion. Furthermore, these tissues are innervated at the periphery. Aging and/or chemically induced degeneration produces distortion and mineralizes the endplates, which is believed to cause significant pain, as well as increase the risk of endplate fracture and collapse of the intradiscal space. Decreased permeability of the endplates is shown to change the mechanical loading environment inside the disc (Natarajan, et al., 2006). The elasto-static behavior of this tissue is usually accepted as linear in the non-degenerated discs (Dooris, et al., 2001) (Schmidt, et al., 2007).

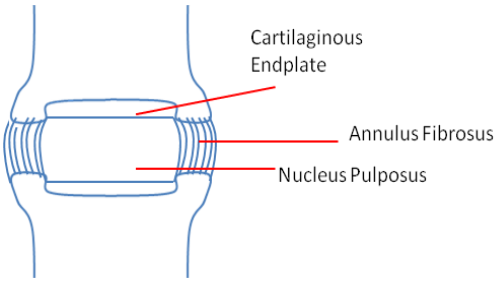

Figure 1.3: Components of the intervertebral disc: Endplates at the superior and inferior boundaries, nucleus at the core surrounded by the annulus at the radial periphery.

The core of the intradiscal space, the “nucleus pulposus”, is a proteoglycan-rich viscous material. Negatively charged glycosaminoglycans (GAG), proteoglycans (PG), Type II collagen and water are the main constituents of this tissue. The random orientation of the collagen fibers

demonstrates the lack of a structured organization, which consequently generates an isotropic mechanical response (Guerin and Elliott 2006). Furthermore, the negative charges and the presence of PGs result in a high swelling pressure throughout the tissue. This pressure is substantially elevated under the application of compressive loads, and balances itself by creating circumferential "hoop" stresses in the annular lamellae (Adams, et al., 2002).

The annulus fibrosus consists of several lamellae wrapped around the nucleus. These individual layers are composed of PGs and Type I collagen. The collagen molecules form a highly organized fiber network, which reinforces the ground material along local orientations and creates the anisotropic material behavior. The orientation of these fibers ranges from 23 to 45 degrees with respect to the horizontal plane, and these orientations vary from the outer to inner annulus (Guerin, et al., 2006).

The anisotropic behavior of the annulus can be described with a transverse isotropy model within a cylindrical coordinate system. Three dimensional finite element modeling (FEM) approaches allow for the geometric representation of individual fibers, and consequently reinforcement in the preferred orientation (Dooris, et al., 2001) (Zander, et al., 2001). This approach gives satisfactory results in terms of predicting the global, structural kinetic response; however modeling of the tissue-level mechanics of the annulus requires a more rigorous technique. Spencer's continuum model for orthotropic materials with multiple fiber families has been employed in previous studies to achieve adequate modeling fidelity (Spencer, 1984). The invariant-based strain energy potentials can be decomposed into individual components of physiological relevance (potentials of the proteoglycan-rich matrix, tissue incompressibility, collagen fibers, etc.) (Wagner, et al., 2004) (Guerin HL, 2007) in order to simulate the nonlinear mechanical behavior of the annulus fibrosus (Figure 1.4).

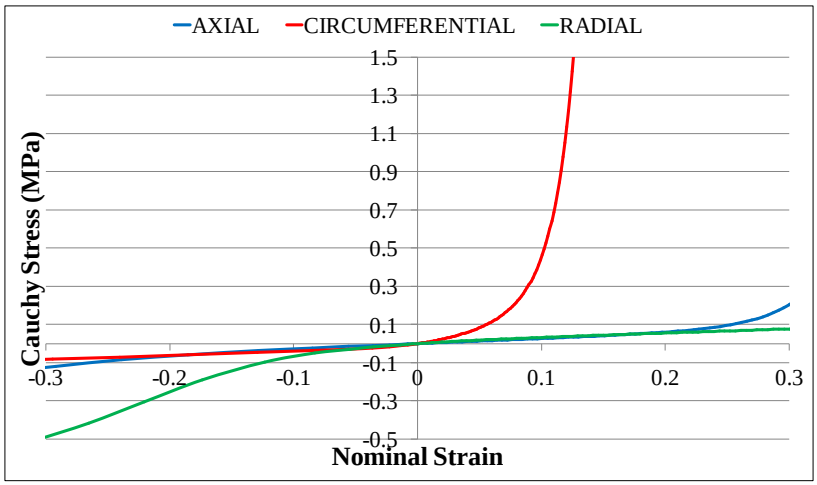

Figure 1.4: Tensile-compressive behavior of annulus fibrosus in three principal loading directions (Wagner, et al., 2004)

1.1.3 Ligaments

Spinal ligaments have a significant effect on the mobility of motion segments, and, therefore, are crucial for understanding and predicting spinal biomechanics (Zander, Rohlmann and Bergmann 2004). Similar to tendons, ligaments primarily consist of Type I collagen, elastin, PGs and water with minor amounts of other proteins and different types of collagen (Panjabi, et al., 1990). With the collagen fibers aligned in the usual loading direction, their mechanical behavior is highly anisotropic. Transverse isotropy is a sufficiently accurate model to describe and model this behavior (Woo, et al., 2005).

The presence of the collagen fiber results in a highly nonlinear static tensile behavior and increases the global strength of the tissue. The mechanical properties of spinal ligaments have been quantified in numerous studies in the past, and substantial differences are observed between the responses of different ligaments (Zander, Rohlmann and Bergmann 2004) (Figure 1.5).

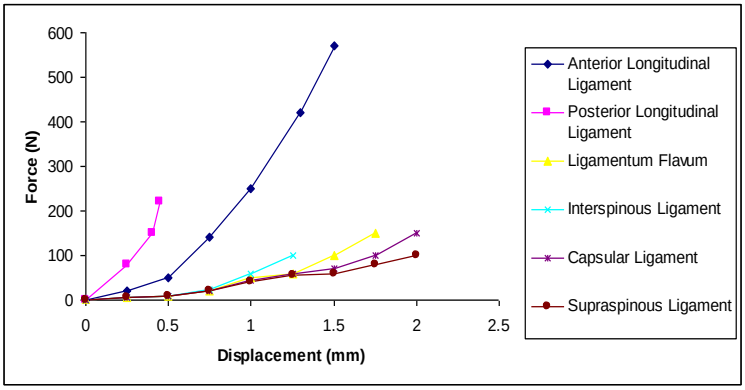

Figure 1.5: Tensile mechanical behavior of spinal ligaments

There are six major spinal ligaments that connect the vertebral bodies and the posterior elements in the lumbar region: Anterior longitudinal ligament (ALL) runs through the entire spine from the sacrum to the cervical region, inserting into the anterior surfaces of the vertebral bodies and covering their associated intervertebral discs. Similarly, the posterior longitudinal ligament (PLL) extends in the same range in the inferior – superior direction, inserting into the posterior surfaces of their associated vertebral bodies along the spinal canal (Figure 1.6).

On the posterior side of the spinal canal, the ligamentum flava (LF) connect the laminae of each vertebral body to its subsequent inferior and superior levels. Likewise, the infraspinous ligament (IFL) inserts into spinous processes at the inferior and superior ends and supraspinous ligament (SSL) inserts into the posterior edges at each level. Capsular ligaments provide additional stability around the facets, covering the entire zygapophyseal joint.

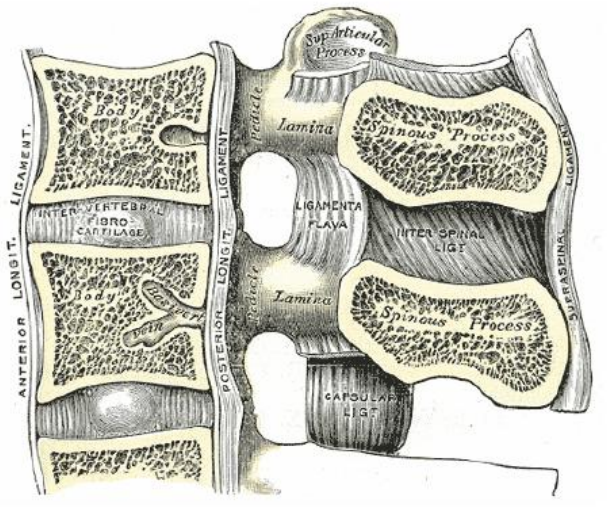

Figure 1.6: Sagittal cut view of lumbar spine showing spinal ligaments in the two dimensional plane (Mosby, 2004).

1.2 DEGENERATIVE DISC DISEASE

The characteristic effects of the degenerative disease and aging on the intervertebral disc are very similar. Consequently, biochemical degradation and reduction in the mechanical properties of the intervertebral discs are common problems in the elderly population due to their tendencies to make traumatic injuries more likely to happen during daily physical activities. *In vitro* experimentation has demonstrated that excessive loading of the disc is likely to fail the vertebral endplate first rather than the disc itself (Adams, et al., 2002). Therefore, herniation and fissures in a healthy disc can only be generated under the combined application of excessive bending and compressive loads (Adams, et al., 1985).

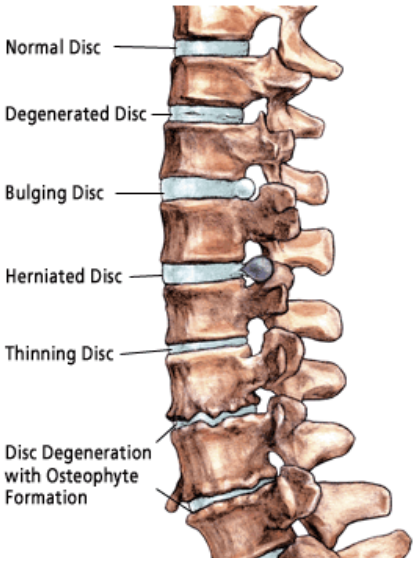

Figure 1.7: Common intervertebral disc related issues (http://www.sandiego-spine.com/subject.php?pn=lumbar-disc-disease-035).

However, during the early stages of degeneration, herniation is more likely to occur due to the significant reduction in the strength of the annulus fibrosus.

In such cases, annular tissue is strained radially in the postero-lateral direction, penetrating into the spinal canal and putting pressure on the spinal cord and nerve roots (Figure 1.7). This resultant "nerve pinching" mechanism is a major source of low back pain, and in many cases, can only be treated operatively. The current gold standard in surgical treatment of the aforementioned problem is fusion, wherein the injured disc tissue is completely removed and two adjacent vertebral bodies are fused to each other using instrumentation. It has been postulated that replacing the nucleus with a hydrogel substance can restore the intradiscal pressure, provided that the damage to the annulus is not too severe. However, the use of artificial discs, which are essentially metal-polymer-metal joint constructs, is becoming more common due their ability to preserve the intact state of mobility (as compared to fusion).

1.2.1 Pathology of Disc Degeneration

The underlying mechanics of lumbar disc degeneration disease is still not entirely clear. Yet, with aging, the biochemical composition of the disc is known to change. Classification of disc degeneration assessment is clinically achieved in the literature by assigning grades depending on the severity of the disease. The "Thompson Scale" is a commonly used grading scheme by clinicians and researchers, and it groups the progression of the morphological changes in the disc into four stages (Figure 1.8). Grade I represents the healthy disc, with the nucleus being a bright colored viscous fluid at the core of the disc, the cartilaginous endplates are highly permeable, and the fibrous layers of the annulus are distinct and organized. At Grade II, a slight discolorization of the nucleus is visible and it appears more like a solid tissue. In Grade III discs, it is not possible to observe the boundary between the annulus and nucleus, the

annular layers are disintegrated and locally ruptured, and the endplates are calcified. Finally, at Grade IV, the annulus and nucleus are completely indistinguishable, the disc height is substantially reduced, and it is not possible to identify the individual layers of the annulus (Thompson, et al., 1990).

The intervertebral disc is the largest avascular tissue in the human body. Therefore, minor disruptions or injuries to the individual components of the tissue might become rather severe in the long-term due to the difficulties in healing. While fissures and tears in the annular lamellae are common during the late stages of degeneration, reductions in mechanical strength of the annulus can lead to excessive bulging and even herniation at earlier time points in the degeneration cascade. A progressive reduction in disc height can be observed, in addition to the formation of osteophytes and loss of integrity of the bony endplate (Goel, et al., 2006). Overall, the degenerative changes in the morphology and mechanics of the disc are significant and often inter-related, and are described in more detail in the following sub-sections.

1.2.2 Changes in the Morphology of the Intervertebral Disc

Degeneration has been postulated to initiate within the nucleus pulposus tissue. Water comprises 90 % of the weight of the healthy nucleus pulposus in children, and its content decreases to 70% in adulthood (Antoniu, et al., 1996). Reduction of hydration initiates inside the nucleus, and subsequently, dehydration begins to affect the remainder of the intervertebral disc. Degenerated nucleus pulposus is shown to include increased levels of matrix-metalloproteinases (MMPs), which stimulate the breakdown of PGs (Stokes, et al., 2005). Furthermore, the total content of Type II collagen is significantly decreased, while there is an increase in the level of Type I collagen content (Andersson, 1998). With these biochemical changes and the increased resemblance of a solid tissue (rather than a fluid-filled structure due

to the reduced water content), the nucleus starts to become a more fibrotic structure. Indeed, in the later stages of degeneration, the annulus and nucleus become histologically indistinguishable.

An immediate loss of functionality and progressive calcification of the cartilaginous endplates accompanies these changes in the nucleus. Blood vessels and nerve endings are observed to grow from the vertebral bodies to inside the disc, since there is limited or no osmotic transportation through the endplates (Bernick, et al., 1982). Cracks and fissures are also common along the surface of the bony endplates.

In addition to increased cross-linking among the collagen fibers, the water content in the annulus is decreased. These microstructural changes in the annulus have a definitive mechanical outcome. Due to the loss of water content and the breakdown of the PGs, the hydrostatic pressurization in the nucleus is lost, and consequently the *in situ* circumferential tension in the annular lamellae disappears (Meakin, et al., 2001). The lack of tension in the annulus tissue increases the catabolic effect of MMPs significantly (Lotz, et al., 2008), leading to a further reduction in the PG content (and thus hydration). Moreover, under *in vivo* compressive loads, this lack of pre-existing tension causes the individual layers to buckle and delaminate, rather than radially bulge. In fact, in the later stages of degeneration, the disintegration of the annular lamellae with rupture and buckling of the collagen fiber bundles can be observed (Iatridis, et al., 2004). Furthermore, due to this increased axial deformation, the intradiscal space becomes narrower.

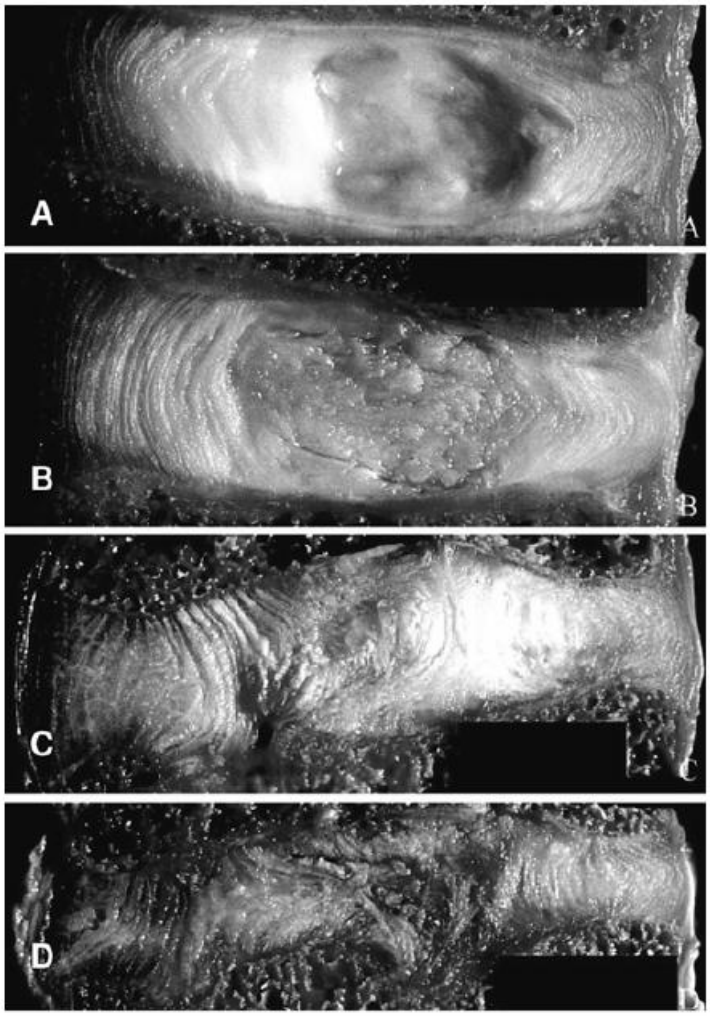

Figure 1.8: Four stages of disc degeneration from Grade I to IV are demonstrated from A to D respectively (Guerin, et al., 2006).

Osteophyte formation often accompanies disc degeneration around the rim of the endplate. It has been hypothesized that this is actually a remodeling phenomena wherein these changes increase the cross sectional area of the endplate and distribute the loads to a broader area (Adams, et al., 2002). However, these mineralized tissues do not display a consistent pattern and usually encompass random geometry. Recently published data suggest that these mineralized deposits contribute to the global resistance of the functional spinal unit primarily under bending loads (Al-Rawahi, et al., 2010). Furthermore, osteoarthritic involvement in the

zygapophyseal joints usually follows disc degeneration due to severe changes in the load-sharing relationship between the anterior and posterior spinal columns (Niosi, et al., 2004).

These degeneration-related changes in the morphology of the intervertebral disc constituents are, in fact, reflected in their biomechanical behavior as well. A rigorous characterization of the material behavior in correlation with the degree of degeneration is necessary in order to accurately assess the effects of the disease on spinal motion segments. The following sections (specifically Chapters 4 and 5) review the existing literature with respect to the alterations of the mechanics of intervertebral disc components due to degeneration. These portions of this dissertation also document the generation of an empirically-based continuum model for degenerated annulus fibrosus.

1.3 TREATMENT

Fusion has remained the gold standard with respect to surgical intervention of disc-related issues in the lumbar spine for the last few decades. Following the removal of the disc tissue, the intradiscal space is filled with bone graft and the injured level and its adjacent segments are reinforced with instrumentation (Figure 1.9) (Kruyt, et al., 2004). This method has been successful in providing pain relief in the short term. However, long-term follow-up studies show that the alteration in the biomechanics and kinematics of the treated segment affect the adjacent levels (Weinhoffer, et al., 1995) (Lee, et al., 1984). An initial increase in the intradiscal pressure and endplate stresses may be contributing to the subsequent degeneration cascade (Eck, et al., 1999).

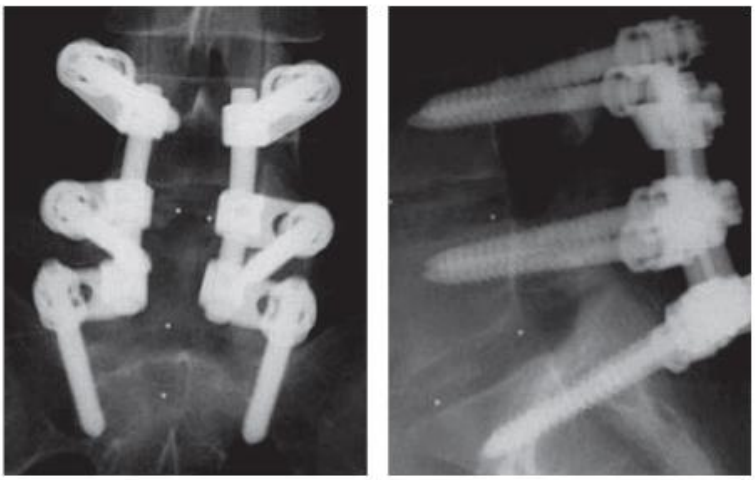

Figure 1.9: Posterior (left) and lateral (right) views of fusion with posterior application of rods and pedicle screws to L4-S1 (Rutherford, et al., 2007).

In an attempt to overcome these shortcomings, the use of dynamic stabilization systems has been proposed as an alternative to the traditional fusion techniques. These posterior spring-rod mechanisms shift the center of rotation posteriorly and are generally intended to unload the anterior column. However, dynamic stabilization is a relatively new concept, and its efficacy still remains unknown since the long term follow-up results are yet to be reported.

Nucleus replacement alone aims at restoring the *in vivo* intradiscal pressure by replacing the nucleus with a hydrogel implant. It is relatively less invasive and is intended to be applied at the early stages of degeneration where the integrity of the annulus and the endplates are preserved. It is hypothesized that a return of nuclear pressure will arrest or prevent further progression of the degeneration (Marcolongo, et al., 2006).

Disc arthroplasty has become more common over the last decade and is much more promising with its potential to restore the kinematics and biomechanics of the injured segment. Fernstrom was the first to try a motion preserving implant instead of fusion during the 1960s. His primitive device was a simple stainless steel sphere that was implanted following the

complete removal of the disc tissue. It remained inside the disc space due to the compressive forces acting on the implant at regions of contact with the endplates. However, the highly limited contact area at both endplates led to stress concentrations and eventually failure/penetration into the vertebral bodies. A second disc arthroplasty design attempt was introduced with the launch of AcroFlex in the following decade. This implant was similar to the state-of-the-art designs in that it filled the intradiscal space completely and was a metal-polymer-metal construct. This implant has evolved through several design iterations and clinical trials. Early mechanical failures of the polymer core led to the current state-of-the-art concept of designing the implant as an artificial joint, where the metal endplates articulate with the polymer core material (Kurtz, 2006).

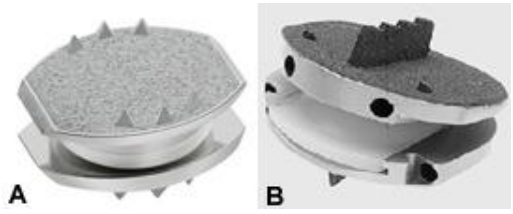

Figure 1.10: Charite (A) and ProDiscL (B) artificial discs. The polymer core is fixed to the inferior endplate inside ProDiscL, while it articulates with both of the endplates in Charite.

Currently, two devices are approved by the FDA and commercially available for surgical use. The Charite and ProDisc designs (Figure 1.10) are both based on the aforementioned metal-polymer-metal design, and include mobile and fixed polymer core material.

1.4 SUMMARY

The literature on the biomechanics of degenerative disc disease is replete. Alterations in the biomechanical properties of the diseased disc tissue and spinal motion segments have been investigated with respect to a spectrum of outcome (e.g., range of motion, elastic modulus, compressibility, etc.). However, without utilization of these data in a constitutive framework, it is not possible to appreciate the progression of degenerative disc disease and appropriate

treatment strategies from a biomechanical perspective. Therefore, we hypothesize that a hybrid approach of modeling and experimentation will enable both a rigorous analysis and a parametric assessment of this problem. Specifically, implementation of material coefficients obtained via well designed mechanical experiments on disc tissue in a global finite element model of spinal motion segments will reveal how the structure-function relationship between the intervertebral disc and spine is altered as a result of degeneration.

In order to meet this objective, this dissertation project is focused on: (1) The generation of a valid finite element model of the human lumbar spine; (2) developing an anisotropic hyperelastic material model of the degenerated annulus fibrosus, and (3) implementation of the latter into the former for a thorough evaluation of the biomechanical impact of disc degeneration to the lumbar spine at a global and local level. It is hypothesized that the load-sharing relationship between the individual components of the intervertebral disc (in particular the ground substance and fibers of the annulus fibrosus) will be altered due to degeneration, and these alterations will be reflected in the global kinematic (nonlinear range of motion response) and mechanical behavior (facet force transmission) of the involved motion segments under pure moment loading. Finally, total disc replacement will be evaluated within this developed framework, in order to mechanically assess this clinically available treatment option.

1.5 SPECIFIC AIMS

Three specific aims were designated for this dissertation project:

Specific Aim #1: Develop a converged and validated finite element model of the healthy human lumbar spine.

In Chapter 2, the soft tissue component load-sharing relationships of a lumbar functional spinal unit (L4/L5) are investigated using finite element method, and the effects of these relationships on the nonlinear moment-rotation predictions are interrogated. This effort and the employed methodology are extended to generate a finite element model of the lumbar spine (L1/L5) in Chapter 3, with particular detail attention ascribed to the mesh refinement and validation protocols.

Specific Aim #2: Develop a nonlinear, anisotropic, constitutive relationship for the mechanical behavior of degenerated human annulus fibrosus, and implement this into the previously developed finite element model.

Chapter 4 describes biaxial and uniaxial tension experiments on healthy and degenerated annulus fibrosus, and the utilization of these data in generation of orthotropic continuum material models. In Chapter 5, these models are implemented in the finite element model of a lumbar functional spinal unit (that is developed and validated in Chapter 2), and the effects of degeneration on local and global biomechanics of the spinal motion segments are reported.

Specific Aim #3: Simulate the implantation of an artificial disc, and evaluate the changes in biomechanical behavior of the spine compared to the healthy and diseased states.

In Chapter 6, implementation of the ProDisc-L into the validated finite element model is documented, and the effects of lumbar disc arthroplasty are assessed within the framework of the healthy and degenerative states of the lumbar intervertebral disc.

REFERENCES

Acaroglu, E., Iatridis, J., Setton, L., Foster, R., Mow, V., & Weidenbaum, M. (1995). Degeneration and aging affect the tensile behavior of human lumbar anulus fibrosus. *Spine* , 2690-2701.

Adams, M., & Hutton, W. (1985). Gradual Disc Prolapse. *Spine* , 524-531.

Adams, M., Bogduk, N., Burton, K., & Dolan, P. (2002). *The Biomechanics of Back Pain.* London: Churchill Livingstone.

Alini, M., Eisenstein, S., Ito, K., Little, C., Kettler, A., Masuda, K., et al. (2007). Are animal models useful for studying human disc disorders/degeneration? *Eur Spine J* , 2-19.

Al-Rawahi, M., Luo, J., Pollintine, P., Dolan, P., & Adams, M. (2010). Mechanical Function of Vertebral Body Osteophytes, as Revealed by Experiments on Cadaveric Spines. *Spine* , In Press.

An, H., & Masuda, K. (2006). Relevance of In Vitro and In Vivo Models for Intervertebral Disc Degeneration. *J Bone Joint Surg Am* , 88-94.

Andersson, G. (1998). What are the age-related changes in the spine? *Baillieres Clin Rheumatol* , 161-173.

Antoniu, J., Steffen, T., & Nelson, F. (1996). The Human Intervertebral Disc: Evidence for Changes in the Biosynthesis and Denaturation of the Extracellular Matrix with Growth, Maturation, Ageing, and Degeneration. *J Clin Invest* , 996-1003.

Bernick, S., & Cailliet, R. (1982). Vertebral Endplate Changes with Aging of Human Vertebrae. *Spine* , 97-102.

Bogduk, N. (1999). *Clinical Anatomy of the Lumbar Spine and Sacrum.* London: Churchill Livingstone.

Crawford, R., Rosenberg, W., & Keaveny, T. (2003). Quantitative computed tomography based finite element models of the human lumbar vertebral body: effect of element size on stiffness, damage, and fracture strength predictions. *Journal of Biomechanical Engineering* , 434-8.

Dooris, A., Goel, V., Grosland, N., Gilbertson, L., & Wilder, D. (2001). Load sharing between anterior and posterior elements in a lumbar motion segment implanted with an artificial disc. *Spine* , E122-E129.

Eck, J., Humphreys, S., & Hodges, S. (1999). Adjacent-segment degeneration after lumbar fusion: a review of clinical, biomechanical, and radiologic studies. *Am J Orthop (Belle Mead NJ).* , 28(6):336-40.

Fazzalari, N., Costi, J., Hearn, T., Fraser, R., Vernon-Roberts, B., Hutchinson, J., et al. (2001). Mechanical and pathologic consequences of induced concentric anular tears in an ovine model. *Spine* , 2575-81.

Freiberg. (1902). Wolff's law and the functional pathogenesis of deformity. *The American Journal of Medical Sciences* , 956-972.

Fujita, Y., Duncan, N., & Lotz, J. (1997). Radial Tensile Properties of the Lumbar Annulus Fibrosus are Site and Degeneration Dependent. *J Orthop Res* , 814-819.

Fujiwara, A., Lim, T., An, H., Tanaka, N., Jeon, C., Andersson, G., et al. (2000). The effect of disc degeneration and facet joint osteoarthritis on the segmental flexibility of the lumbar spine. *Spine* , 3036-3044.

Goel, V., Sairyo, K., Vishnubhotla, S., Biyani, A., & Ebraheim, N. (2006). Spine Disorders: Implications for Bioengineers. In E. A. Kurtz SM, *SPINE Technology Handbook* (pp. 145-182). London, UK: Elsevier.

Guan, Y., Yoganandan, N., Moore, J., Pintar, F., Zhang, J., Maiman, D., et al. (2007). Moment-rotation responses of the human lumbosacral spinal column. *Journal of Biomechanics* , 1975-80.

Guerin, H., & Elliott, D. (2006). Degeneration affects the fiber reorientation of human annulus fibrosus under tensile load. *Journal of Biomechanics* , 1410-1418.

Guerin, H., & Elliott, D. (2007). Quantifying the contributions of structure to annulus fibrosus mechanical function using a nonlinear, anisotropic, hyperelastic model. *Journal of Orthopaedic Research* , 508-516.

Guerin, H., & Elliott, D. (2006). Structure and properties of soft tissues in the spine. In E. A. Kurtz SM, *SPINE Technology Handbook* (pp. 35-62). London: Elsevier.

Hsieh AH, H. D. (2009). Degenerative anular changes induced by puncture are associated with insufficiency of disc biomechanical function. *Spine* , 998-1005.

Iatridis JC, M. P. (1999). Compression-induced changes in intervertebral disc properties in a rat tail model. *Spine* , 996-1002.

Iatridis JC., S. L. (1998). Degeneration affects the anisotropic and nonlinear behaviors of human anulus fibrosus in compression. *J Biomech* , 535-544.

Iatridis. (1999). Shear Mechanical Properties of Human Lumbar Annulus Fibrosus. *J Orthop Res* , 732-737.

Iatridis, J., & Gwynn, I. (2004). Mechanisms for Mechanical Damage in the Intervertebral Disc Annulus Fibrosus. *J Biomech* , 1165-1175.

Korecki CL, C. J. (2008). Needle puncture injury affects intervertebral disc mechanics and biology in an organ culture model. *Spine* , 235-41.

Krismer M, H. C. (2000). Motion in lumbar functional spine units during side bending and axial rotation moments depending on the degree of degeneration. *Spine* , 2020-2027.

Kruyt, M., van Gaalen, S., Oner, F., Verbout, A., de Bruijn, J., & Dhert, W. (2004). Bone tissue engineering and spinal fusion: the potential of hybrid constructs by combining osteoprogenitor cells and scaffolds. *Biomaterials* , 1463-1473.

Kurtz, S. (2006). Total Disc Arthroplasty. In E. A. Kurtz S, *SPINE Technology Handbook* (pp. 303-369).

Lee, C., & Langrana, N. (1984). Lumbosacral spinal fusion: a biomechanical study. *Spine* , 574–581.

Lotz. (2004). Animal models of intervertebral disc degeneration: lessons learned. *Spine* , 657-663.

Lotz, J., Hadi, T., Bratton, C., Reiser, K., & Hsieh, A. (2008). Anulus fibrosus tension inhibits degenerative structural changes in lamellar collagen. *Eur Spine J* , 1149-1159.

Marcolongo, M., Cannella, M., & Massey, C. (2006). Nucleus Replacement of the Intervertebral Disc. In E. A. Kurtz SM, *SPINE Technology Handbook* (pp. 281-301).

Meakin, J., Redpath, T., & Hukins, D. (2001). The Effect of Partial Removal of the Nucleus Pulposus from the Intervertebral Disc on the Response of the Human Annulus Fibrosus to Compression. *Clinical Biomechanics* , 121-128.

Mimura, M., Panjabi, M., Oxland, T., Crisco, J., Yamamoto, I., & Vasavada, A. (1994). Disc degeneration affects the multidirectional flexibility of the lumbar spine. *Spine* , 1371-80.

Mosby. (2004). *Gray's Anatomy.*

Natarajan, R., Williams, J., & Andersson, G. (2006). Modeling changes in intervertebral disc mechanics with degeneration. *Journal of Bone and Joint Surgery Supplement 2* , 36-40.

Niosi, C., & Oxland, T. (2004). Degenerative mechanics of the lumbar spine. *Spine J* , 202S-208S.

Panjabi, M., & White, A. (1990). *Clinical Biomechanics of the Spine.* Philadelphia: Lippincott Williams & Wilkins.

Rohlmann A, Z. T. (2006). Analysis of the influence of disc degeneration on the mechanical behaviour of a lumbar motion segment using the finite element method. *J Biomech* , 2484-2490.

Ruberté LM, N. R. (2009). Influence of single-level lumbar degenerative disc disease on the behavior of the adjacent segments--a finite element model study. *J Biomech.* , 341-8.

Rutherford, E., Tarplett, L., Davies, E., Harley, J., & King, L. (2007). Lumbar Spine Fusion and Stabilization: Hardware, Techniques, and Imaging Appearances. *Radiographics* , 1737-1749.

Schmidt H, H. F. (2009). Dependency of disc degeneration on shear and tensile strains between annular fiber layers for complex loads. *Med Eng Phys* .

Schmidt H., K. A. (2007). The risk of disc prolapses with complex loading in different degrees of disc degeneration - a finite element analysis. *Clin Biomech* , 988-998.

Schmidt, H., Heuer, F., Drumm, J., Klezl, Z., Claes, L., & Wilke, H. (2007). Application of a calibration method provides more realistic results for a finite element model of a lumbar spinal segment. *Clinical Biomechanics* , 377-84.

Spencer, A. (1984). Constitutive theory for strongly anisotropic solids. In Spencer, *Continuum Theory of the Mechanics of Fibre-Reinforced Composites* (pp. 1-32). New York: Springer Verlag.

Stokes, I., & Iatridis, J. (2005). Biomechanics of the Spine. In H. R. Mow VC, *Basic Orthopaedic Biomechanics and Mechano-Biology* (pp. 529-561). Philadelphia: Lippincott Williams & Wilkins.

Thompson, J., Pearce, R., Schechter, M., Adams, M., Tsang, I., & Bishop, P. (1990). Preliminary evaluation of a scheme for grading the gross morphology of the human intervertebral disc. *Spine* , 411-415.

Wagner, D., & Lotz, J. (2004). Theoretical model and experimental results for the nonlinear elastic behavior of human annulus fibrosus. *Journal of Orthopaedic Research* , 901-909.

Weinhoffer, S., Guyer, R., Herbert, M., & Griffith, S. (1995). Intradiscal pressure junction and the lumbosacral junction (so-called measurements above an instrumented fusion). *Spine* , 526–531.

Wilke HJ, K. A. (1997). Are sheep spines a valid biomechanical model for human spines? *Spine* , 2365-2374.

Williams JR, N. R. (2007). Inclusion of regional poroelastic material properties better predicts biomechanical behavior of lumbar discs subjected to dynamic loading. *J Biomech* , 1981-7.

Woo, S., Lee, T., Abramowitch, S., & Gilbert, T. (2005). Structure and function of ligaments and tendons. In H. R. Mow VC, *Basic Orthopaedic Biomechanics and Mechano-biology* (pp. 301-342). Philadelphia: Lippincott Williams & Wilkins.

Zander T, R. A. (2006). Effect of a posterior dynamic implant adjacent to a rigid spinal fixator. *Clin Biomech (Bristol, Avon)* , 767-74.

Zander, T., Rohlmann, A., & Bergmann, G. (2004). Influence of ligament stiffness on the mechanical behavior of a functional spinal unit. *Journal of Biomechanics* , 1107-1111.

Zander, T., Rohlmann, A., Calisse, J., & Bergmann, G. (2001). Effect of bone graft characteristics on the mechanical behavior of the lumbar spine. *Clinical Biomechanics* , S73-S80.

CHAPTER 2:

The Micromechanical Role of the Annulus Fibrosus Components under Physiological Loading of the Lumbar Spine

(This chapter was published as a Research Article (with Dr. Jose J Garcia and Dr. Christian M. Puttlitz acting as the co-authors of the manuscript) in the Journal of Biomechanical Engineering (132, 061007 (2010)). The text and figures have been adapted with permission from the journal's publisher, American Society of Mechanical Engineering (ASME).)

2.1 INTRODUCTION

The moment-rotation response of spinal motion segments (vertebra-disc-vertebra constructs) is highly nonlinear (Panjabi, et al., 1990). This behavior is often characterized by an initial “neutral zone”, wherein large deformations occur under very small loads, followed by an “elastic region” wherein the response is approximately linear. The presence of the neutral zone has been attributed to the lack of full tension (“slackness”) in the spinal soft tissues, which is established during loading, as well as the creep-related shifting of the hysteresis curve (Panjabi, 1992) (Wilke, et al., 1998). While the effect of ligament mechanics on spinal motion segment kinematics is relatively clear (Zander, et al., 2006), the relationship between the local mechanical properties of the disc and spinal kinematics has not been explicitly established.

The mechanical properties of isolated annulus fibrosus samples under quasi-static loading conditions have been well characterized via numerous experimental and modeling studies (Klisch, et al., 1999) (Elliott, et al., 2001). Simple hyperelastic material models have been successfully employed to represent the ground substance, and the mechanical behavior of the fibers has been described with exponential models (Eberlein, et al., 2001) (Wagner, et al., 2004). However, without translation of these efforts into larger scale modeling of spinal motion segments, the effects of these findings on the global behavior of the spine cannot be appreciated. This length scale “link” is a prerequisite for the successful modeling of other conditions of interest, in particular, degenerative disc disease. Understanding the individual roles of the various spinal components at the tissue level and how they contribute to global mechanics is requisite in order for the biomechanics of disc degeneration to be accurately interpreted. Further, these tissue level property-global function relationships are important for devising sound treatment strategies.

While part of the nonlinearity of the kinematic behavior of the spinal motion segments appears to be a consequence of the heterogeneous structure and mechanical properties of the disc tissues, the specific load-sharing relationship between the collageneous fiber network and the ground substance of the annulus fibrosus is not clear within this global framework. This can be explicitly clarified with a "hybrid" modeling approach wherein a strain energy potential capable of simulating the annulus fibrosus mechanical properties is implemented into a relatively larger scale (single motion segment) finite element model. Earlier continuum approaches in modeling of the annulus have focused on establishment of this methodology (Eberlein, et al., 2001) (Wagner, et al., 2004) (Eberlein, et al., 2004). With the application of a rigorous validation protocol, this approach can reveal the specific roles that the disc constituents play under physiological motions, and how these specific constituent roles change with disease and the application of treatment.

Therefore, the objectives of this study were twofold: (1) Generate a valid, high resolution finite element model of a lumbar functional spinal unit (FSU) capable of reproducing the nonlinear kinematic response over physiologically relevant pure-moment loading range; and (2) quantify and compare the individual contributions of the annular ground substance and collagen fiber network during load bearing on the relative local (tissue level) and global (FSU level) scales.

2.2 METHODS

2.2.1 Reconstruction of Geometry

Using computed tomography (CT) scans of a 49 year old female cadaver, a high resolution finite element model of the L4/L5 FSU was generated. Image segmentation was

conducted in AMIRA (ver. 4.0, Mercury Computer Systems Inc, Chelmsford, MA), and the resultant three dimensional surfaces were imported into TRUEGRID (XYZ Scientific Applications Inc, Livermore, CA) and meshed. Mesh refinement was achieved through convergence of strain energy density (SED) predictions for individual tissues (Ayturk, et al., 2009). The final mesh consisted of 8-noded hexagonal elements with approximately 230,000 degrees of freedom (Figure 2.1). This model was subsequently imported into ABAQUS CAE (ver. 6.8, SIMULIA, Providence, RI) for further model development.

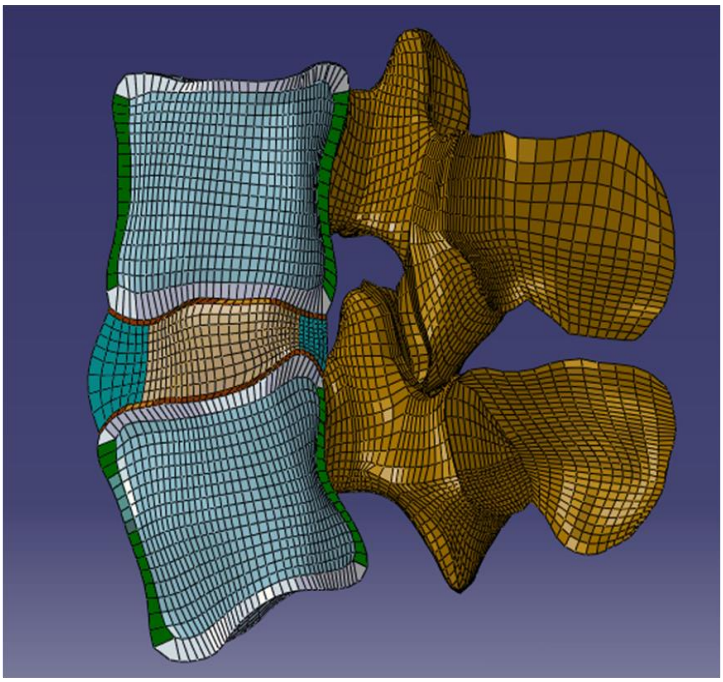

Figure 2.1: A sagittal cut-view of the functional spinal unit. Cortical (green) and trabecular (light blue) bone, posterior elements (brown), bony (grey) and cartilaginous (red) endplates, annulus (light green) and nucleus (light brown) are demonstrated.

2.2.2 Material Properties

Linearly elastic and transversely isotropic material models were imported from the literature to simulate the mechanical behavior of the osseous tissues (Ueno, et al., 1987) (Whyne, et al., 2001). The material constants of the trabeculae were based on CT image data

using previously reported linear regression formulae based on Hounsfield attenuation units (Crawford, et al., 2003). Ligaments were modeled as tension-only, nonlinear springs with previously reported force-displacement relationships (Rohlmann, et al., 2006). The nucleus pulposus was modeled as nearly incompressible (Poisson's ratio: ν = 0.49) and linearly elastic (Dooris, et al., 2001).

The mechanical behavior of the annulus fibrosus was modeled with an orthotropic continuum approach where the mechanical contributions of the fibers and the ground substance were defined over the same physical volume. Utilizing Spencer's invariant-based method for modeling fiber reinforced composites (Spencer, 1984), a strain energy function was developed for the annulus ($W_{annulus}$) as a cumulative function of two separate components (W_{matrix} and W_{fiber}):

$$W_{annulus} = W_{matrix} + W_{fiber} \tag{2.1}$$

The matrix term was chosen as a third-order reduced polynomial (i.e. Yeoh material) in order to simulate the nonlinearity of the stress-strain response of the ground substance. The governing equation for the incompressible material was taken as:

$$W_{matrix} = C_{10}(\bar{I}_1 - 3) + C_{20}(\bar{I}_1 - 3)^2 + C_{30}(\bar{I}_1 - 3)^3 \tag{2.2}$$

where C_{10}, C_{20} and C_{30} are material coefficients and $\bar{I}_1$ is the first invariant of deviatoric component of the Cauchy-Green strain tensor. The coefficients were obtained using optimization schema in ABAQUS CAE in order to give the best fit to the stress-strain response of healthy annulus tissue in the radial direction (Fujita, et al., 1997) (Figure 2.2). Differentiation of Eq. (2.2) with respect to stretch yielded the stress-strain relationship based on stretch and the invariants, in which the error was then minimized with a linear least-squares approximation

ABAQUS tool (ABAQUS, 2008). The fibers were represented as an exponential function of the strain invariants, similar to previous examples in the literature (Eberlein, et al., 2001) (Wagner, et al., 2004) (Guerin, et al., 2007):

$$W_{fiber} = \frac{a_3}{b_3}\left(e^{b_3(I_4-1)^2} + e^{b_3(I_6-1)^2} - 2\right) \quad (2.3)$$

where I_4 and I_6 represent the fourth and sixth invariants of the Cauchy-Green strain tensor (C), respectively:

$$C = F^T F \qquad I_4 = a_0 C a_0 \qquad I_6 = b_0 C b_0 \quad (2.4)$$

where a_0 and b_0 represent the direction cosines of the two fiber families in the undeformed configuration, and F represents the deformation gradient (Holzapfel, 2000). The material coefficients a_3 and b_3 were calibrated to fit the mechanical response of the annulus tissue in the circumferential and axial directions (Wagner, et al., 2004) under tension and compression. The final strain energy function was coded into a user subroutine (UANISOHYPER). Minimum allowable values of the invariants I_4 and I_6 were constrained such that the fibers were activated only under tensile loads. The fiber angles were specified to vary between 26° to 45° from the outer layer to the inner layer of the annulus (Schmidt, et al., 2007), respectively, and they were implemented using the local *ORIENTATION command. The material properties chosen for all tissues are summarized in Table 2.1.

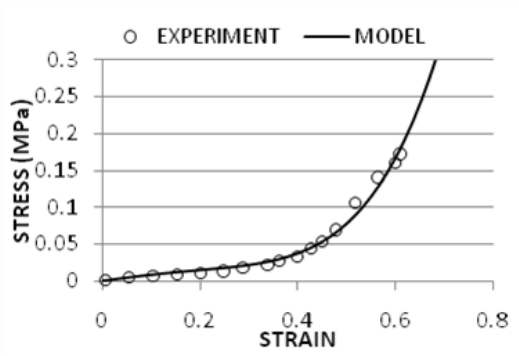

Figure 2.2: Tensile mechanical behavior of the annulus material in the radial direction. Experimental data were adapted from graphical data published in (Fujita, et al., 1997).

Material	Elastic Modulus (MPa)	Poisson Ratio	Reference
Cortical Bone	E_{11} =8000	ν_{12} = 0.4	(Ueno, et al., 1987)
	E_{22} = 8000	ν_{13} = 0.35	
	E_{33} = 12000	ν_{23} = 0.3	
Trabecular Bone	*Based on CT images*	(Crawford, Rosenberg and Keaveny 2003)	
Posterior Elements	E = 3500	ν = 0.3	(Dooris, Goel, et al., 2001)
Bony Endplates	E = 1000	ν = 0.3	(Whyne, et al., 2001)
Facet Cartilage	Neo-Hookean, C_{10} = 2		(Noailly, et al., 2005)
Annulus Fibrosus	Fiber reinforced Yeoh Material		
	C_{10} = 0.0146, C_{20} = -0.0189 C_{30} = 0.041		
	a_3 =0.03, b_3 = 120.0 (b_3 is unitless)		
Nucleus Pulposus	E = 1	ν = 0.49	(Dooris, et al., 2001)
Cartilaginous Endplate	E = 23.8	ν = 0.4	(Lu, et al., 1996)
Ligaments	*Exponential force-displacement curves*		(Rohlmann, et al., 2006)

Table 2.1: Summary of the mechanical properties used in the model

2.2.3 Validation & Model Predictions

Validation of the model was performed following the stepwise protocol previously suggested by Heuer et al. (Heuer, et al., 2007). The FSU was reduced by removal of all ligaments, followed by a complete nucleotomy. Then, during the re-addition of each component, the range of motion (ROM) predictions were compared to available experimental data. The resting pressure inside the nucleus (as described below) and the nonlinear properties of the ligaments were calibrated to provide the best fit when necessary. During the application of this calibration scheme, the FSU was tested under pure moments up to 7.5 Nm in the three principal directions (flexion-extension, lateral bending and axial rotation), without the application of a compressive pre-load as the aforementioned scenario has been shown to yield comparable results with the *in vivo* kinematic behavior (Wilke, et al., 2001).

Given that the model was used to predict the loading-motion response and relevant internal mechanical parameters, complete validation of the finite element model of the spine cannot be based on kinematic data alone. Hence, the intradiscal nuclear pressure (both in the

prescribed pure-moment-loading scenario and under the application of purely compressive loads) (Figure 2.3), vertebral bone strain (Figure 2.4), and disc bulge (Table 2.2) predictions (defined as the maximum nodal displacement in the area of interest) of the model were also compared with previously published experimental data. While a rather thorough approach is essential to ensure the accuracy of other mechanical predictions, the validation methodology described herein has been constrained to the parameters that are relevant to the scope of this work. A complete description of the entire battery of validation metrics is contained elsewhere (Ayturk, 2007).

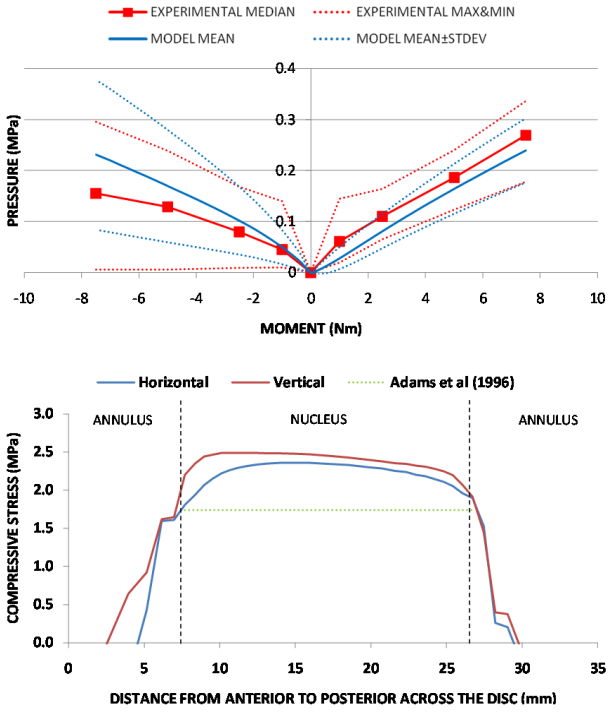

Figure 2.3: (Top) Intradiscal nuclear pressure predictions of the intact model under flexion (+ moment) and extension (- moment) loading. The mean and standard deviation values reported for the model represent the nodal variation of the model's predictions within the nucleus pulposus. The experimental data represent the median, maximum and minimum of a pool of tested specimens, as indicated by the legend (Heuer, et al., 2007). (Bottom) Change in the horizontal and vertical compressive stress components in the antero-posterior direction while the FSU is under compression with the application of 2000N. Dashed lines represent the physical boundaries between the annulus and the nucleus.

2.2.4 Annulus Component Prediction Modeling

In addition to ROM, SED predictions were reported for the fiber and ground substance components as a measure of their individual mechanical responses and contributions. Specifically, SED was interpreted as an indicator of the load-sharing relationship between the fibers and the ground substance since it inherently removes any confounding disparities due to volumetric differences between these components that is associated with the aforementioned continuum approach in modeling the annulus fibrosus.

Since the disc maintains a homeostatic, non-zero stress/strain condition in its resting, reference configuration (Wilke, et al., 1999), the nucleus was pressurize d by inducing positive (expansive) isotropic volumetric strain (using the *THERMAL STRAIN option) on the corresponding nodes at the beginning of each analysis. Consequently, the model predictions were non-zero when no load was applied, and therefore, the "change" in each parameter of interest with respect to this no load reference state was reported. At the end of pressurization, the nodal predictions (of the deviatoric component of the stress tensor) in the nucleus pulposus were 0.1 ± 0.04 MPa (mean ± standard deviation), consistent with previously reported in vivo nuclear pressure measurements taken in the transverse position (Thompson, et al., 2003). All solutions were

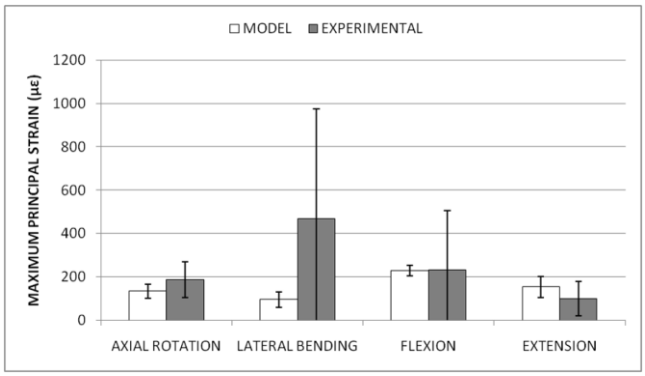

Figure 2.4: Maximum principal strain predictions at the anterolateral cortical surface of L4 under the application of 3Nm of pure moment. Model predictions indicate the mean and standard deviation of nodal predictions in the anterolateral cortical region, while the experimental data indicate the mean and standard deviation in the measurements from a sample pool (n=6) (Ayturk, 2007).

obtained using ABAQUS Standard (ver. 6.8, SIMULIA, Providence, RI) running on a high-performance workstation (Model: xw8400, Hewlett-Packard Company, Palo Alto, CA).

	ANNULUS + NUCLEUS		INTACT	
	MODEL	**HEUER ET AL**	**MODEL**	**HEUER ET AL**
Flexion	2.29	2.21	1.88	1.63
Lateral Bending	1.36	1.32	1.5	1.11

Table 2.2: The magnitude of maximum outward disc bulge under pure moments of 7.5 Nm. ANNULUS + NUCLEUS represents the condition where all ligaments and posterior elements are removed. Both the model predictions and experimental data (Heuer, Schmidt and Wilke 2008) are in mm.

2.3 RESULTS

2.3.1 Validation Data

The moment-rotation responses of the FSU in all three directions (flexion, extension, unilateral bending and unilateral axial rotation) were in reasonable agreement with the experimental data (Figure 2.5) following pressurization of the nucleus and calibration of the ligament properties. In the first case, where the only load-bearing soft tissue was the annulus, the kinematic behavior was initially very compliant. According to the criterion specified by Thompson et al. (Thompson, et al., 1990) for defining the neutral zone, these annulus-only models predicted neutral zones with magnitudes of 5.98°, 5.6°, 1.41° and 2.28° for flexion, extension, lateral bending and axial rotation, respectively (in agremeent with the findings of (Heuer, et al., 2007)). As expected, the total ROM predictions were reduced with the addition of each soft tissue component in all loading scenarios. In the intact condition, these values were 5.12°, 3.89°, 4.88° and 3.48° in flexion, extension, lateral bending and axial rotation, respectively.

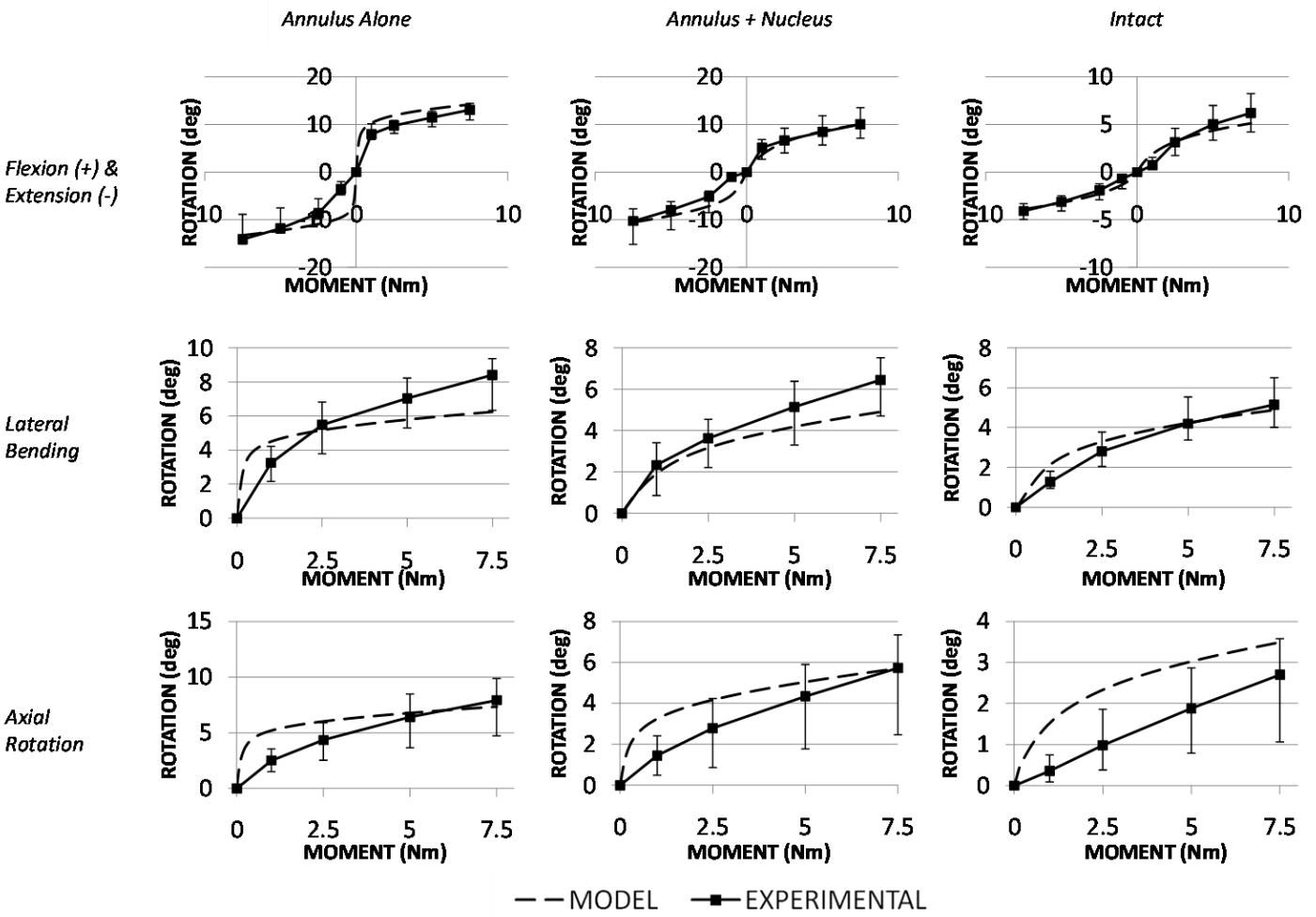

Figure 2.5: Moment-rotation response of the FSU with the annulus alone, annulus and nucleus and in intact condition. Pure moments were applied under flexion/extension (+/-), lateral bending and axial rotation. Experimental data were adapted from graphical data in (Heuer, et al., 2007) and indicate the median, minimum and maximum of the measurements.

The intradiscal nuclear pressure predictions of the model (mean values of 239 kPa and 231 kPa for flexion and extension, respectively) were in good agreement with experimental data from the literature (Figure 2.3). Furthermore, simulation of a 2000 N compression experiment yielded mean stress predictions of 2.2 MPa and 2.37 MPa in the horizontal and vertical directions, respectively, which are comparable to previously published measured values of nuclear pressure 1.74 $\pm$ 0.52 MPa (mean $\pm$ standard deviation) as reported by (Adams, et al., 1996). Strain predictions in the anterolateral cortical surface of L4 were underestimated under lateral bending; however, the predictions for the other loading cases loosely approximated the experimental data. All loading scenario predictions were within one standard deviation of the experimental mean (Figure 2.4). Similarly, the maximum disc bulge predictions when the ligaments and posterior elements were removed (2.29 mm and 1.36 mm in flexion and lateral bending, respectively) compared well to the experimental data, as well as the predictions for the intact case (1.88 mm and 1.5 mm in flexion and lateral bending, respectively) (Table 2.2).

2.3.2 Annulus Constituent Predictions

In the reference configuration, the SED predictions for the ground substance and the fibers were 0.65 MPa and 0.4 MPa, respectively. Overall, the SED predictions for the fibers increased at a higher rate than those for the ground substance with respect to increasing rotation (Figure 2.6). Specifically, under lateral bending and axial rotation, the SED predictions for the ground substance continued to increase at an approximately constant rate before and after the end of the neutral zone with respect to rotation. On the other hand, the slope of the SED predictions for the fiber component continually increased with additional applied loading beyond the neutral zone. The annulus SED predictions of the intact model were higher under

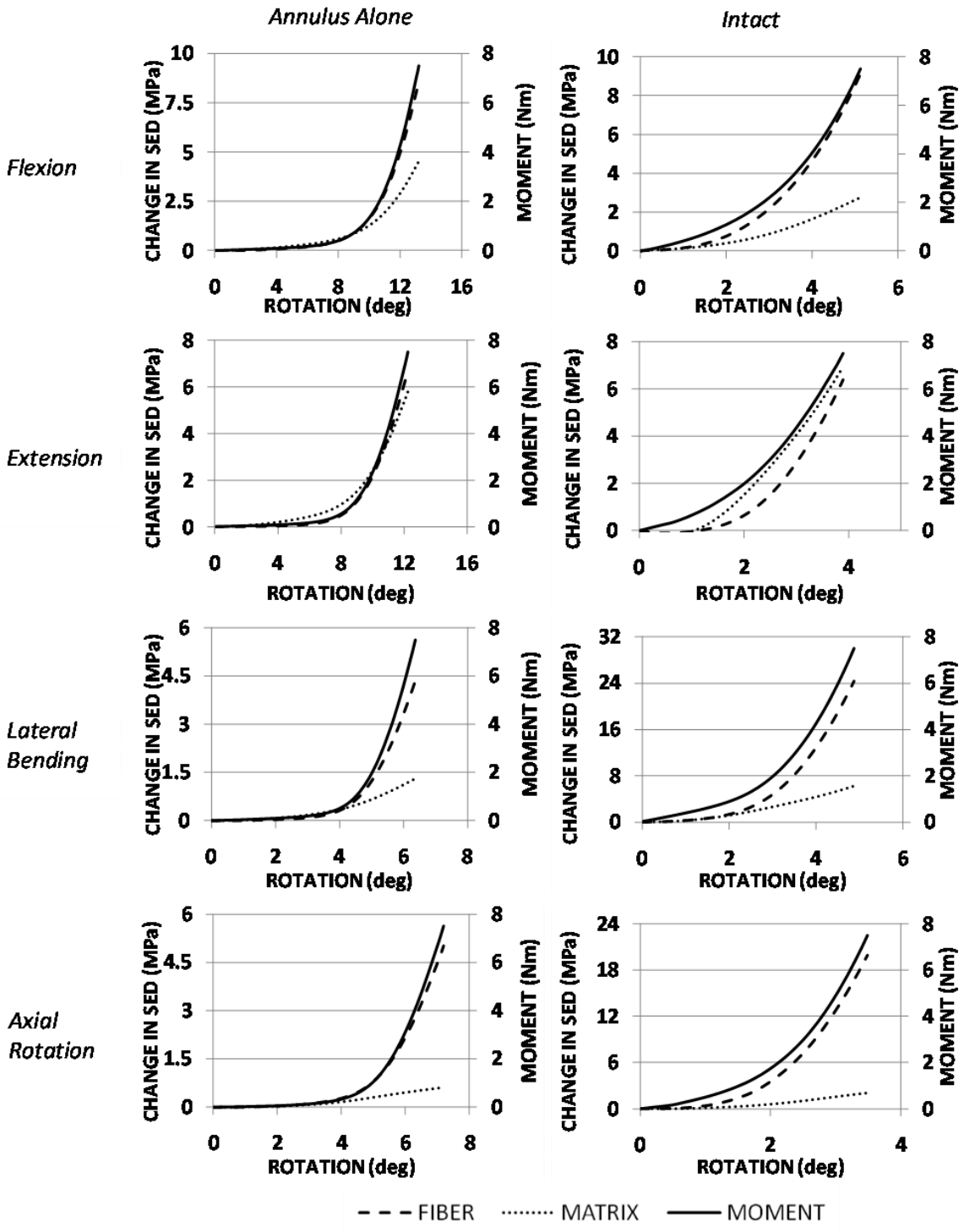

Figure 2.6: Total SED predictions for the annulus ground substance and fibers, and applied moment with respect to global rotation for the model with annulus alone (left) and in the intact condition (right).

lateral bending and axial rotation than those of the model with the annulus alone, in spite of the reduction in the ROM. The highest SED predictions of the model with the annulus alone were under loading in flexion. On the other hand, following the addition of the nucleus, the posterior elements and the ligaments, the highest change in SED predictions for the intact model were observed during lateral bending loading.

The load sharing between the collageneous fibers and the ground substance was approximately equal under extension when the model was run with the annulus alone (53.7 % and 46.3 %, respectively) and when fully intact (47.9 % and 52.1%, respectively; Figure 2.7). However, in the other loading directions, the total SED predictions for the fiber component were substantially greater than the matrix SED predictions. Specifically, the fibers carried the greatest share of the mechanical loads under axial rotation in both the intact condition (90.5 %) and with the annulus alone (89.2 %; Figure 2.7). The local SED predictions demonstrate the same pattern, wherein the ground substance appears to bear a greater amount of the load in areas where the disc is under compression and the fibers bear a higher amount of load in the areas under tension (Figure 2.8). Moreover, the SED predictions for the

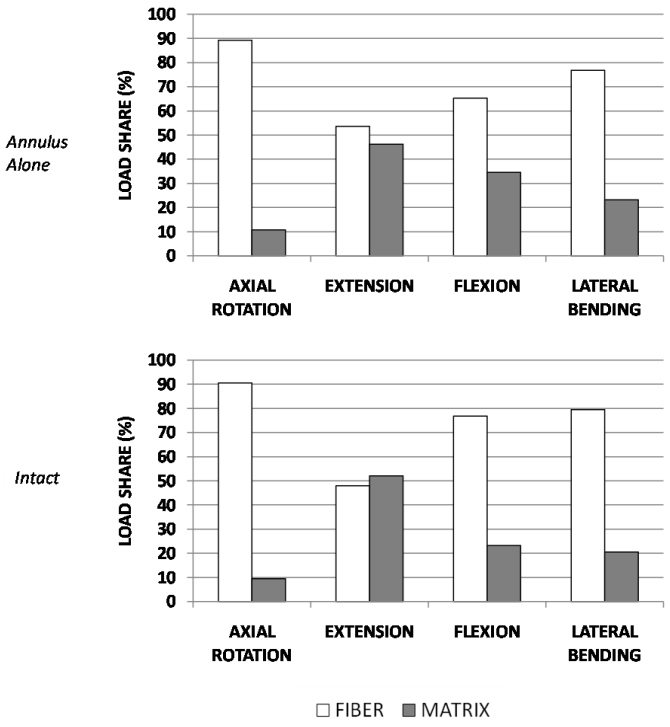

Figure 2.7: Load-sharing between the fibers and ground substance of the annulus (as measured using the SED) under 7.5 Nm of loading in all directions with the annulus alone as the load bearing soft tissue (top) and in the intact condition (bottom).

fibers increased from the inner layers towards the outer layers of the annulus, where outward bulging of the disc was observed. Specifically in areas under tensile loads, SED predictions for the fibers were highest in the intermediate layers rather than the extrema. When the ligaments, posterior elements and nucleus were removed, bulging of the internal layers of the annulus was observed to be towards the nuclear cavity, consistent with previous findings associated with advanced disc degeneration (Seroussi, et al., 2005) (Lotz, et al., 1998).

2.4 DISCUSSION

In this work, some of the underlying causes of nonlinearity in the kinematic behavior of lumbar spinal motion segments were investigated using a finite element modeling approach. Specifically, the individual contributions of the ground substance and collageneous fibers to the mechanical behavior of annulus fibrosus were quantified under different loading conditions. The generated finite element model was capable of simulating the nonlinear kinematic response of the L4/L5 FSU. This capability is requisite in order to ensure that the proper fidelity of the model's predictions over physiologically relevant loading ranges is valid, as opposed to validation in a pointwise manner. Clinical conditions of interest, particularly disc degeneration, cannot be accurately simulated without predicting the changes in the nonlinearity of the moment-rotation response and the hypermobility of the motion segment (Mimura, et al., 1994). Only under these circumstances would the attempts at modeling the effect of treatment strategies that aim to regenerate the diseased disc tissue (such as dynamic stabilization devices) be meaningful.

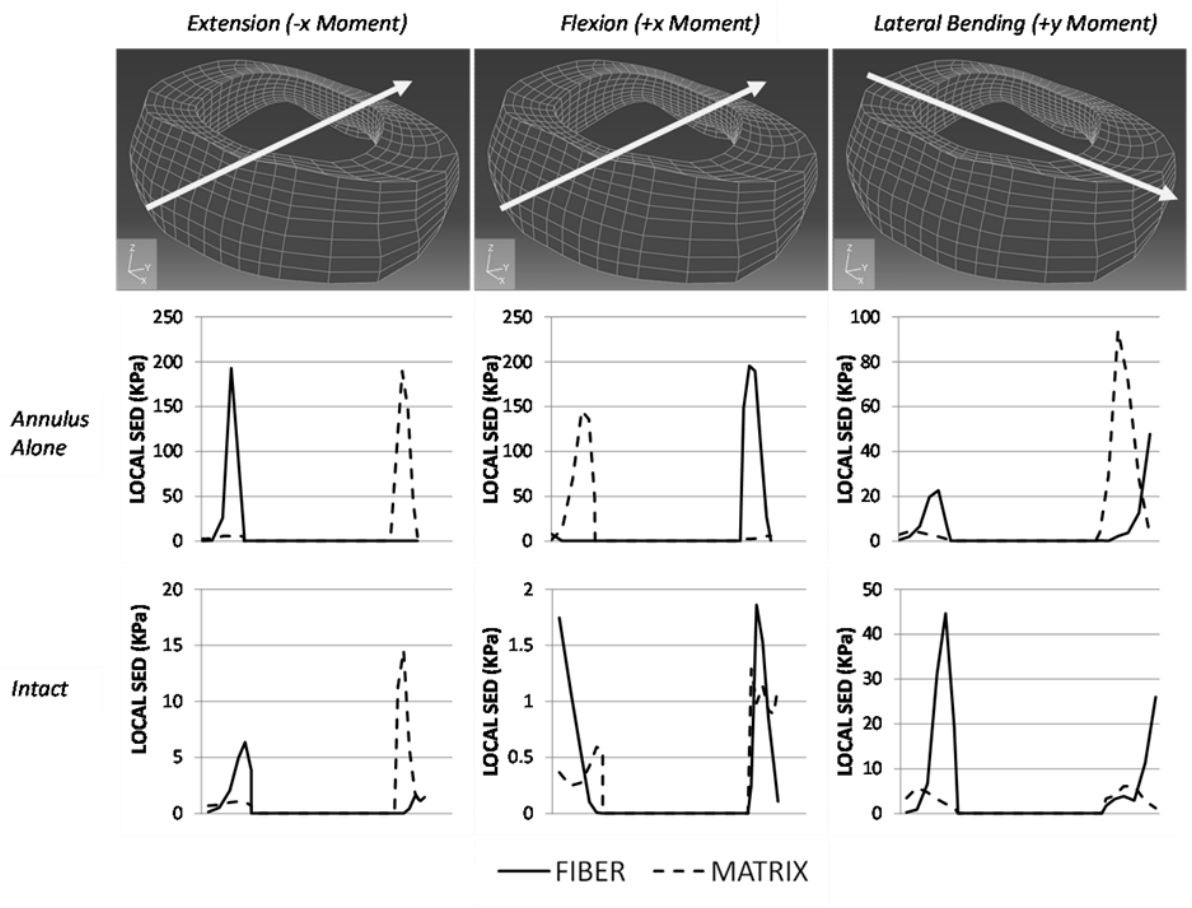

Figure 2.8: Local annular SED distribution in the anteroposterior direction under extension (left) and flexion (middle) and in the medial-lateral direction under lateral bending (right). The white arrows indicate the positions of the nodes in the annulus corresponding to the horizontal axes of the charts below. The plots demonstrate the local SED predictions for the ground substance and the fibers with the annulus alone (middle) and the FSU in the intact condition (bottom). The blue (ground substance) and red (fiber) curves represent the component SED predictions under 7.5 Nm of pure moment loading.

The initially compliant kinematic response of the reduced FSU with only the annulus as the load bearing soft tissue in all loading directions was followed by a global stiffening effect that was coincident with the stiffening of the collageneous fibers (Figure 2.6). Structurally, this initial compliance could be due to the uncrimping of the annular fibers *in situ*, while a similar strain-based stiffening of the ground substance was not observed. The continuous recruitment of collageneous fibers under mechanical loading regimes has been shown to increase the stiffness of the global construct for ligamenteous (Hurschler, et al., 1997) and tendinous (Hansen, et al., 2002) tissues. Furthermore, the use of an exponential model to represent the mechanical behavior of the fibers proved to be an accurate method towards simulating the nonlinearity of the spinal motion segments, similar to other collageneous tissue constructs.

The total SED predictions in all loading directions (except for extension) indicate that the fibrous network in the annulus is the major load-bearing component of the tissue under 7.5 Nm of pure moment loading. In light of the previous observations, this confirms that the mechanical properties of the fibers are the dominant determinants with respect to the resultant kinematic response in the elastic zone. Moreover, while these fibers are activated within areas under local tensile loading, they also appear to bear substantial amounts of load within the outer lamellae of the annulus where outward bulging is frequently observed (Figure 2.8). The large differences between the predictions for the “intact” and “annulus alone” cases under lateral bending and axial rotation show that nucleus pressurization is the primary mechanism that induces higher loads on the annulus fibrosus on a global scale (Figure 2.6). The maximum fiber strains in the annulus have been reported to be located in the posterior and posterolateral regions under pure moment loading (Heuer, et al., 2008). Our SED predictions confirm these findings. These mechanical data correlate with the most frequent clinical findings related to annular damage such as herniation and annular tears (Adams, et al., 2002).

While the dynamically-derived and experimental neutral zone measurements cannot be used for direct quantitative comparisons to quasi-static load-displacement data, the model predictions reflect the experimental findings of relatively "*large deformations under very small loads*" (Panjabi, 1992) (Thompson, et al., 2003). Consequently, the "late" stiffening of the fibers plays a definitive role in bounding the neutral zone (Wilke, et al., 1998). This limitation of the neutral zone is particularly relevant during various stages of the degeneration cascade, such as when the resting nuclear pressure is reduced or the mechanical functionality of the nucleus pulposus is completely lost.

In addition to deterioration of the ground substance through increased catabolic activity, disc degeneration has been shown to significantly reduce the re-orientation capability of the fibrous network under loading (Guerin, et al., 2006). Within this framework, the activation of the fibers is "delayed" under loading, resulting in generation of resistive forces only at higher deformations as compared to the healthy case (Figure 2.6). This finding is also in agreement with previous reports of increased neutral zone magnitude as a result of degeneration, which is typically interpreted as hypermobility in the clinical setting (Mimura, Panjabi, et al., 1994).

As it is the case for any modeling work, there is a number of limitations with the current study. While there is a certain variation in the morphology and mechanical properties of the intervertebral disc throughout its geometry (Holzapfel, et al., 2005), it was assumed to be spatially homogeneous, except for the variation in the fiber orientation. Moreover, the viscoelastic response of the soft tissues was omitted by assuming that all the loads were applied under quasi-static loading conditions, and predictions were compared with experimental data collected under relatively slow loading rates to be consistent.

The development of the current model provides a high fidelity tool for investigating the global effects of degeneration-induced changes in the annulus fibrosus on the local scale. In addition, many regenerative treatment schemas currently under development seek to locally alter both the nucleus pulposus and annulus fibrosus, such that these changes produce a more normal return of global intervertebral mechanics. Future studies utilizing this model will focus on identifying specific mechanical target criteria (e.g. acceptable ranges for restoration of nucleus pressure) for these treatments.

2.5 CONCLUSION

The nonlinear kinematic behavior of the L4/L5 FSU was simulated with a finite element modeling approach. Specifically, the individual contributions of the ground substance and collageneous fibers to the mechanical behavior of annulus fibrosus were quantified under pure moment load application. The collageneous fibers were found to bear the majority of the load in all loading scenarios except for extension, and they also conferred a substantial effect on the nonlinear kinematic behavior of the lumbar spine. These data explicitly establish that fiber recruitment is a critical component in determining the range of motion and neutral zone magnitudes of spinal motion segments.

REFERENCES

ABAQUS. (2008). *Abaqus Theory Manual (ver 6.8).* Providence, RI: Dassault Systemes SIMULIA Corp.

Adams, M., Bogduk, N., Burton, K., & Dolan, P. (2002). *The Biomechanics of Back Pain.* London: Churchill Livingstone.

Adams, M., McNally, D., & Dolan, P. (1996). "Stress" Distributions Inside Intervertebral Discs. *J Bone Joint Surg Br* , 78(6):965-972.

Ayturk, U. (2007). *Development and validation of a three dimensional high resolution nonlinear finite element model of an L3/L4 funcitonal spinal unit, Master's Thesis.* Fort Collins, CO: Colorado State University.

Ayturk, U., & Puttlitz, C. (2009). The effect of mesh refinement on the predictions of finite element models of spine. *ASME Summer Bioengineering Conference.* Lake Tahoe, CA.

Crawford, R., Rosenberg, W., & Keaveny, T. (2003). Quantitative computed tomography based finite element models of the human lumbar vertebral body: effect of element size on stiffness, damage, and fracture strength predictions. *Journal of Biomechanical Engineering* , 434-8.

Dooris, A., Goel, V., Grosland, N., Gilbertson, L., & Wilder, D. (2001). Load sharing between anterior and posterior elements in a lumbar motion segment implanted with an artificial disc. *Spine* , E122-E129.

Eberlein, R., Holzapfel, G., & Forhlich, M. (2004). Multi-Segment FEA of the Human Lumbar Spine Including the Heterogeneity of the Annulus Fibrosus. *Comput Mech* , 34:147-163.

Eberlein, R., Holzapfel, G., & Schulze-Bauer, C. (2001). An anisotropic model for annulus tissue and enhanced finite element analyses of intact lumbar disc bodies. *Computer Methods in Biomechanics and Biomedical Engineering* , 209-230.

Elliott, D., & Setton, L. (2001). Anisotropic and inhomogeneous tensile behavior of the human anulus fibrosus: experimental measurement and material model predictions. *J Biomech Eng* , 123(3):256-263.

Fujita, Y., Duncan, N., & Lotz, J. (1997). Radial tensile properties of the lumbar annulus fibrosus are site and degeneration dependent. *J Orthop Res* , 814-9.

Guerin, H., & Elliott, D. (2006). Degeneration affects the fiber reorientation of human annulus fibrosus under tensile load. *Journal of Biomechanics* , 1410-1418.

Guerin, H., & Elliott, D. (2007). Quantifying the contributions of structure to annulus fibrosus mechanical function using a nonlinear, anisotropic, hyperelastic model. *Journal of Orthopaedic Research* , 508-516.

Hansen, K., Weiss, J., & Barton, J. (2002). Recruitment of tendon crimp with applied tensile strain. *J Biomech Eng* , 72-7.

Heuer, F., Schmidt, H., & Wilke, H. (2008). The relation between intervertebral disc bulging and annular fiber associated strain for simple and complex loading. *J Biomech* , 1086-1094.

Heuer, F., Schmidt, H., Claes, L., & Wilke, H. (2007). Stepwise reduction of functional spinal structures increase vertebral translation and intradiscal pressure. *J Biomech* , 795-803.

Heuer, F., Schmidt, H., Klezl, Z., Claes, L., & Wilke, H. (2007). Stepwise reduction of functional spinal structures increase range of motion and change lordosis angle. *Journal of Biomechanics* , 271-280.

Holzapfel, G. (2000). *Nonliear Solid Mechanics.* Wiley.

Holzapfel, G., Schulze-Bauer, C., Feigl, G., & Regitnig, P. (2005). Single-lamellar mechanics of the human lumbar anulus fibrosus. *Biomechanics and Modeling in Mechanobiology* , 125-140.

Hurschler, C., Loitz-Ramage, B., & Vanderby, R. J. (1997). A structurally based stress-stretch relationship for tendon and ligament. *J Biomech Eng* , 392-9.

Klisch, S., & Lotz, J. (1999). Application of a fiber-reinforced continuum theory to multiple deformations of the annulus fibrosus. *J Biomech* , 32(10):1027-1036.

Lotz, J., Colliou, O., Chin, J., Duncan, N., & Liebenberg, E. (1998). Compression-induced degeneration of the intervertebral disc: an in vivo mouse model and finite-element study. *Spine* , 2493-506.

Lu, Y., Hutton, W., & Gharpuray, V. (1996). Do bending, twisting, and diurnal fluid changes in the disc affect the propensity to prolapse? A viscoelastic finite element model. *Spine* , 2570-9.

Mimura, M., Panjabi, M., Oxland, T., Crisco, J., Yamamoto, I., & Vasavada, A. (1994). Disc degeneration affects the multidirectional flexibility of the lumbar spine. *Spine* , 1371-80.

Noailly, J., Lacroix, D., & Planell, J. (2005). Finite element study of a novel intervertebral disc substitute. *Spine* , 2257-64.

Panjabi, M. (1992). The stabilizing system of the spine. Part II. Neutral zone and instability hypothesis. *J Spinal Dis* , 5(4):390-7.

Panjabi, M., & White, A. (1990). *Clinical Biomechanics of the Spine.* Philadelphia: Lippincott Williams & Wilkins.

Rohlmann, A., Zander, T., Schmidt, H., Wilke, H., & Bergmann, G. (2006). Analysis of the influence of disc degeneration on the mechanical behaviour of a lumbar motion segment using the finite element method. *J Biomech* , 2484-2490.

Schmidt, H., Heuer, F., Drumm, J., Klezl, Z., Claes, L., & Wilke, H. (2007). Application of a calibration method provides more realistic results for a finite element model of a lumbar spinal segment. *Clinical Biomechanics* , 377-84.

Seroussi, R., Krag, M., Muller, D., & Pope, M. (2005). Internal deformations of intact and denucleated human lumbar discs subjected to compression, flexion, and extension loads. *J Orthop Res* , 122-31.

Spencer, A. (1984). Constitutive theory for strongly anisotropic solids. In Spencer, *Continuum Theory of the Mechanics of Fibre-Reinforced Composites* (pp. 1-32). New York: Springer Verlag.

Thompson, J., Pearce, R., Schechter, M., Adams, M., Tsang, I., & Bishop, P. (1990). Preliminary evaluation of a scheme for grading the gross morphology of the human intervertebral disc. *Spine* , 411-415.

Thompson, R., Barker, T., & Pearcy, M. (2003). Defining the Neutral Zone of sheep intervertebral joints during dynamic motions: an in vitro study. *Clin Biomech* , 89-98.

Ueno, K., & Liu, Y. (1987). A three dimensional nonlinear finite element model of lumbar intervertebral joint in torsion. *J Biomech Eng* , 200-9.

Wagner, D., & Lotz, J. (2004). Theoretical model and experimental results for the nonlinear elastic behavior of human annulus fibrosus. *Journal of Orthopaedic Research* , 901-909.

Weiss, J., Maker, B., & Govindjee, S. (1996). Finite element implementation of incompressible, trasnversely isotropic hyperelasticity. *Comput Methods Appl Mech Engrg* , 107-128.

Whyne, C., Hu, S., & Lotz, J. (2001). Parametric Finite Element Analysis of Vertebral Bodies Affected by Tumors. *J Biomech* , 34(10):1317-1324.

Wilke, H., Neef, P., Caimi, M., Hoogland, T., & Claes, L. (1999). New In Vivo Measurements of Pressures in the Intervertebral Disc in Daily Life. *Spine* , 24(8):755-762.

Wilke, H., Rohlmann, A., Neller, S., Schultheiss, M., Bergmann, G., Graichen, F., et al. (2001). Is it Possible to Simulate Physiologic Loading Conditions by Applying Pure-Moments? A Comparison of In Vivo and In Vitro Load Components in an Internal Fixator. *Spine* , 26(6):636-642.

Wilke, H., Wenger, K., & Claes, L. (1998). Testing criteria for spinal implants: recommendations for the standardization of in vitro stability testing of spinal implants. *European Spine Journal* , 7(2):148-154.

Zander, T., Rohlmann, A., Burra, N., & Bergmann, G. (2006). Effect of a posterior dynamic implant adjacent to a rigid spinal fixator. *Clin Biomech (Bristol, Avon)* , 37(7):767-74.

CHAPTER 3:

Parametric Convergence Sensitivity and Validation of a Finite Element Model of Human Lumbar Spine

(This chapter was accepted for publication as a Research Article (with Dr. Christian M. Puttlitz acting as a co-author) in Computer Methods in Biomechanics and Biomedical Engineering in March 2010. The text and figures have been adapted with permission from the journal's publisher, Taylor & Francis UK.)

3.1 INTRODUCTION

Finite element modeling of spine has been an appealing alternative to biomechanical experimentation and an established methodology in assessment of the performances of medical devices and conducting basic science research (Shirazi-Adl, et al., 1984) (Lu, et al., 1996) (Zander, et al., 2001) (Schmidt, et al., 2007) (Natarajan, et al., 2006) (Jones, et al., 2008). Due to the rigorous nature of the development process (as a result of the geometric and mechanical behavior complexity), it is possible to predict mechanical parameters of interest that cannot be measured through experimentation.

The geometry of spinal segments is quite complex (Bogduk, 1999), and representation with generic shapes may lead to over-simplification of the problem. A more frequently used and accurate method is reconstruction of CT-based imaging data (Goel, et al., 1995) (Liebschner, et al., 2003). The individual material properties of the spinal tissues are gathered through extensive testing and are well documented in the literature. Bony tissues are usually represented with linearly elastic material models since they are subject to relatively infinitesimal strains (small strain theory) *in vivo* (Ueno, et al., 1987) (Dooris, et al., 2001) (Whyne, et al., 2001). The properties of soft tissue components, on the other hand, are highly nonlinear, and their associated deformations are relatively large. The annulus fibrosus, in particular, is of special interest, due to the aforementioned nonlinearity and its morphology-related anisotropy (Fujita, et al., 1997) (Klisch, et al., 1999) (Elliott, et al., 2001) (Wagner, et al., 2004). The composite structure of the tissue can be modeled by the definition of the geometric components discretely (Shirazi-Adl, et al., 1984) (Goel, et al., 1995) or with a continuum approach that assumes the tissue is homogeneous at the micro-level (Eberlein, Holzapfel and Schulze-Bauer 2001) (Eberlein, Holzapfel and Frohlich 2004).

Verification and validation are inherent requirements in the development of a reliable finite element model (Anderson, et al., 2007) (Jones, et al., 2008). The former is associated with confirming that the problem of interest is appropriately formulated and solved. In addition to specific computational factors such as the choice of iterative solution technique, verification of mesh convergence is particularly important. Under static boundary conditions, this requirement can be accomplished by verifying the minimization of the system's potential energy (Zienkiewicz, et al., 2000) (Morris, 2008). In the spine, where the material and geometric non-uniformities can affect the predictive outcome, mesh convergence is of particular importance (Marks, et al., 1993). Unfortunately, mesh convergence is often omitted in finite element modeling of spinal segments, and to the best of our knowledge, a thorough assessment of how the changes in mesh resolution affect the predictions have not been reported to date. Relatively few studies have attempted to demonstrate mesh convergence explicitly (Villaraga, et al., 1999) (Liebschner, et al., 2003) (Williams, et al., 2007), and these investigations have generally been limited to analysis of global stiffness or displacement predictions. An extensive convergence study is warranted in all spinal modeling attempts, wherein the change in strain energy density (as an indicator of mechanical response) with respect to mesh resolution should be minimized. Consequently, one of the goals of this study is to demonstrate the convergence behavior of all spinal tissues separately and evaluate how they compare to the overall stiffness and displacement parameters that have been traditionally used in previously published spinal modeling endeavors.

The second aforementioned requirement, validation, has been generally kept limited to comparisons of spinal range of motion predictions (ROM). While this might be sufficient if the use of the model will be restricted to these motion (kinematic or kinetic) parameters, validation with respect to ROM predictions only does not necessarily ensure the accuracy of other internal

mechanical parameter predictions of interest such as stress or strain mappings. With the availability of miniature strain gages and pressure measurement devices for experimental studies, there is an increased amount of data on intradiscal pressure (Adams, et al., 1996) (Heuer, et al., 2007) facet forces (Wilson, et al., 2006) (Sawa, et al., 2008) and bony strain (Frei, et al., 2001) available in the literature that might serve the validation purposes. Taking such a thorough validation approach would ensure the fidelity of the clinically relevant predictions, and consequently increase the utility of the model.

Therefore, the primary objective of this paper is to generate a finite element model of the healthy human lumbar spine (L1-L5) and, (1) verify mesh convergence for each tissue constituent and (2) perform an extensive validation using both kinematic/kinetic and stress/strain data.

3.2 METHODS

3.2.1 Mesh Generation

The model geometry was reconstructed using computed tomography (CT) scans of a cadaveric specimen (age=49) with no known bone disease or spinal abnormality. A set of 220 two-dimensional images (0.5 mm thick with 1 mm spacing) taken in the transverse plane was imported into AMIRA (ver. 4.0, Mercury Computer Systems Inc, Chelmsford, MA). The resultant in-plane pixel resolutions were 0.35 mm x 0.35 mm with a third voxel dimension (in the superior-inferior direction) of 0.5 mm.

The three-dimensional components of the mesh were generated in TrueGrid (XYZ Scientific Applications Inc, Livermore, CA). The vertebra and intervertebral disc geometries were subsequently imported, with each surface being sectioned into simpler shaped sub-geometries.

Rectangular shaped boundary blocks (BB) consisting of eight-noded elements were then morphed into these sub-geometries and were merged at the intersections to form a complete mesh of the L1-L5 geometry. Cartilaginous endplate (0.8 mm) and facet cartilage thicknesses (1.25 mm) were based on previously reported measurements (Bogduk, 1999) (Womack, et al., 2008). Six major ligaments (anterior longitudinal ligament (ALL), posterior longitudinal ligament (PLL), facet capsules (FC), ligamentum flavum (LF), infraspinous ligament (ISL) and supraspinous ligament (SSL)) were simulated with one-dimensional spring elements.

3.2.2 Material Properties

The mechanical behavior of cortical and trabecular bone were simulated with linearly elastic and transversely isotropic material models (Ueno, et al., 1987). Trabecular regions inside the vertebral bodies were assigned homogeneous material properties while the solid mesh was refined. Then, during validation, these values were modified based on the CT attenuation data using previously reported linear regression formulae (Crawford, et al., 2003):

$$E_{33} = -34.7 + 3230\rho \tag{3.1}$$

$$E_{11} = E_{22} = 0.33E_{33} \tag{3.2}$$

where ρ is the bone mineral density (calibrated using a phantom image), E_{33} is the elastic modulus in the longitudinal direction, and E_{11} and E_{22} are the elastic moduli in the planar directions. The spring elements representing the ligaments were assigned previously reported exponential force-displacement relationships (Nolte, et al., 1990) (Rohlmann, et al., 2006):

$$F = ae^{b(\varepsilon - c) - 1} \tag{3.3}$$

where a, b and c are material constants and ε is strain based on displacement. The nucleus pulposus was modeled as a linearly elastic and almost incompressible solid (v =0.49) (Dooris, et al., 2001). Finally, mechanical behavior of the annulus fibrosus was modeled with an orthotropic

continuum approach. The contributions of the fibers and the ground substance to the mechanical behavior were explicitly defined as components of a strain energy function (W):

$$W_{annulus} = W_{matrix} + W_{fiber} \tag{3.4}$$

Using Spencer's classic approach (Spencer, 1984), the individual energy terms were defined as functions of Cauchy-Green strain tensor invariants:

$$W_{matrix} = C_{10}(\bar{I}_1 - 3) + C_{20}(\bar{I}_1 - 3)^2 + C_{30}(\bar{I}_1 - 3)^3 \tag{3.5}$$

$$W_{fiber} = \frac{a_3}{b_3}\left(e^{b_3(I_4-1)^2} + e^{b_3(I_6-1)^2} - 2\right) \tag{3.6}$$

Further details of the function are given elsewhere (Ayturk, et al., 2010). Both terms (3.5) and (3.6) were coded into an ABAQUS user subroutine (UANISOHYPER) and the fiber term was constrained so that the fibers would become active only under tensile loads. The local fiber orientation was specified to range from 26° to 45° between the outer and inner layers, respectively (Schmidt, et al., 2007). The implemented material properties are summarized in Table 3.1.

Material	**Elastic Modulus (MPa)**	**Poisson Ratio**	**Reference**
Cortical Bone	E_{11} =8000	ν_{12} = 0.4	(Ueno and Liu, 1987)
	E_{22} = 8000	ν_{13} = 0.35	
	E_{33} = 12000	ν_{23} = 0.3	
Trabecular Bone	*Based on CT images*		(Crawford et al., 2003)
Posterior Elements	E = 3500	ν = 0.3	(Dooris et al., 2001)
Bony Endplates	E = 1000	ν = 0.3	(Whyne et al., 2001)
Facet Cartilage	Neo-Hookean, C_{10} = 2		(Noailly et al., 2005)
Annulus Fibrosus	Fiber reinforced Yeoh Material		
	C_{10} = 0.0146, C_{20} = -0.0189 C_{30} = 0.041		
	a_3 =0.03, b_3 = 120.0 (b_3 is unitless)		
Nucleus Pulposus	E = 1	ν = 0.49	(Dooris et al., 2001)
Cartilaginous Endplate	E = 23.8	ν = 0.4	(Lu et al., 1995)
Ligaments	*Exponential force-displacement curves*		(Rohlmann et al., 2006)

Table 3.1: Summary of the mechanical properties used in the model

3.2.3 Loading and Boundary Conditions

Model predictions were calculated under pure moment loading for all cases reported herein. Moments up to 7.5 Nm were applied at the superior endplate of L1 in three principal loading directions (flexion (+)/extension (-), unilateral bending and uniaxial rotation) while the model was kinematically constrained at the inferior endplate of L5. Facet joint articulation in all levels was simulated as a finite sliding contact problem with no friction between cartilaginous surfaces.

Since the disc maintains a homeostatic, non-zero stress/strain condition in its resting, reference configuration, the nucleus was pressurized by inducing positive (expansive) isotropic volumetric strain (using the *THERMAL STRAIN option) on the corresponding nodes at the beginning of each analysis. Consequently, the model predictions were non-zero when no load was applied, and therefore, the "change" in each parameter of interest with respect to this no load reference state was reported. At the end of pressurization, the mean of the nodal predictions (of the volumetric component of the stress tensor) in the nuclei pulposi was 0.11 MPa, consistent with previously reported in vivo nuclear pressure measurements taken in the transverse lying position (Wilke, et al., 1999). All solutions were obtained using ABAQUS Standard (ver. 6.8, SIMULIA, Providence, RI) running on a high-performance workstation (Model: xw8400, Hewlett-Packard Company, Palo Alto, CA).

	ELEMENTS	NODES	DEGREES OF FREEDOM
LOW	44422	54178	158187
MEDIUM	88536	101069	300000
HIGH	184646	205401	605154

Table 3.2: Summary of changes in mesh density

3.2.4 Mesh Convergence

In order to ensure that the predictions of the model were unaffected by the mesh resolution, mesh refinement was verified. By modification of the mesh seeds at each boundary block, the total degrees of freedom in the model were varied to yield three separate mesh resolutions (Table 3.2). The number of nodes, elements and total degrees of freedom were approximately doubled at each consecutive step. According to the densities of each mesh, the three corresponding models were labeled as LOW, MEDIUM and HIGH (Figure 3.1).

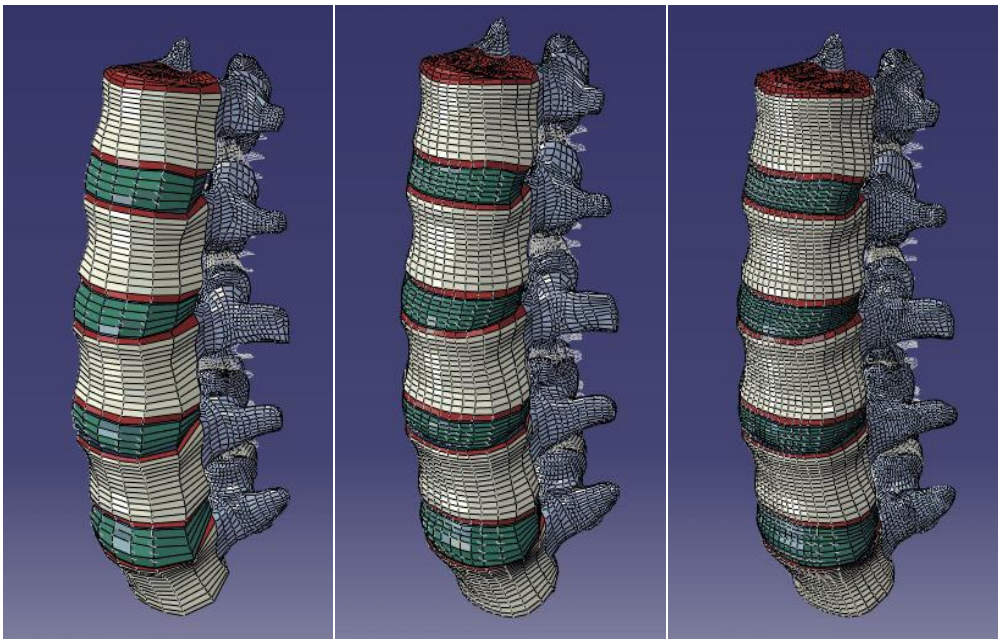

Figure 3.1: The model with three mesh resolutions: (left) LOW, (middle) MEDIUM and (right) HIGH.

Under pure moment loading in the three principal rotations (flexion/extension, lateral bending and axial rotation) the mean strain energy density (SED) (defined as strain energy per instantaneous volume) corresponding to each constituent tissue was calculated. The predictions with three different mesh resolutions were compared, and those within $\pm$ % 5 of the HIGH results were considered converged.

In order to eliminate indirect effects of load sharing between the anterior and posterior columns (which becomes a variable when the mesh resolution is changed), all models were initially tested without the ligaments and posterior elements and SED predictions were reported. Full models were subsequently tested in order to evaluate the final range of motion predictions.

3.2.5 Validation

The predictions of the converged (MEDIUM resolution) model were validated through comparison with data from previously conducted experiments (Ayturk 2007) and the available literature. The following details the specific parameter predictions that were included in this validation procedure:

1. *Range of motion (ROM)*

The kinematic predictions of the converged model were compared with the results of an experimental study from the literature (Panjabi, et al., 1994), where specimens were tested under pure-moment loading in the flexion/extension, lateral bending and axial rotation directions.

2. *Intradiscal nuclear pressure (IDP)*

The intradiscal pressure predictions of the model in flexion and extension were compared to available experimental data. The pressure measurements from two studies (Ayturk, 2007) (Heuer, et al., 2007) were gathered, where the nuclear pressure changes under pure moment loading in flexion and extension were quantified. The predictions of the model at the L23 and L34 levels were compared with experimental data under 3 Nm, and predictions at L45 level were compared with experimental data under 7.5 Nm.

3. *Maximum principal strain on anterolateral cortical bone*

Maximum principal strain predictions on the anterolateral surfaces of L2, L3 and L4 vertebral bodies were quantified under 3Nm of pure moment loading and compared with experimental data (Ayturk, 2007)(n=6). The predictions at 16 nodes (that formed an approximately 7x12 mm rectangular region) were averaged, and treated as the model outcome.

4. Facet force transmission under extension and axial rotation

Facet force transmission predictions under extension and axial rotation were compared with experimental data from the literature (Wilson, et al., 2006) (Niosi, et al., 2008) (Sawa, et al., 2008).

5. Deformation in the anterior longitudinal ligament

The deformation predictions for the anterior longitudinal ligament between levels L2 and L3 in extension were compared with experimental measurements (Ayturk, 2007) (n=6).

3.3 RESULTS

3.3.1 Mesh Convergence

Percentage changes between LOW and MEDIUM resolutions and HIGH resolution mesh are summarized in Figure 3.2. Changes in mesh density had the largest impact on the FE predictions under axial rotation loading. Specifically, the differences between SED predictions of LOW and HIGH resolution models for cartilaginous and bony endplates were 72 % and 39 %, respectively. The loading case least affected by the change in mesh resolution was flexion. In all loading scenarios, the largest differences between the predictions of the LOW and MEDIUM resolution meshes were observed in the cartilaginous and bony endplates. However, no

consistent difference between the convergence behaviors of soft and hard tissues was observed. ROM did not correlate with the overall SED predictions, and was not found to be an indicator of mechanical prediction convergence. The difference between the predictions of the MEDIUM and HIGH resolution models was less than 5 % in most cases. Therefore the MEDIUM resolution mesh was considered converged.

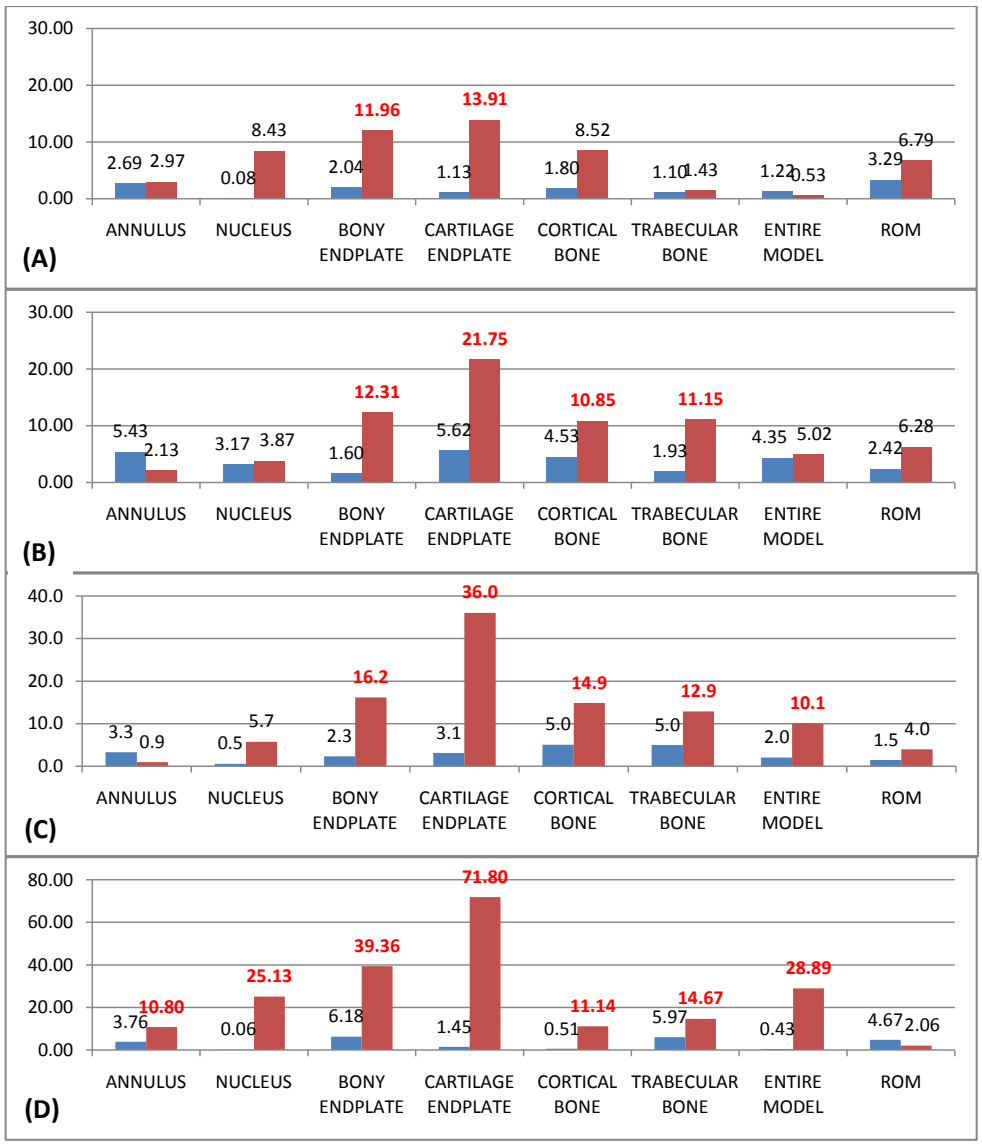

Figure 3.2: Summary of convergence data. (A), (B), (C) and (D) indicate loading in flexion, extension, lateral bending and axial rotation, respectively. Percentile differences of strain energy predictions of low and medium resolution models (red and blue colors, respectively) under 7.5 Nm of pure moment with respect to the high resolution model are given. Values greater than 10% are highlighted with red color.

3.3.2 Validation

1. ROM

The nonlinearity of the moment –rotation relationship in all levels was accurately simulated. The ROM predictions were generally within one standard deviation of the sample mean for all levels and loading directions throughout the entire loading regimes (Figure 3.3 and Figure 3.4). ROM magnitudes under 7.5 Nm pure-moment loading in all directions are summarized in Table 3.3. Among all loading scenarios, the greatest ROM was predicted in flexion while the least was predicted under axial rotation. Furthermore, the L4/L5 level was the most flexible level under all loading regimes in comparison to the other spinal levels.

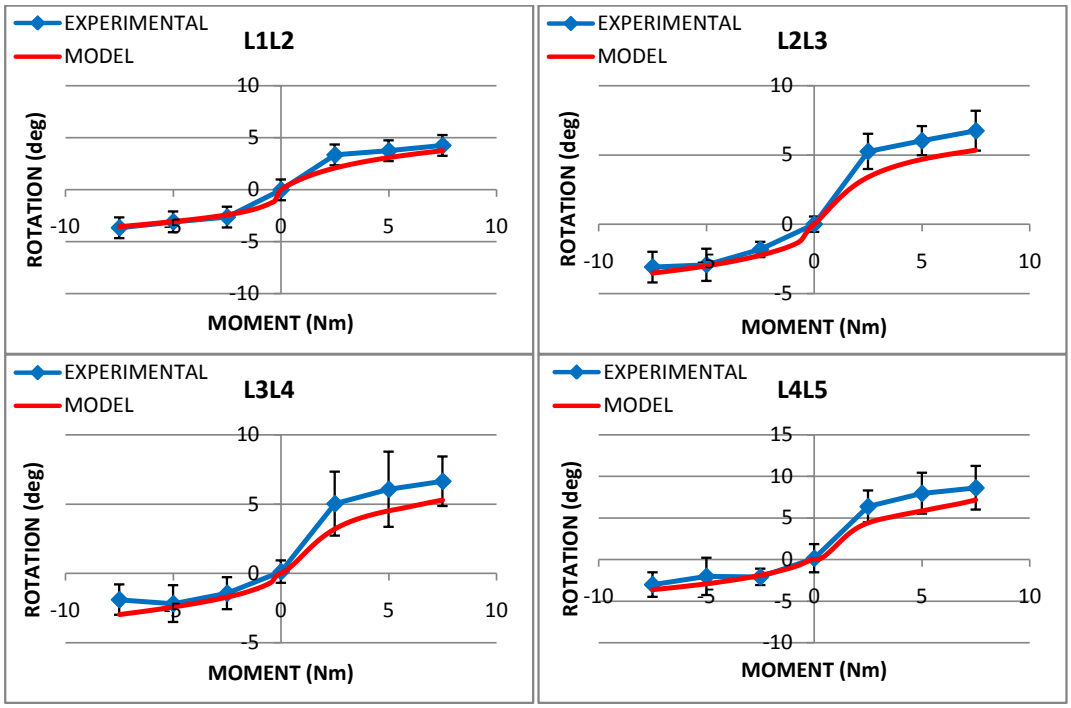

Figure 3.3: The intersegmental rotation predictions of the model compared with experimental data under flexion (+) and extension (-) loading. The experimental data represent the mean rotations and the error bars indicate one standard deviation.

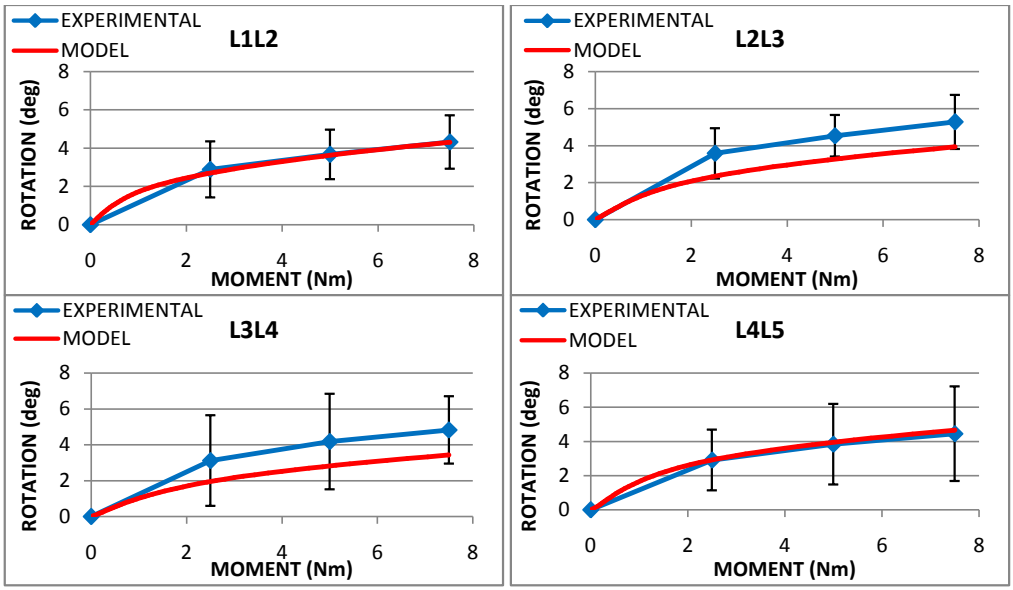

Figure 3.4: The intersegmental rotation predictions of the model compared with experimental data under lateral bending. The experimental data represent the mean rotations and the error bars indicate one standard deviation.

	L1/L2	L2/L3	L3/L4	L4/L5	L1/L5
Flexion/Extension	7.31	8.89	8.25	10.81	35.27
Unilateral Bending	4.32	3.93	3.43	4.66	16.34
Uniaxial Rotation	2.72	2.83	2.27	3.60	11.41

Table 3.3: ROM predictions under 7.5 Nm pure-moment loading in three directions. All values are in degrees.

2. IDP

The intradiscal pressure predictions of the model were in good agreement with the experimental data (Figure 3.5). The mean of the pressure predictions for all levels was 114 KPa at the resting position. 568 and 498 KPa mean pressures were predicted under 7.5 Nm of loading in flexion and extension, respectively. Furthermore, the IDP predictions in flexion were greater than those in extension.

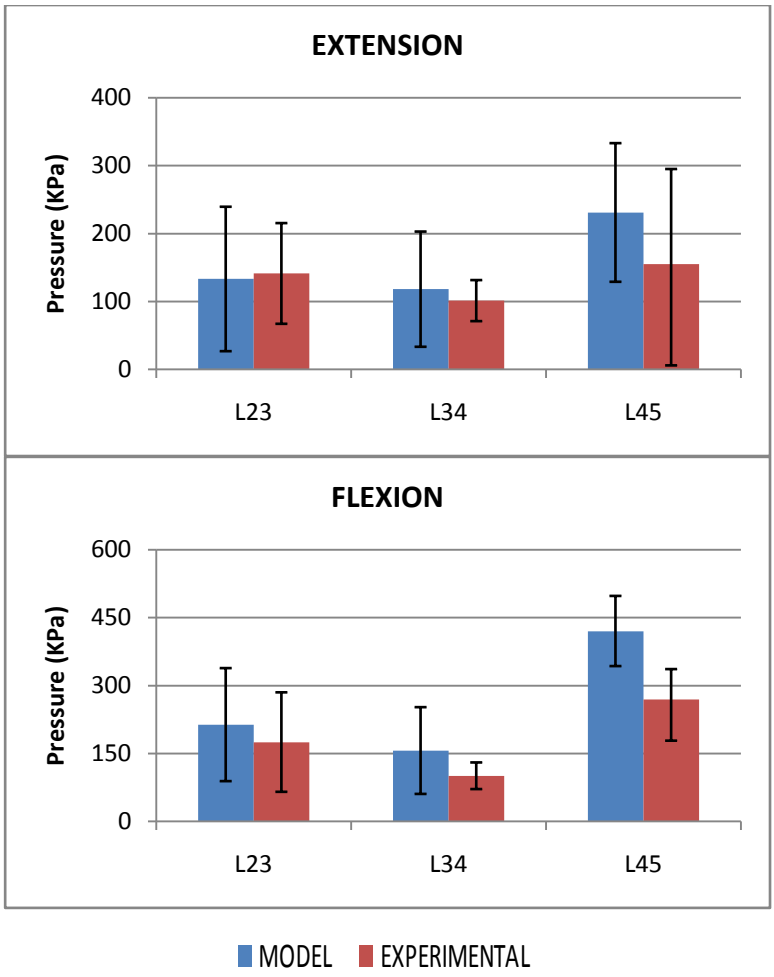

Figure 3.5: Intradiscal nuclear pressure predictions of the model at levels L23, L34 and L45 compared with experimental data (Ayturk 2007) (Heuer F 2007). The predictions for the L45 level were quantified under 7.5 Nm of pure moment loading while the L23 and L34 data were quantified under 3 Nm. "MODEL" indicates the nodal mean of the pressure predictions while the error bars indicate the standard deviation corresponding to this dataset. "EXPERIMENTAL" indicates the mean of the measurements from the tested specimens while the error bars indicate the corresponding standard deviation.

3. Maximum principal strain on anterolateral cortical bone

Strain predictions were generally in agreement with the experimental data (Figure 3.6). The mean anterolateral cortical strain predictions were 188, 193 and 72 microstrain at levels L2, L3 and L4, respectively, under axial rotation loading; and 101, 201 and 78 microstrain at levels L2, L3 and L4, respectively, under lateral bending. In lateral bending, the model predictions

underestimated the experimental mean, although these predictions remained within one standard deviation of the mean.

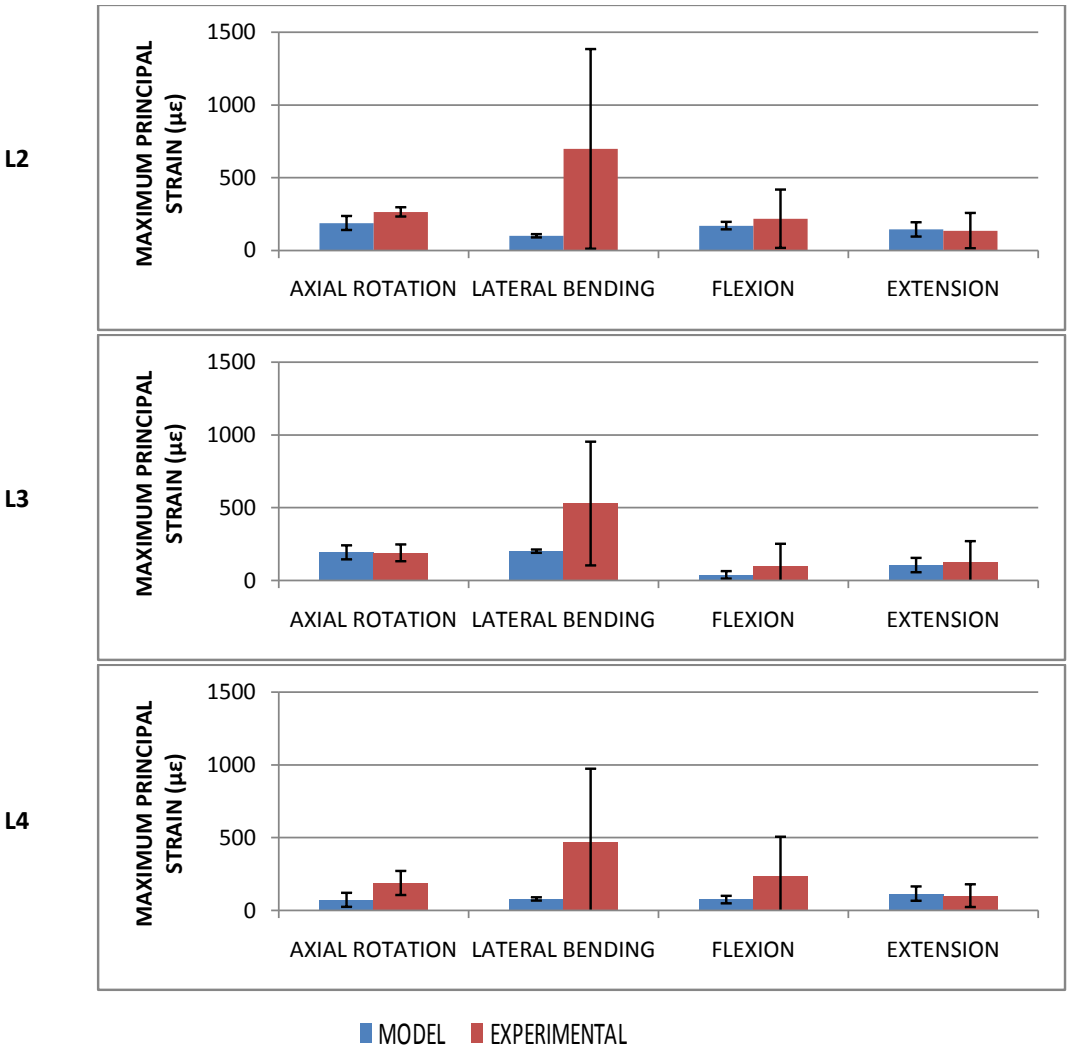

Figure 3.6: Anterolateral cortical bone strain predictions of the model under 3 Nm pure moment loading compared to experimental data (Ayturk 2007). "MODEL" indicates the mean of the model nodal predictions on the anterolateral surfaces while the error bars indicate the standard deviation of this dataset. "EXPERIMENTAL" indicates the mean of the measurements from a sample population and the error bars indicate the corresponding standard deviations.

4. Facet force transmission under extension and axial rotation

Facet force transmission predictions under extension and axial rotation were in good agreement with experimental data from the literature (Figure 3.7). The average force predictions in the facets of all levels were 44 and 86 N under extension and axial rotation, respectively. The facet force - applied moment relationship was observed to be approximately linear.

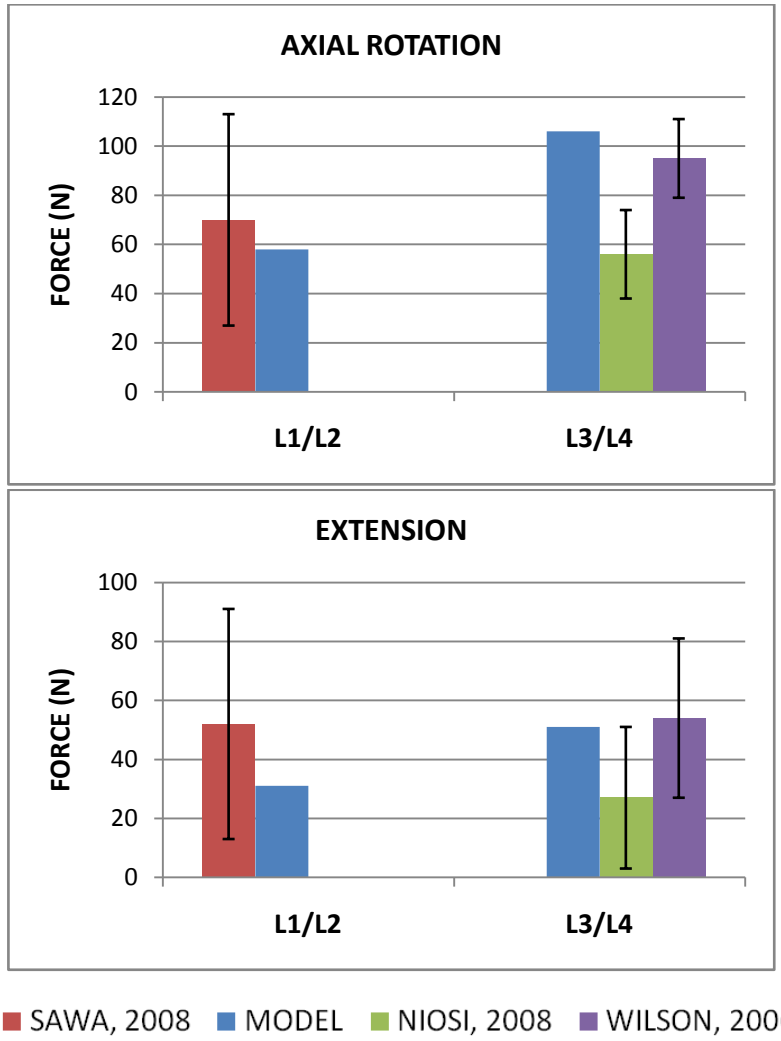

Figure 3.7: Facet force transmission predictions under 7.5 Nm of pure-moment loading in extension and axial rotation compared with experimental data (Sawa AG 2008) (W. D. Niosi CA 2008) (Wilson DC 2006).

5. Deformation in the anterior longitudinal ligament

The deformation predictions for the anterior longitudinal ligament between levels L2 and L3 were consistent with experimental measurements (Figure 3.8). The ALL at these levels supported tensile loads of 78 and 240 N under 3 and 7.5 Nm of pure-moment loading in extension, respectively. Furthermore, the ALL forces at all spinal levels were predicted to be higher than those forces transmitted through the facets. Flexion resulted in complete relaxation of the ALL at all levels, as the associated spring elements were placed in compression.

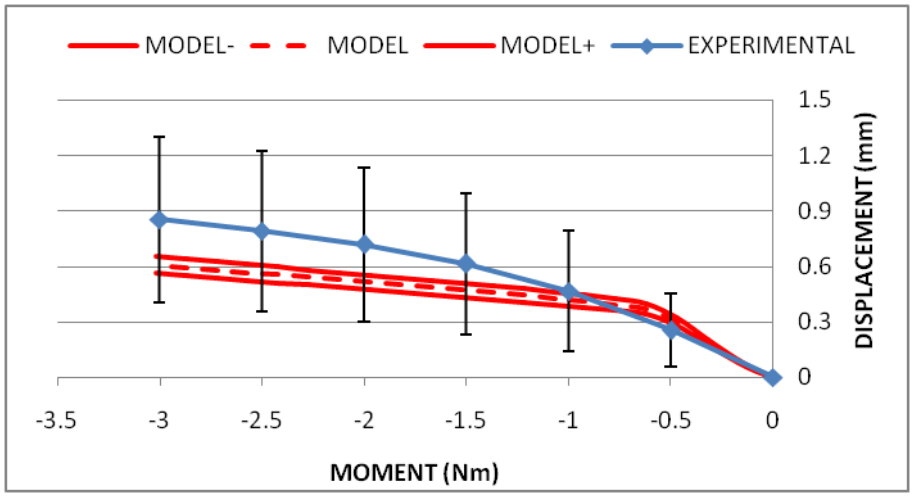

Figure 3.8: Anterior longitudinal ligament strain between levels L2 and L3. The model data were presented as mean (dashed line) and mean ± standard deviation (solid lines) of the predictions, whereas the experimental data were presented as mean (solid line) ± standard deviation of the sample population.

3.4 DISCUSSION

3.4.1 Mesh Convergence

SED predictions were most sensitive to changes in mesh resolution in lateral bending and axial rotation. Our results indicate that, the convergence behavior of finite element models of spine is highly direction-dependent. Among the loading conditions simulated, axial rotation appears to be "the worst case", therefore this particular loading mechanism should be

employed as a conservative criterion in spinal convergence studies. This may be due to the fact that the geometry of the vertebral column is highly heterogeneous and that axial rotation induces more local shear stresses (as opposed to normal stresses) altering the model's potential energy minimization. Furthermore, ROM was not specifically sensitive to changes in mesh density. The predicted percentage differences in all loading scenarios and motion levels corresponded to less than 1°. The differences between the sensitivity of internal energy and global displacement predictions is intuitive with respect to finite element modeling (Zienkiewicz, et al., 2000) (Morris, 2008) and yet the data presented herein show that convergence based solely on the kinematics/kinetics (such as ROM) or global stiffness predictions does not necessitate that convergence of other mechanical internal parameters (i.e. stress, strain, etc.) is satisfied.

Among all tissues, energy predictions for the bony and cartilaginous endplates were the most sensitive to changes in mesh resolution. Both of these tissues were consistently modeled with single-element-thickness in all meshes, therefore this particular result might be interpreted as the result of altering mesh density in the planar directions. Furthermore, the annulus fibrosus and nucleus pulposus tissues were found to be sensitive to changes in mesh resolution under axial rotation (Figure 3.2). The stresses generated on the intervertebral disc, and the alterations in these mechanical conditions as a result of disease or treatment are of high clinical interest, and therefore establishing the convergence behavior and validation of the model with respect to these stress predictions is critical. Our data indicate that the local shear loads can yield large deviations in the stress predictions if the intervertebral disc mesh is not converged, and therefore, the verification of the mesh refinement is a crucial step in the development of finite element models of spine. No consistent difference was observed between soft and hard tissue convergence behavior in the loading scenarios simulated here.

Geometric non-uniformities are known to have a negative effect on the convergence behavior of finite element models (Marks, et al., 1993) (Morris, 2008), specifically when the designated parameter is SED. Given the complex geometry of the posterior vertebral region, convergence of local stress predictions in this area should be specifically confirmed, in addition to employing the global criteria and methodology described here.

3.4.2 Validation

An extensive validation protocol was applied to ensure the accuracy of the model predictions. ROM prediction validity was established over the nonlinear range of 0-7.5Nm. This is particularly important when assessing the performance of prosthetic devices and the effect of degenerative changes due to potential alterations in the nonlinearity of the motion patterns. The work of Panjabi et al. alone was used as the basis of the validation effort outlined in this paper since the rotation response of the lumbar spine was documented under varying moments for all lumbar levels. The application of a 100 N compressive load was not simulated in this study, and we would anticipate that this produced slightly larger ranges of motion predictions than would be expected had the 100 N load been applied. Furthermore, the relative rotations were calculated based on the motion of the superior endplates of each vertebra, and the direct comparison of the experimental data to the model predictions had the underlying assumption that the vertebrae act as rigid bodies (with respect to the soft tissue structures) within the range of interest, an assumption that is implicit in any experimental study that uses stereophotogrammetry to calculate intervertebral rotations. Nevertheless, there is a wide range of "physiologic" ROM values documented in the literature, and the magnitudes of the values reported herein are in good agreement with them (Panjabi and White 1990) (Mimura, et al., 1994) (Noailly, et al., 2005) (Guan, et al., 2007). The coupled motion predictions of the model

under lateral bending and axial rotation were also found to be in good agreement with previously published data (Panjabi, et al., 1988).

Due to the large stress gradients in the nuclei pulposi, the mean and the variation of nodal predictions were reported for IDP. Our earlier work shows that the modeling approach presented here yields minimal stress variation throughout the nucleus pulposus under pure compression (Ayturk, et al., 2010), consistent with previously reported experimental data (Adams, McNally and Dolan 1996). Consequently, while the "hydrostatic pressure environment" assumption holds true for compression loading scenarios, our data suggest that this is not necessarily the case under pure-moment loading. To reach a more definitive conclusion, further experimental studies are warranted.

Our previous work (Chapter 2) and the nonlinearity of the ROM results presented herein show that the exponential force-displacement relationship is a good model to simulate spinal ligament mechanics. While it might not be possible to experimentally measure force, LVDT or strain gage based devices as well as stereophotogrammetry techniques may be employed in displacement measurement, which in turn can be used in the validation of computational model predictions. The results presented here are limited to measurements of ALL deformation; however, further experimentation under different types of loading can yield valuable information that can be utilized towards this goal.

Strain predictions in the anterolateral cortical surfaces of the vertebral bodies were in good agreement with experimental measurements, despite the relatively large variations in these measurements. Furthermore, under compressive loads alone, the strain predictions in the bony endplates (data not shown) were consistent with previously reported results (Frei, et al., 2001). Altogether, these results show that the vertebral geometry represented here and the

associated material models are capable of realistically simulating bony deformation in the lumbar spine.

The exact function of the facet joints and their contributions to spinal biomechanics are contemporary active research topics (Serhan, et al., 2007). Furthermore, the feasibility and reliability of the currently available means of force measurement continues to be debated (Wilson, et al., 2006) (Sawa, et al., 2008). Nevertheless, the force predictions reported herein were in agreement with previously reported experimental measurements, and show that the load sharing mechanism between the anterior and posterior columns was realistically simulated. Further predictions on contact pressure and area would require a very accurate representation of facet cartilage geometry.

This study had several limitations. The poroviscoelastic nature of the spinal tissues was omitted by assuming that all the loads were applied under quasi-static loading conditions, and that the individual tissue constituents were solid continua. The experimental data cited herein for the purpose of validation were also collected under similar loading conditions. Part of the data used for validation (IDP, ligament deformation and cortical bone strain) were collected under pure-moment loading up to 3 Nm, therefore the validation attempt was limited to this particular magnitude for the aforementioned parameters. Furthermore, predictions for variables other than ROM and ligament deformation were approximately linear throughout the reported loading ranges, therefore only the pointwise data corresponding to 7.5 Nm were presented. Lastly, the goal of this modeling endeavor was to simulate only the lumbar (L1-L5) spine, and hence, the sacrum and the lumbosacral disc were not included in this model. Future work will include caudal extension of the model to include these important mechanical and clinical structures of the spine. Moreover, relatively complex loading scenarios (Rohlmann, et al.,

2009) will also be investigated in order to evaluate the impact of individual muscle forces on spinal biomechanics *in vivo*.

3.5 CONCLUSION

A finite element model of the human lumbar spine was generated. Mesh refinement was achieved through convergence of SED predictions for each tissue constituent. The converged model was then validated based on ROM, IDP, bone strain, ligament (ALL) deformation and facet force predictions. Changes in mesh resolution most profoundly affected the mechanical predictions on the bony and cartilaginous endplates, as well as the intervertebral disc components under axial rotation. Mesh resolution had a minimal impact on ROM, as expected. The nonlinearity of the intersegmental ROM was accurately simulated for all levels, and the predictions for the aforementioned parameters were in good agreement with previously reported experimental data. The validated model can be utilized in studying the effects of degeneration on the lumbar spine biomechanics, as well as the contemporary treatment strategies.

REFERENCES

Adams, M., McNally, D., & Dolan, P. (1996). "Stress" Distributions Inside Intervertebral Discs. *J Bone Joint Surg [Br]* , 965-972.

Anderson, A., Ellis, B., & Weiss, J. (2007). Verification, Validation and Sensitivity Studies in Computational Biomechanics. *Computer Methods in Biomechanics and Biomedical Engineering* , 10:171-184.

Ayturk, U. (2007). *Development and validation of a three dimensional high resolution nonlinear finite element model of an L3/L4 funcitonal spinal unit, Master's Thesis.* Fort Collins, CO: Colorado State University.

Ayturk, U., Garcia, J., & Puttlitz, C. (2010). The Micromechanical Role of the Annulus Fibrosus Components Under Physiological Loading of the Lumbar Spine. *J Biomech Eng* , 132(6):061007.

Bogduk, N. (1999). *Clinical Anatomy of the Lumbar Spine and Sacrum.* London: Churchill Livingstone.

Crawford, R., Rosenberg, W., & Keaveny, T. (2003). Quantitative computed tomography based finite element models of the human lumbar vertebral body: effect of element size on stiffness, damage, and fracture strength predictions. *Journal of Biomechanical Engineering* , 434-8.

Dooris, A., Goel, V., Grosland, N., Gilbertson, L., & Wilder, D. (2001). Load sharing between anterior and posterior elements in a lumbar motion segment implanted with an artificial disc. *Spine* , E122-E129.

Eberlein, R., Holzapfel, G., & Frohlich, M. (2004). Multi-segment FEA of the human lumbar spine including the heterogeneity of the annulus fibrosus. *Computational Mechanics* , 147-63.

Eberlein, R., Holzapfel, G., & Schulze-Bauer, C. (2001). An anisotropic model for annulus tissue and enhanced finite element analyses of intact lumbar disc bodies. *Computer Methods in Biomechanics and Biomedical Engineering* , 209-230.

Elliott, D., & Setton, L. (2001). Anisotropic and inhomogeneous tensile behavior of the human anulus fibrosus: experimental measurement and material model predictions. *J Biomech Eng* , 256-263.

Frei, H., Oxland, T., Rathonyi, G., & Nolte, L. (2001). The effect of nucleotomy on lumbar spine mechanics in compression and shear loading. *Spine* , 26:2080-9.

Fujita, Y., Duncan, N., & Lotz, J. (1997). Radial tensile properties of the lumbar annulus fibrosus are site and degeneration dependent. *J Orthop Res* , 814-9.

Goel, V., Monroe, B., Gilbertson, L., & Brinckmann, P. (1995). Interlaminar shear stresses and laminae separation in a disc. Finite element analysis of the L3-L4 motion segment subjected to axial compressive loads. *Spine* , 20(6):689-98.

Guan, Y., Yoganandan, N., Moore, J., Pintar, F., Zhang, J., Maiman, D., et al. (2007). Moment-rotation responses of the human lumbosacral spinal column. *Journal of Biomechanics* , 1975-80.

Heuer, F., Schmidt, H., Claes, L., & Wilke, H. (2007). Stepwise reduction of functional spinal structures increase vertebral translation and intradiscal pressure. *J Biomech* , 795-803.

Heuer, F., Schmidt, H., Klezl, Z., Claes, L., & Wilke, H. (2007). Stepwise reduction of functional spinal structures increase range of motion and change lordosis angle. *Journal of Biomechanics* , 271-280.

Jones, A., & Wilcox, R. (2008). Finite element analysis of the spine: towards a framework of verification, validation and sensitivity analysis. *Med Eng Phys* , 30:1287-304.

Klisch, S., & Lotz, J. (1999). Application of a fiber-reinforced continuum theory to multiple deformations of the annulus fibrosus. *J Biomech* , 32(10):1027-1036.

Liebschner, M., Kopperdahl, D., Rosenberg, W., & Keaveny, T. (2003). Finite element modeling of the human thoracolumbar spine. *Spine* , 28:559-565.

Lu, Y., Hutton, W., & Gharpuray, V. (1996). Do bending, twisting, and diurnal fluid changes in the disc affect the propensity to prolapse? A viscoelastic finite element model. *Spine* , 2570-9.

Marks, L., & Gardner, T. (1993). The use of strain energy as a convergence criterion in the finite element modelling of bone and the effect of model geometry on stress convergence. *Journal of Biomedical Engineering* , 15-474,476.

Mimura, M., Panjabi, M., Oxland, T., Crisco, J., Yamamoto, I., & Vasavada, A. (1994). Disc degeneration affects the multidirectional flexibility of the lumbar spine. *Spine* , 1371-80.

Morris, A. (2008). A Practical Guide to Reliable Finite Element Modeling. In *Chap.4 What's Energy Got to Do with It?* (pp. 79-112). West Sussex, England: Wiley.

Natarajan, R., Williams, J., & Andersson, G. (2006). Modeling changes in intervertebral disc mechanics with degeneration. *Journal of Bone and Joint Surgery Supplement 2* , 36-40.

Niosi, C., Wilson, D., Zhu, Q., Keynan, O., Wilson, D., & Oxland, T. (2008). The effect of dynamic posterior stabilization on facet joint contact forces: an in vitro investigation. *Spine* , 19-26.

Noailly, J., Lacroix, D., & Planell, J. (2005). Finite element study of a novel intervertebral disc substitute. *Spine* , 2257-64.

Nolte, L., Panjabi, M., & Oxland, T. (1990). Biomechanical Properties of Lumbar Spinal Ligaments. In G. Heimke, U. Soltesz, & A. Lee, *Clinical Implant Materials* (pp. 663-668). Heidelberg: Elsevier.

Panjabi, M., & White, A. (1990). *Clinical Biomechanics of the Spine.* Philadelphia: Lippincott Williams & Wilkins.

Panjabi, M., Oxland, T., Yamamoto, I., & Crisco, J. (1994). Mechanical behavior of the human lumbar and lumbosacral spine as shown by three-dimensional load-displacement curves. *Journal of Bone and Joint Surgery* , 413-24.

Panjabi, M., Yamamoto, I., Oxland, T., & Crisco, J. (1988). How does posture affect coupling in the lumbar spine? . *Spine* , 14: 1002-1011.

Rohlmann, A., Zander, T., Rao, M., & Bergmann, G. (2009). Realistic loading conditions for upper body bending. . *J Biomech* , 42: 884-890.

Rohlmann, A., Zander, T., Schmidt, H., Wilke, H., & Bergmann, G. (2006). Analysis of the influence of disc degeneration on the mechanical behaviour of a lumbar motion segment using the finite element method. *J Biomech* , 2484-2490.

Sawa, A., & Crawford, N. (2008). The use of surface strain data and a neural networks solution method to determine lumbar facet joint loads during in vitro spine testing. *J Biomech* , 2647-53.

Schmidt, H., Heuer, F., Drumm, J., Klezl, Z., Claes, L., & Wilke, H. (2007). Application of a calibration method provides more realistic results for a finite element model of a lumbar spinal segment. *Clinical Biomechanics* , 377-84.

Serhan, H., Varnavas, G., Dooris, A., Patwadhan, A., & Tzermiadianos, M. (2007). Biomechanics of the posterior lumbar articulating elements. *Neurosurgical focus* , 22(1):E1.

Shirazi-Adl, S., Shrivastava, S., & Ahmed, A. (1984). Stress analysis of the lumbar disc-body unit in compression. A three-dimensional nonlinear finite element study. *Spine* , 120-34.

Spencer, A. (1984). Constitutive theory for strongly anisotropic solids. In Spencer, *Continuum Theory of the Mechanics of Fibre-Reinforced Composites* (pp. 1-32). New York: Springer Verlag.

Ueno, K., & Liu, Y. (1987). A three dimensional nonlinear finite element model of lumbar intervertebral joint in torsion. *J Biomech Eng* , 200-9.

Villaraga, M., Anderson, R., Hart, R., & Dinh, D. (1999). Contact analysis of a posterior cervical spine plate using a three-dimensional canine finite element model. *J Biomech Eng* , 121: 206-214.

Wagner, D., & Lotz, J. (2004). Theoretical model and experimental results for the nonlinear elastic behavior of human annulus fibrosus. *Journal of Orthopaedic Research* , 901-909.

Whyne, C., Hu, S., & Lotz, J. (2001). Parametric finite element analysis of vertebral bodies affected by tumors. *J Biomech* , 34:1317-24.

Wilke, H., Neef, P., Caimi, M., Hoogland, T., & Claes, L. (1999). New in vivo measurements of pressures in the intervertebral disc in daily life. *Spine* , 755-62.

Williams, J., Natarajan, R., & Andersson, G. (2007). Inclusion of regional poroelastic material properties better predicts biomechanical behavior of lumbar discs subjected to dynamic loading. *J Biomech* , 1981-7.

Wilson, D., Niosi, C., Zhu, Q., Oxland, T., & Wilson, D. (2006). Accuracy and repeatability of a new method for measuring facet loads in the lumbar spine. *J Biomech* , 348-53.

Womack, W., Woldtvedt, D., & Puttlitz, C. (2008). Lower cervical spine facet cartilage thickness mapping. *Osteoarthritis Cartilage* , 16: 1018-1023.

Zander, T., Rohlmann, A., Calisse, J., & Bergmann, G. (2001). Effect of bone graft characteristics on the mechanical behavior of the lumbar spine. *Clinical Biomechanics* , S73-S80.

Zhu, Q., Park, Y., Sjovold, S., Niosi, C., Wilson, D., Cripton, P., et al. (2008). Can extra-articular strains be used to measure facet contact forces in the lumbar spine? An in-vitro biomechanical study. *Proc Inst Mech Eng H* , 171-84.

Zienkiewicz, O., & Taylor, R. (2000). The Finite Element Method Volume 1 The Basis. In *Chap. 15 Adaptive Finite Element Refinement* (pp. 401-426). Woburn, MA: Butterworth-Heinemann.

CHAPTER 4:

Development of Orthotropic Continuum Models of Healthy and Degenerated Annulus Fibrosus Based on a Biaxial Testing Protocol

4.1 INTRODUCTION

Collageneous orthopaedic tissues commonly exhibit nonlinear and anisotropic mechanical behavior. The annulus fibrosus in particular owes its unique material behavior to the highly organized collagen fiber network embedded within its proteoglycan-rich matrix. The distribution of local fiber orientations is heterogeneous in the radial direction, ranging from 23° to 45° with respect to the horizontal plane from the external layers to the internal layers, respectively (Guerin, et al., 2006).

The anisotropic nature of the annulus makes the associated modeling endeavors challenging. A "hybrid geometry" approach was commonly employed in the early spinal finite element models, with discrete geometric representations of the ground substance and the fibers (Shirazi-Adl, et al., 1984) (Dooris, et al., 2001) (Zander, et al., 2001). These efforts were primarily focused on the simulation of spinal kinematics, rather than accurately representing the local mechanics of the intervertebral disc. More recent experimental studies quantified the mechanical behavior of the annulus fibrosus tissue in physiologically relevant loading directions, providing a basis for constitutive modeling attempts. The continuum modeling framework suggested by Spencer for specific applications of fiber-reinforced composites has typically been utilized to this end (Spencer, 1984). The invariant-based strain energy potentials can be decomposed into individual components of physiological relevance (potentials of the PG-rich matrix, tissue incompressibility, collagen fibers, etc.) (Wagner, et al., 2004) (Guerin HL, 2007) in order to simulate the nonlinear mechanical behavior of the annulus fibrosus.

The aforementioned continuum approach becomes particularly relevant when attempting to model the degenerative effects on the biomechanical behavior of the annulus fibrosus. Briefly, degenerative disc disease alters the morphology of the annulus through

increased breakdown of PG molecules, loss of hydration, reduction in Type I collagen content and organization. Previous modeling studies have related these structural changes to the mechanics of the tissue (O'Connell, et al., 2009), however, direct utilization of the continuum approach (based on experimental data) in spinal motion segment modeling has only been reported for the healthy condition (Eberlein, et al., 2001) (Ayturk, et al., 2010).

Degenerative disease has been shown to reduce the shear modulus (Iatridis, 1999) and failure stress (Acaroglu, et al., 1995) of the annulus fibrosus, while increasing its permeability and compressive modulus (Iatridis, et al., 1998). The mobility of spinal segments has been reported to typically increase during the earlier stages of the degenerative cascade (Mimura, et al., 1994) and decrease with increasing severity of the disease (Krismer, et al., 2000). To the best of our knowledge, these mechanical changes at the tissue and motion segment levels have not been rigorously related. However, the aforementioned continuum modeling framework, previously established in the literature, has the potential to be directly implemented in finite element models of the spine and provides a possible causational and investigational link between the microscopic and macroscopic mechanics of the intervertebral disc. A fundamental requirement of this application would be the computational stability of the developed material models, which may be satisfied by utilizing convex strain energy functions (i.e. functions with positive definite hessian matrices).

Material behavior characterization by using strain energy functions is possible through direct experimentation on the tissue of interest. Specifically, biaxial tension tests conducted under plane stress conditions provide extensive data that might also serve as a robust basis for validation purposes. While the plane stress assumption is a limitation of these particular protocols and associated modeling attempts, additional validation tests in out-of-plane

directions may extend the utility of these models to three dimensions (Holzapfel, et al., 2009). The biaxial testing procedure was initially established via modeling of cardiovascular tissues through numerous studies (Sacks, et al., 2003), and more recently has been extended to include the annulus fibrosus (Bass, et al., 2004). Conducting a biaxial testing protocol on healthy and degenerated annulus fibrosus tissue has the potential to generate a large enough dataset (which will include stress-strain data collected under numerous physiologically-relevant loading conditions) that is necessary for the development of relevant continuum models.

Therefore, the objective of this study was to generate a strain energy function that is capable of simulating the mechanical behavior of healthy and degenerated human annulus fibrosus. Thus, the specific aims were:

(1) To develop an experimental dataset by performing uniaxial and biaxial tension tests on healthy and degenerated annulus fibrosus tissues;

(2) To develop material models (which satisfy the computational stability requirements of large scale finite element applications) of these tissues by fitting a strain energy function to the generated data, and to determine if significant differences in material parameters exist between the healthy and degenerated tissues.

4.2 METHODS

4.2.1 Specimen Preparation

A total of 15 intervertebral discs were harvested from six fresh-frozen cadaveric spines. These tissues were scanned using magnetic resonance imaging (MRI). The resultant images were graded according to the Thompson degeneration scale (Thompson, et al., 1990) by a practicing orthopaedic spine surgeon (Dr. Vikas Patel, Associate Professor, University of Colorado, Denver),

and the discs were grouped as either healthy (Grades I-II, n=7) or degenerated (Grades III-IV, n=8) (Figure 4.1). Two specimens were extracted from each disc for biaxial testing in the axial-circumferential directions and uniaxial testing in the radial direction. Rectangular-shaped specimens (2mm thickness) were dissected from the outer anterolateral layers (in the circumferential direction, 6mm x 11mm) and anterior region (in the radial direction, 7mm x 8mm) of the annuli fibrosi with a diamond-bladed band saw (Model:30, Exakt Advanced Technologies, Germany) for biaxial and uniaxial mechanical testing, respectively (Figure 4.2). All specimens were evaluated to confirm that no macroscopic abnormalities (including tears and delamination of layers) that could alter the mechanical behavior were present. In order to account for swelling effects upon thawing and saline absorption, the thickness of each sample was additionally measured *post hoc* by taking digital images of diagonal cross-sections with a microscope (Stereomaster, Fisher Scientific, Waltham, MA). The resultant images were processed with ImageJ (NIH, Bethesda, MD) (Figure 4.3), and the mean thickness was quantified (2.3 $\pm$ 0.4 mm for biaxial samples and 2.4 $\pm$ 0.2 mm for uniaxial samples) using pixel-based coordinate data.

Figure 4.1: Sagittal MR images of representative healthy (left) and degenerated (right) discs.

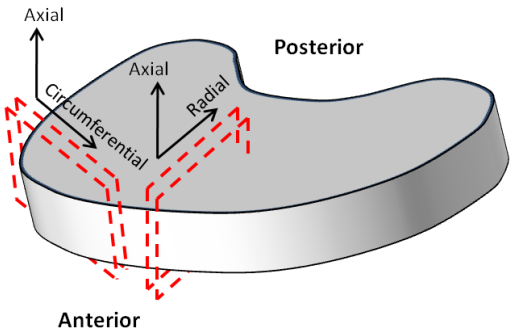

Figure 4.2: The specimen dissection orientations for the uniaxial and biaxial experiments.

4.2.2 Mechanical Testing

The biaxial samples were firmly sutured at all four edges (4-0 suture, monofilament, Surgipro II, Syneture, Mansfield, MA) and positioned in a custom-built biaxial testing system. Four markers were created by staining the surface of each specimen with black ink, in order to form an approximately square-shaped grid. Hydration was maintained by keeping the specimens on the surface of a saline-filled pool throughout the entire experiment. Pilot experiments identified the target stretch ratio to be 1.1 (deformation rate was 0.1mm/sec in the circumferential direction, and the rate in the axial direction was set to yield simultaneous loading) while the maximum allowable Lagrangian stress was set to be 0.7 MPa. All specimens were tested in four biaxial loading configurations, with the ratio of nominal engineering strains in the axial-circumferential directions being equal to 1-0, 0-1, 1-1 and 2-1 (Sacks, et al., 1993). In order to establish the reference state, specimens were first pre-loaded to 0.2 N in both directions and allowed to relax for 15 minutes prior to each test. Then, five cycles of preconditioning were applied to each sample, and the load/deformation data were collected on the last cycle. A 30 minute relaxation period was established between the application of each loading condition,

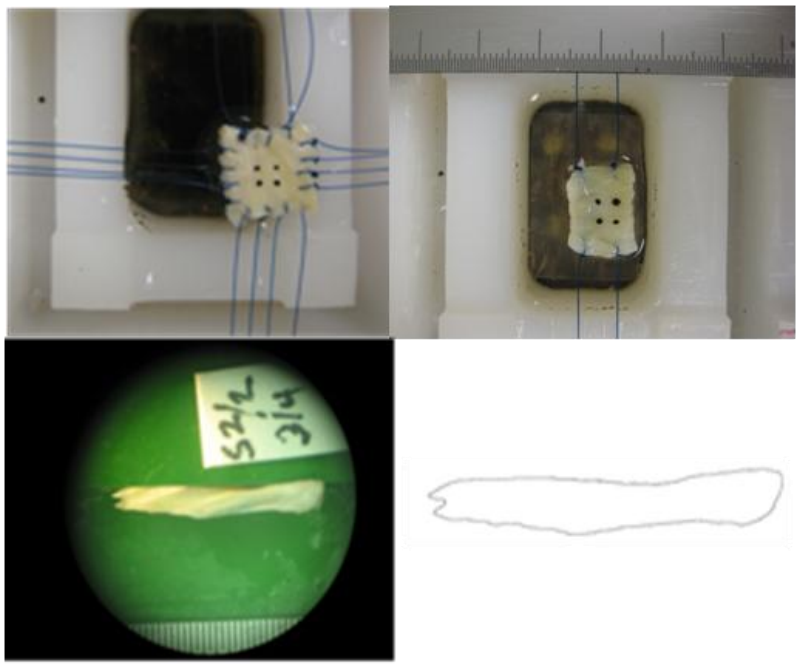

Figure 4.3: A biaxial sample being tested in circumferential and axial directions (left), diagonal cross-section of the specimen (middle) and the isolated image used for thickness quantification (right).

and this protocol was repeated until all loading scenarios were completed.

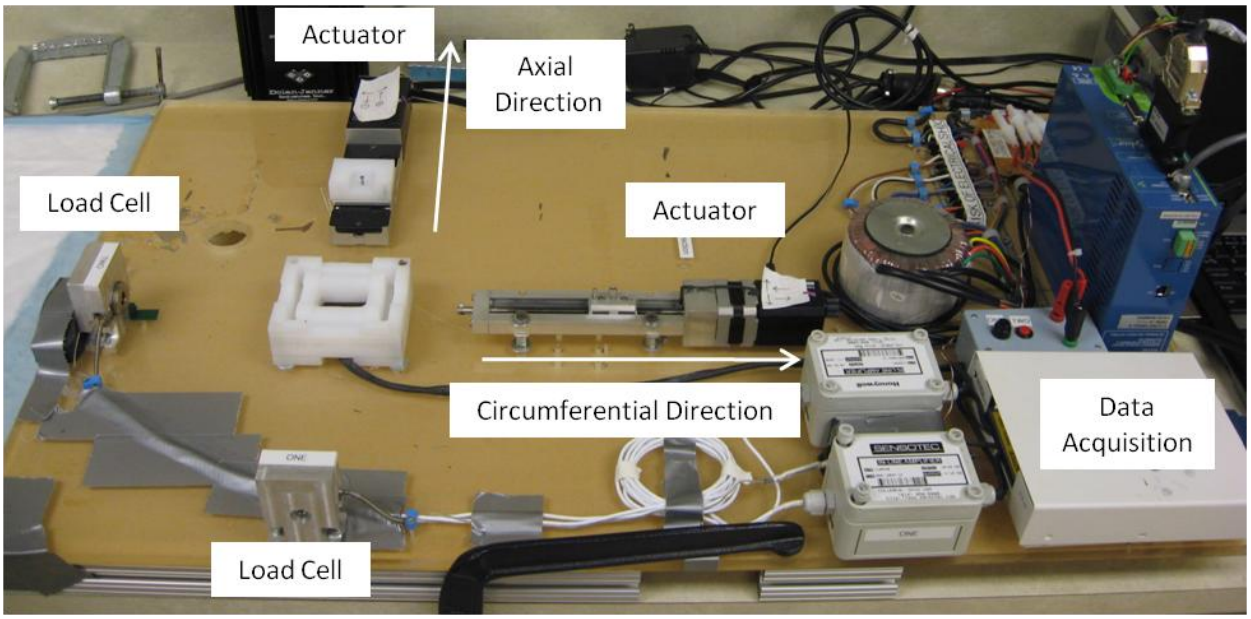

Figure 4.4: The biaxial testing system utilized in the tension experiments.

The applied loads were measured with two load cells (10lb range, Model 31, Honeywell, Columbus, OH), positioned in the planar testing fixture (Figure 4.4) in line with the axial and circumferential directions. The Lagrangian stress (T) was calculated by dividing the measured force by the undeformed cross-sectional area (defined as the product of measured thickness and the width normal to the loading direction), and later transformed to the Cauchy stress (σ) (Sacks, et al., 2003):

$$T = \frac{P}{l\,t} \qquad \sigma = F\,T \tag{4.1}$$

where P represents the measured force, l and t represents the width and thickness of the sample, respectively, and F represents the deformation gradient (see below). A digital camera (resolution = 7.1 MP, Canon PowerShot A560, Lake Success, NY) positioned above the specimen optically recorded the deformation of the specimen surface, and the corresponding digital

images were processed with a custom-written tracking code that quantified the displacement of the four markers (resolution ~ 2.5 μm/pixel). Principal stretches were calculated based on the aforementioned displacements wherein the shear strain was assumed to be negligible (Holzapfel, et al., 2009). Thus, the deformation map was defined as:

$$x_1 = \lambda_1 X_1 + K_1 X_2 \qquad x_2 = \lambda_2 X_2 + K_2 X_1 \qquad x_3 = \lambda_3 X_3 \qquad (4.2)$$

where x_n and X_n represents the position vectors in the deformed and undeformed configurations, respectively, and λ_n represents the stretch ratios in the principal directions. Due to the zero-shear assumption ($K_n = 0$), the deformation gradient is simplified:

$$F = \begin{bmatrix} \lambda_1 & & \\ & \lambda_2 & \\ & & \lambda_3 \end{bmatrix} \qquad (4.3)$$

The displacement measurements and the differentiation of Eq. 4.1 yielded the in-plane stretch ratios. The out-of-plane stretch ratio was calculated by assuming incompressibility of the tissue:

$$J = \det(F) = 1 \qquad \lambda_3 = \frac{J}{\lambda_1 \lambda_2} \qquad (4.4)$$

The calculated principal stretch ratios were paired with the corresponding Cauchy stress measurements and used for constitutive modeling and data fitting. The uniaxial samples were tested using the aforementioned protocol, by being loaded solely in the radial direction with a target stretch ratio equal to 1.4.

4.2.3 Constitutive Modeling

A modified version of a previously developed anisotropic strain energy function (Gasser, et al., 2006) was utilized for the constitutive modeling efforts, where the total energy density

was the sum of the matrix (W_{matrix}) and fiber (W_{fiber}) terms (with the strain invariants I_1, I_4 and I_6 being the independent variables (Spencer, 1984)):

$$I_1 = tr(C) \qquad I_4 = a_0 C a_0 \qquad I_6 = b_0 C b_0 \tag{4.5}$$

$$W = W_{matrix} + W_{fiber} \tag{4.6}$$

A second-order, reduced-polynomial function (Eq. 4.7) was chosen to model the matrix term, due to its predictive capability in simulating the nonlinear tensile behavior of the samples in the radial direction and its computational stability within the stretch magnitudes of interest (less than 1.5 stretch ratio):

$$W_{matrix} = C_{10}(I_1 - 3) + C_{20}(I_1 - 3)^2 \tag{4.7}$$

By definition, the fiber component induces an exponential increase in the stress predictions, however higher values of κ (the fiber dispersion parameter, defined between 0 and 0.33 (Gasser, et al., 2006)) simulate a reduced level of organization in the collagen network and lead to smaller stress predictions for the fiber component:

$$W_{fiber} = \frac{k_1}{2k_2} \sum_{\alpha=4,6} (e^{k_2[(1-3\kappa)(I_\alpha - 1) + \kappa(I_1 - 3)]^2} - 1) \tag{4.8}$$

k_1 and k_2 on the other hand, represent the baseline stiffness and the nonlinearity of the collagen fiber behavior, respectively. Both tissues were modeled as incompressible (as indicated in the previous section (Eq. 4.4)). The theoretical Cauchy stress was calculated by differentiating the total energy density (W) by the right-Cauchy-Green strain tensor (C), and applying the appropriate transformation (Holzapfel, et al., 2009) (Holzapfel, 2000):

$$\sigma = 2J^{-1} F^T \frac{\partial W}{\partial C} F \tag{4.9}$$

Finally, the Cauchy stress components (in a condensed form) in the principal directions are expressed as:

$$\sigma_1 = 2\frac{\partial W}{\partial I_1}\left({\lambda_1}^2 - {\lambda_3}^2\right) + 2\frac{\partial W}{\partial I_4}(cos\theta)^2{\lambda_1}^2 + 2\frac{\partial W}{\partial I_6}(sin\theta)^2{\lambda_1}^2 \qquad (4.10)$$

$$\sigma_2 = 2\frac{\partial W}{\partial I_1}\left({\lambda_2}^2 - {\lambda_3}^2\right) + 2\frac{\partial W}{\partial I_4}(sin\theta)^2{\lambda_2}^2 + 2\frac{\partial W}{\partial I_6}(cos\theta)^2{\lambda_2}^2 \qquad (4.11)$$

with the subscripts 1 and 2 corresponding to the axial and circumferential directions, respectively. The mechanical contribution of the fiber term in the radial direction was assumed to be negligible, and consequently the coefficients C_{10} and C_{20} were optimized based on the uniaxial experimental data. The coefficients k_1, k_2 and κ associated with the fiber term, were fit based on the stress/stretch data compiled with biaxial testing. All fitting procedures were performed with the *fmincon* function in MATLAB (Mathworks, Natick, MA) through minimization of the sum of squared errors in the stress predictions. The pooled results from the tests on healthy and degenerated tissue were compared with a two-tailed student's t-test, with significance set at $p<0.05$ (SigmaStat ver 3.1.1, Systat Software, Inc., Chicago, IL). Normality was established for the k_1 and k_2 parameters with log transformations.

4.3 RESULTS

Both healthy and degenerated samples demonstrated a nonlinear stress-strain response in the uniaxial loading experiments (Figure 4.5). Increasing the strain in the circumferential direction from 0-1 to 2-1 loading configurations did not progressively lead to a stiffer response in the axial direction. The mean Pearson's correlation coefficients for the uniaxial fitting protocols were 0.99 and 0.95 for the degenerated and healthy specimens, respectively. For the biaxial protocols, specifically in one dimensional circumferential (0-1) and axial (1-0) loading, the

mean correlation coefficients were 0.97 and 0.79 for the healthy specimens, and 0.89 and 0.81 for the degenerated specimens, respectively.

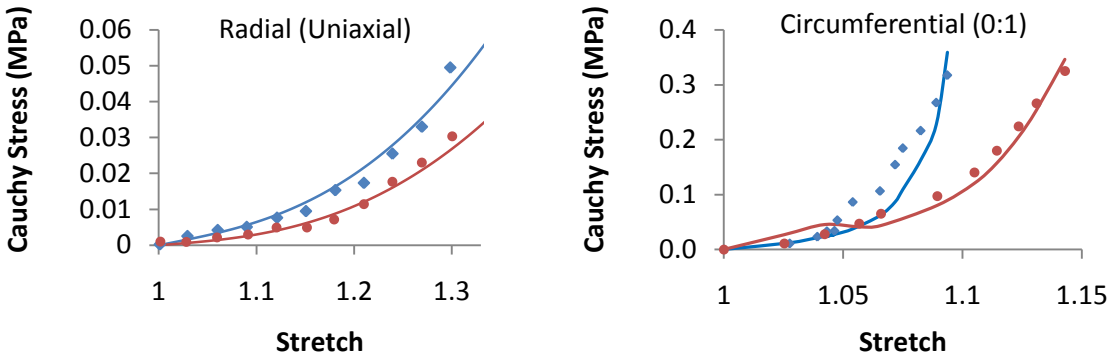

Figure 4.5: Typical stress measurements from uniaxial (left) and biaxial (right) tests on healthy and degenerated samples. Solid lines represent model fits (blue: healthy, red: degenerated).

Among the optimized coefficients, the healthy (Figure 4.6) and degenerated (Figure 4.7) groups yielded significant differences with respect to k_2 ($p=0.013$) and the fiber dispersion parameter (κ) ($p=0.027$) (Table 4.1). Specifically, the mean stress measurements in the uniaxial tests yielded slightly more compliant results for the degenerated samples, however, no significant differences were found for C_{10} ($p=0.221$) or C_{20} ($p=0.446$). Healthy specimens were typically more compliant under axial (1-0) loading and stiffer under circumferential loading (0-1) than degenerated specimens (Figure 4.5), but this did not yield significant differences in the k_1 parameter ($p=0.102$) (Table 4.1).

	C_{10}	C_{20}	k_1	k_2*	κ*
Healthy	0.0154 (0.0146)	0.0743 (0.0612)	2.05 (1.76)	86.53 (149.12)	0.113 (0.111)
Degenerated	0.0100 (0.0083)	0.0695 (0.0612)	3.12 (1.87)	179.42 (152.82)	0.245 (0.052)

Table 4.1: The optimized coefficients for both groups. Data represent mean (stdev) values, * indicates statistical significance ($p<0.05$). C_{10}, C_{20} and k_1 are in MPa, and k_2 and κ are unitless.

4.4 DISCUSSION

A single orthotropic continuum model applied to both degenerated and healthy annulus fibrosus tissue has been developed in this study. The morphology-related changes in the mechanics of the tissue have been reported previously, and similar modeling efforts attributed these alterations to specific components within the annulus. One of the aims of this particular study was to extend the aforementioned modeling efforts by employing a convex strain energy function, with the potential of being implemented in a large-scale finite element model of the intervertebral disc.

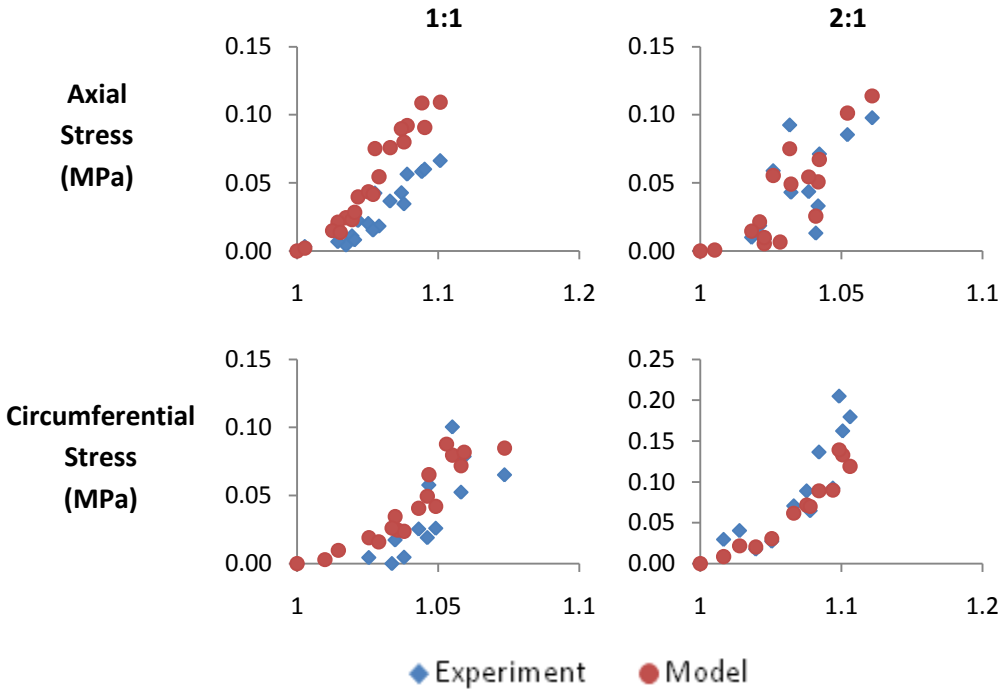

Figure 4.6: Model predictions and experimental stress measurements for a particular healthy sample in 1:1 and 2:1 (axial:circumferential) loading conditions.

The biaxial experiments yielded results similar to what's been previously reported (O'Connell, et al., 2009); particularly a typical increase and reduction in stress measurements in axial (1-0) and circumferential loading (0-1) as a result of degeneration, respectively. These patterns were manifested in the optimization results as significant increases in k_2 and κ due to

degeneration (Figures 4.5, 4.6 and 4.7). The C_{10} and C_{20} coefficients were optimized based on the uniaxial tension tests performed on the samples extracted in the radial direction. The assumption that the fiber component does not contribute to tensile load bearing in the radial direction has been commonly repeated in similar modeling studies in the literature. There are mixed reports with respect to the effect of degeneration on the elastic properties of annulus in the radial direction, with some studies indicating significant differences (O'Connell, et al., 2009) (Smith, et al., 2008) while others have reported no significant effects (Acaroglu, et al., 1995) (Fujita, et al., 1997). The current study did not find any differences in the material coefficients due to degeneration. Fujita et al. tested the largest number of specimens (n=183) among all the studies cited here, and noted that the differences in radial mechanical behavior was only evident when the specimens were extracted from the middle layers of the anterior region of the annulus fibrosus. This might explain the non-significant outcome of our experiments and previously reported data, wherein the sample pools were relatively limited.

The increase in κ was particularly relevant to the changes in the microstructure, as it is an indicator of the uniformity of fiber orientations throughout the modeled continuum. A detailed description of the effects of variation in dispersion on stress and energy predictions is published elsewhere (Gasser, et al., 2006). Briefly, within this particular modeling framework, increased dispersion reduces the stress and energy generation due to fiber stretch (Eq. 4.2). On the other hand, the increase in k_2 results in higher nonlinearity in the fibers' stress-stretch mechanical behavior. While the changes in κ yield a more compliant response at relatively small deformations (0:1), the increase in k_2 demonstrates the generation of higher stresses at large deformations (1:0). Thus, our results indicate that **degeneration produces *increased dispersion* in the collagen fiber orientation and an associated increase in anisotropy of the nonlinearity**

with regard to the annulus' mechanical behavior. Based upon these findings, we postulate that this "mechanical disorganization" may be the leading contributing factor to the biomechanical incompetence of the annulus fibrosus (and the intervertebral disc) at large with degeneration.

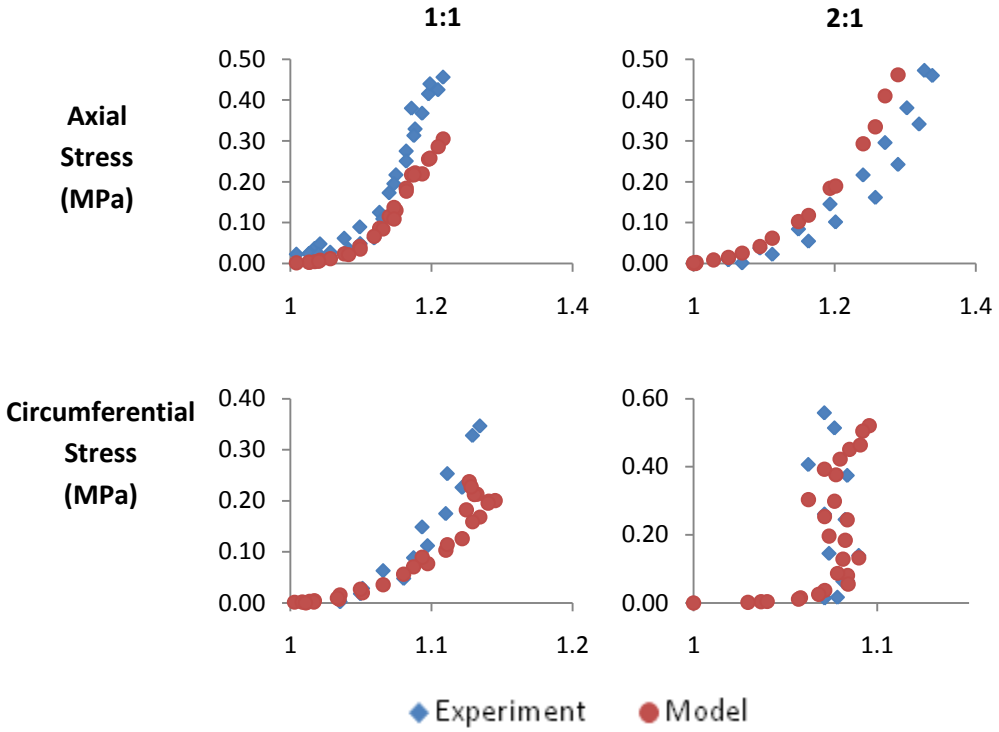

Figure 4.7: Model predictions and experimental stress measurements for a particular degenerated sample in 1:1 and 2:1 (axial:circumferential) loading conditions.

The superposition of discrete energy terms (such as matrix and fiber in this case) in order to formulate the mechanical behavior of collageneous soft tissues is quite common (Sacks, et al., 2003) (Wagner, et al., 2004) (Guerin, et al., 2007). Furthermore, the fiber behavior is typically represented as an exponential function, due to the accurate representation of the nonlinear behavior of the collagen (Weiss, et al., 1996). In comparison to previous reports of the fiber component coefficients (k_1 and k_2), the mean values determined for these parameters in this study were greater in the current study for both groups (Table 4.1). However, these differences are most likely due to the inclusion of a dispersion effect in our model and the

exclusion of an explicit fiber-matrix interaction component. The latter typically represents the shear contribution in the modeled continuum, and is not included in the present study in order to simplify the implementation of the strain energy formulation. Consequently, in comparison to previous work in the literature, the fiber component predictions in the current study may be regarded as the "lumped" sum of the fiber and the fiber-matrix interaction effects.

One of the important outcomes of this study is that the developed strain energy models may be implemented in larger scale finite element models of the spine in order to assess the biomechanical effects of degenerative disc disease on spinal motion segments. These applications would still include the inherent continuum assumption regarding the tissue microstructure. However, individual coefficients corresponding to the matrix or fiber components as well as fiber orientation may be modified depending on the specific region of the annulus that is being modeled within the intervertebral disc. This approach may more accurately represent the known spatial heterogeneity of the annulus.

4.5 CONCLUSION

In this work, two orthotropic continuum models of healthy and degenerated human annulus fibrosus were generated. Significant differences in the nonlinearity and dispersion of collagen fibers were found between two groups. The employed strain energy function was previously shown to be unconditionally convex, which is a requirement in order to achieve computational stability (Gasser, et al., 2006). Therefore, future work will focus on the implementation of our results into a large-scale finite element model, and subsequently, investigation of the effects of disc degeneration at the motion-segment level.

ACKNOWLEDGEMENTS

Mr. Jim zumBrunnen's assistance with statistical methods and analyses is gratefully acknowledged.

REFERENCES

Acaroglu, E., Iatridis, J., Setton, L., Foster, R., Mow, V., & M., W. (1995). Degeneration and aging affect the tensile behavior of human lumbar anulus fibrosus. *Spine* , 2690-2701.

Adams, M., Bogduk, N., Burton, K., & Dolan, P. (2002). *The Biomechanics of Back Pain.* London: Churchill Livingstone.

Ayturk, U., Garcia, J., & Puttlitz, C. (2010). The Micromechanical Role of the Annulus Fibrosus Components Under Physiological Loading of the Lumbar Spine. *J Biomech Eng* , 132(6):061007.

Bass, E., Ashford, F., Segal, M., & Lotz, J. (2004). Biaxial testing of human annulus fibrosus and its implications for a constitutive formulation. *Ann Biomed Eng* , 32(9):1231-42.

Dooris, A., Goel, V., Grosland, N., Gilbertson, L., & DG., W. (2001). Load sharing between anterior and posterior elements in a lumbar motion segment implanted with an artificial disc. *Spine* , E122-E129.

Eberlein, R., Holzapfel, G., & Schulze-Bauer, C. (2001). An anisotropic model for annulus tissue and enhanced finite element analyses of intact lumbar disc bodies. *Computer Methods in Biomechanics and Biomedical Engineering* , 209-230.

Fujita, Y., Duncan, N., & Lotz, J. (1997). Radial tensile properties of the lumbar annulus fibrosus are site and degeneration dependent. *J Orthop Res* , 814-9.

Gasser, T., Ogden, R., & Holzapfel, G. (2006). Hyperelastic modelling of arterial layers with distributed collagen fibre orientations. *J R Soc Interface* , 3, 15–35.

Guerin, H., & Elliott, D. (2006). Degeneration affects the fiber reorientation of human annulus fibrosus under tensile load. *Journal of Biomechanics* , 1410-1418.

Guerin, H., & Elliott, D. (2007). Quantifying the contributions of structure to annulus fibrosus mechanical function using a nonlinear, anisotropic, hyperelastic model. *Journal of Orthopaedic Research* , 508-516.

Guerin, H., & Elliott, D. (2006). Structure and properties of soft tissues in the spine. In E. A. Kurtz SM, *SPINE Technology Handbook* (pp. 35-62). London: Elsevier.

Holzapfel, G. (2000). *Nonliear Solid Mechanics.* Wiley.

Holzapfel, G., & Ogden, R. (2009). On planar biaxial tests for anisotropic nonlinearly elastic solids. A continuum mechanical framework. . *Mathematics and Mechanics of Solids* , 14:474–489.

Iatridis. (1999). Shear Mechanical Properties of Human Lumbar Annulus Fibrosus. *J Orthop Res* , 732-737.

Iatridis, J., Setton, L., Foster, R., Rawlins, B., Weidenbaum, M., & Mow, V. (1998). Degeneration affects the anisotropic and nonlinear behaviors of human anulus fibrosus in compression. *J Biomech* , 535-544.

Krismer, M., Haid, C., Behensky, H., Kapfinger, P., Landauer, F., & Rachbauer, F. (2000). Motion in lumbar functional spine units during side bending and axial rotation moments depending on the degree of degeneration. *Spine* , 2020-2027.

Mimura, M., Panjabi, M., Oxland, T., Crisco, J., Yamamoto, I., & Vasavada, A. (1994). Disc degeneration affects the multidirectional flexibility of the lumbar spine. *Spine* , 1371-80.

Natarajan, R., Williams, J., & Andersson, G. (2006). Modeling changes in intervertebral disc mechanics with degeneration. *Journal of Bone and Joint Surgery Supplement 2* , 36-40.

O'Connell, G., Guerin, H., & Elliott, D. (2009). Theoretical and uniaxial experimental evaluation of human annulus fibrosus degeneration. *J Biomech Eng* , 131(11):111007.

Sacks, M., & Chuong, C. (1993). Biaxial mechanical properties of passive right ventricular free wall myocardium. *J Biomech Eng* , 115(2): 202-5.

Sacks, M., & Sun, W. (2003). Multiaxial mechanical behavior of biological materials. *Annu Rev Biomed Eng* , 5:251-84.

Schmidt, H., Heuer, F., Drumm, J., Klezl, Z., Claes, L., & Wilke, H. (2007). Application of a calibration method provides more realistic results for a finite element model of a lumbar spinal segment. *Clinical Biomechanics* , 377-84.

Shirazi-Adl, S., Shrivastava, S., & Ahmed, A. (1984). Stress analysis of the lumbar disc-body unit in compression. A three-dimensional nonlinear finite element study. *Spine* , 120-34.

Smith, L., Byers, S., Costi, J., & Fazzalari, N. (2008). Elastic fibers enhance the mechanical integrity of the human lumbar anulus fibrosus in the radial direction. *Ann Biomed Eng* , 36(2):214-23.

Spencer. (1984). Constitutive theory for strongly anisotropic solids. In Spencer, *Continuum Theory of the Mechanics of Fibre-Reinforced Composites* (pp. 1-32). New York: Springer Verlag.

Thompson, J., Pearce, R., Schechter, M., Adams, M., Tsang, I., & Bishop, P. (1990). Preliminary evaluation of a scheme for grading the gross morphology of the human intervertebral disc. *Spine* , 411-415.

Wagner, D., & Lotz, J. (2004). Theoretical model and experimental results for the nonlinear elastic behavior of human annulus fibrosus. *Journal of Orthopaedic Research* , 901-909.

Weiss, J., Maker, B., & Govindjee, S. (1996). Finite element implementation of incompressible, trasnversely isotropic hyperelasticity. *Comput Methods Appl Mech Engrg* , 107-128.

Zander, T., Rohlmann, A., Calisse, J., & Bergmann, G. (2001). Effect of bone graft characteristics on the mechanical behavior of the lumbar spine. *Clinical Biomechanics* , S73-S80.

CHAPTER 5:

Finite Element Modeling of Degeneration-Related Changes in Lumbar Spine Biomechanics

5.1 INTRODUCTION

Degenerative disc disease leads to significant alterations in the biomechanics of the intervertebral disc, as indicated by the reported changes in range of motion of lumbar spinal segments and the mechanical behavior of the annulus fibrosus (Acaroglu, et al., 1995) and nucleus pulposus (Johannessen, et al., 2005). Severe changes in the morphology of relevant intervertebral disc constituents, particularly the nucleus pulposus and annulus fibrosus (Setton, et al., 2006), (Thompson, et al., 1990) are potential sources for these observed alterations in material behavior.

While it is not possible to pinpoint the exact initiation of degeneration, dehydration in the nucleus pulposus (which is also an outcome of aging (Antoniu, et al., 1996)) is the most likely event that triggers the degradation in the remainder of the disc. The increased breakdown of hydrophilic proteoglycan (PG) molecules (Stokes, et al., 2005) and the change in the ratio of Type I / Type II collagen content (Andersson, 1998) are simultaneous with the measured reduction in the aggregate modulus of the tissue (Johannessen, et al., 2005). Although calcification of the endplate is a commonly observed phenomenon (Bernick, et al., 1982), recent data suggest that the permeability is also increased as a result of degeneration and aging (Rodriguez, et al., In Press). However, parametric modeling analyses predict that the influence of endplate mechanical properties on the overall mechanics of the disc is relatively insignificant (Hsieh, et al., 2005).

In addition to increased cross-linking among the collagen fibers, the water content in the annulus is decreased with degeneration. Due to the loss of hydration and the breakdown of the PGs, the hydrostatic pressurization in the nucleus is lost, and consequently the *in situ* circumferential tension in the annular lamellae is reduced (Meakin, et al., 2001). The lack of

tension in the annulus tissue increases the catabolic effect of matrix-metalloproteinases (MMPs) significantly (Lotz, et al., 2008), leading to a further reduction in the PG content (and thus, hydration). Moreover, under *in vivo* compressive loads, this loss of circumferential tension causes the individual layers to buckle and delaminate (as opposed to the physiological radial bulge that is commonly observed (Guerin, et al., 2006)). In fact, in the later stages of degeneration, the disintegration of the annular lamellae with rupture and buckling of the collagen fiber bundles has been reported (Iatridis, et al., 2004). Clearly, these microstructural changes in the annulus have a definitive mechanical outcome on the clinically relevant mechanics of the intervertebral disc.

Studies on the elastic behavior of the annulus fibrosus have shown that degeneration increases the toe-region modulus under circumferential tension, but does not affect the elastic modulus of the linear region (Guerin, et al., 2006) and significantly reduces the Poisson ratio (Acaroglu, et al., 1995). The shear modulus has also been shown to increase with degeneration (Iatridis, 1999), whereas the linear elastic modulus under radial tension remains unchanged (Fujita, et al., 1997). The permeability of degenerated annulus fibrosus tissue has been found to be reduced as compared to that of the healthy tissue (Natarajan, et al., 2006). Iatridis has shown that there is a reduction in the compressive aggregate modulus (Iatridis, et al., 1998). Although there is no clear trend in the changes with respect to the elastic properties of the annulus as a result of degeneration, its strength has been shown to decrease in all loading directions (Acaroglu, et al., 1995) (Fujita, et al., 1997). Failure stresses in the radial and circumferential directions are reduced significantly, and Acaroglu has shown that the failure strain energy density is also significantly reduced (Acaroglu, et al., 1995).

There have been few attempts at simulating the aforementioned effects of disc degeneration on the global kinetic and mechanical behavior of lumbar spine segments (Rohlmann, et al., 2006) (Schmidt, et al., 2007). The associated models included the severe changes in geometry, formation of osteophytes and compressibility of the annulus and nucleus (Schmidt, et al., 2009) (Ruberté, et al., 2009) (Williams, et al., 2007) (Zander, et al., 2006). However, the material models used to represent the healthy and degenerated annulus fibrosus or nucleus pulposus have not been explicitly validated. Instead, these studies included the inherent assumption that these parameters do not have significant effects on the local stress concentrations under *in vivo* loading conditions and the associated resultant rotation responses. The validity of this assumption can only be demonstrated with extensive analyses that include mechanical testing of healthy and degenerated disc tissue and implementation of the findings in a validated finite element model of the spine.

Overall, although there is a number of studies on the effects of degeneration on intervertebral disc mechanics (Wagner, et al., 2004) (Schmidt, et al., 2007) (Guerin, et al., 2007), development of material models of the degenerated tissue has been limited (O'Connell, et al., 2009). Our recent analyses and modeling efforts on healthy and degenerated annulus fibrous tissue have resulted in the generation of orthotropic continuum models that can be implemented in large scale finite element models. The classic methodology we employed (originally suggested by Spencer (Spencer, 1984)) involves the assumption that there exists an energy potential that is capable of accurately describing the mechanical behavior of the material of interest, with this potential expressed as a function of the strain invariants. The calibration procedure required data-fitting on the *in vitro* response of the tissue in all principal loading directions, as well as its biaxial response to certain load combinations (see Chapter 4). Subsequently, the objective of this study was to implement the aforementioned continuum

models in a finite element model of a lumbar functional spinal unit in order to document the microscopic and macroscopic biomechanical changes induced by degenerative disc disease.

5.2 METHODS

5.2.1 Finite Element Model Development

A previously developed and validated finite element model of the L4/L5 functional spinal unit was utilized (Ayturk, et al., 2010). Briefly, the geometry of the model was based on computed tomography (CT) scans of a cadaveric specimen, and the refined mesh consisted of 8-noded hexagonal elements with approximately 230,000 degrees of freedom. The material properties of all osseous tissues and part of the soft tissues were based on data retrieved from the literature. Specifically, the properties of healthy and degenerated annulus fibrosus were assigned based on biaxial tension tests performed in our laboratory (as explained in detail in Chapter 4 and briefly summarized below). Ligaments were modeled as tension-only, nonlinear springs with previously reported force-displacement relationships. Validation of the original model was performed based on range of motion, intradiscal pressure, vertebral bone strain and disc bulge under pure-moment and pure-compression loading scenarios. Pertaining to the comparative purposes of this study, the material properties of the intervertebral disc constituents were modified, and the progression of degeneration was simulated using three model variants:

1. *Healthy (H):* Coefficients calculated for nondegenerate annulus and nucleus were implemented. Prior to the application of rotational loads, the nucleus was pressurized by an isotropic volumetric expansion in order to simulate its swelling pressure, and subsequent contribution to the generation of circumferential tension in the annulus.

2. *Degenerated Nucleus (DN):* The aforementioned pressurization step was removed, and material properties for the degenerated nucleus were implemented. Ossification of the cartilaginous endplate was simulated by assigning bony endplate properties to the cartilage layer elements.

3. *Degenerated Annulus and Nucleus (DA):* In addition to the changes described in the DN condition, the empirically-derived material coefficients for the degenerated annulus were implemented.

While the material properties and *in situ* nuclear pressure were altered in the degeneration scenarios, osteophytes, local tears or similar macroscopic abnormalities were not modeled. Rather than attempting to simulate these defects that are usually specific to a particular individual and random in nature, the focus was limited to the effects of measured changes in tissue mechanical behavior. Furthermore, the properties of ligaments were consistent for each group; however, this led to an increased "buckling effect" due to the modeled degeneration. Specifically, in the healthy disc scenario, pressurization of the disc resulted in the generation of pre-stresses in the ligaments, which, because this pressurization step was eliminated in the degeneration models, were not developed the in DN and DA scenarios.

5.2.2 Modeling the Intervertebral Disc

The annulus fibrosus was modeled as an incompressible orthotropic continuum, with its total strain energy density defined as the sum of the matrix (W_{matrix}) and fiber (W_{fiber}) components:

$$W = \mathrm{W}_{\mathrm{matrix}} + \mathrm{W}_{\mathrm{fiber}} \tag{5.1}$$

$$W_{matrix} = C_{10}(I_1 - 3) + C_{20}(I_1 - 3)^2 \quad (5.2)$$

$$W_{fiber} = \frac{k_1}{2k_2}\sum_{\alpha=4,6}(e^{k_2[(1-\kappa)(I_1-3)+\kappa(I_\alpha-1)]^2} - 1) \quad (5.3)$$

The independent variables (I_n) represent the invariants of the Green deformation tensor:

$$C = F^T F \qquad I_4 = a_0 C a_0 \qquad I_6 = b_0 C b_0 \quad (5.4)$$

where F represents the deformation gradient and a_0 and b_0 represent the direction cosines of the two fiber families in the undeformed configuration. Details of the invariants and relevant tensor derivations are given elsewhere (Spencer, 1984) (Holzapfel, 2000). The material coefficients C_{10}, C_{20}, k_1, k_2 and κ were based on biaxial tension tests performed in our laboratory on healthy and degenerated annuli fibrosi (Ayturk, et al., 2011). The nucleus pulposus was modeled as a linearly elastic solid, with the appropriate material properties based on previously published experimental data (Johannessen, et al., 2005). The coefficients employed in all three conditions are listed in Table 5.1.

Material	Elastic Modulus (MPa)	Poisson Ratio	Reference
Cortical Bone	E_{11} =8000	ν_{12} = 0.4	(Ueno and Liu, 1987)
	E_{22} = 8000	ν_{13} = 0.35	
	E_{33} = 12000	ν_{23} = 0.3	
Trabecular Bone	*Based on CT images*		(Crawford et al., 2003)
Posterior Elements	E = 3500	ν = 0.3	(Dooris et al., 2001)
Bony Endplates	E = 1000	ν = 0.3	(Whyne et al., 2001)
Facet Cartilage	Neo-Hookean, C_{10} = 2		(Noailly et al., 2005)
Annulus Fibrosus			
	H & DN	C_{10} = 0.0154, C_{20} = 0.0743, k_1 = 2.05, k_2 = 86.53, κ = 0.113	
	DA	C_{10} = 0.01, C_{20} = 0.0695, k_1 = 3.12, k_2 = 179.42, κ = 0.245	
Nucleus Pulposus	H	E = 1 ν = 0.49	(Johannessen, et al., 2005)
	DN & DA	E = 0.44 ν = 0.4	
Cartilaginous Endplate	E = 23.8	ν = 0.4	(Lu et al., 1995)
Ligaments	*Exponential force-displacement curves*		(Rohlmann et al., 2006)

Table 5.1: Summary of the mechanical properties used in the model for all three experimental variants.

The total strain energy function was coded into a user subroutine (UANISOHYPER) in ABAQUS. For solution of specific boundary problems, the Cauchy stress (σ_{ij}) and elasticity

tensors (E_{ijkl}) have to be defined as functions of the deformation gradient. The derivation of both tensors requires the differentiation of the total energy density function:

$$\sigma_{ij} = 2J^{-1}F^T \frac{\partial W}{\partial C_{ij}} F \qquad E_{ijkl} = 4\frac{\partial^2 W}{\partial C_{ij}\partial C_{kl}} \tag{5.5}$$

where the derivatives with respect to the Right-Cauchy-Green strain tensor (C_{ij}) are the only variables dependent on the energy function. Application of the chain rule yields:

$$\frac{\partial W}{\partial C_{ij}} = \sum_{n=1,4,6} \frac{\partial W}{\partial I_n}\frac{\partial I_n}{\partial C_{ij}} \tag{5.6}$$

and the derivative of the total energy density with respect to the invariants become the only "user-defined" component in the coding process. The relevant first and second derivatives of the function (Eq. 5.1) were implemented in the subroutine, and the remaining calculations and transformations (Eq. 5.5) were performed by the finite element solution algorithm (ABAQUS Standard, see below). Minimum allowable values of the invariants I_4 and I_6 (1 for both) were constrained such that the fibers were activated only under tensile loads. The fiber angles were specified to vary between 26° to 45° from the outer layer to the inner layer of the annulus (Guerin, et al., 2006), respectively, and they were implemented using the local *ORIENTATION command.

5.2.3 Model Predictions & Boundary Conditions

All models were constrained at the inferior endplate of L5. Pure-moments up to 7.5 Nm were applied in three principal loading directions (flexion/extension, lateral bending and axial rotation). All solutions were obtained using ABAQUS Standard (ver. 6.9, SIMULIA, Providence, RI) running on a high-performance workstation (Model: xw8400, Hewlett-Packard Company, Palo Alto, CA).

5.3 RESULTS

Degeneration of the annulus fibrosus increased the range of motion (ROM) in all loading directions except for lateral bending. The most notable kinematic changes were predicted in extension and axial rotation. In extension, a 42% increase in ROM was predicted in the DN scenario (with respect to the H condition), while the change in the DA scenario was approximately 28% (Figure 5.1). Axial rotation ROM predictions for the DA case were larger than that in the DN case (4.1° and 3.7°, respectively). The greatest ranges of motion were consistently predicted in flexion loading for all three model variants.

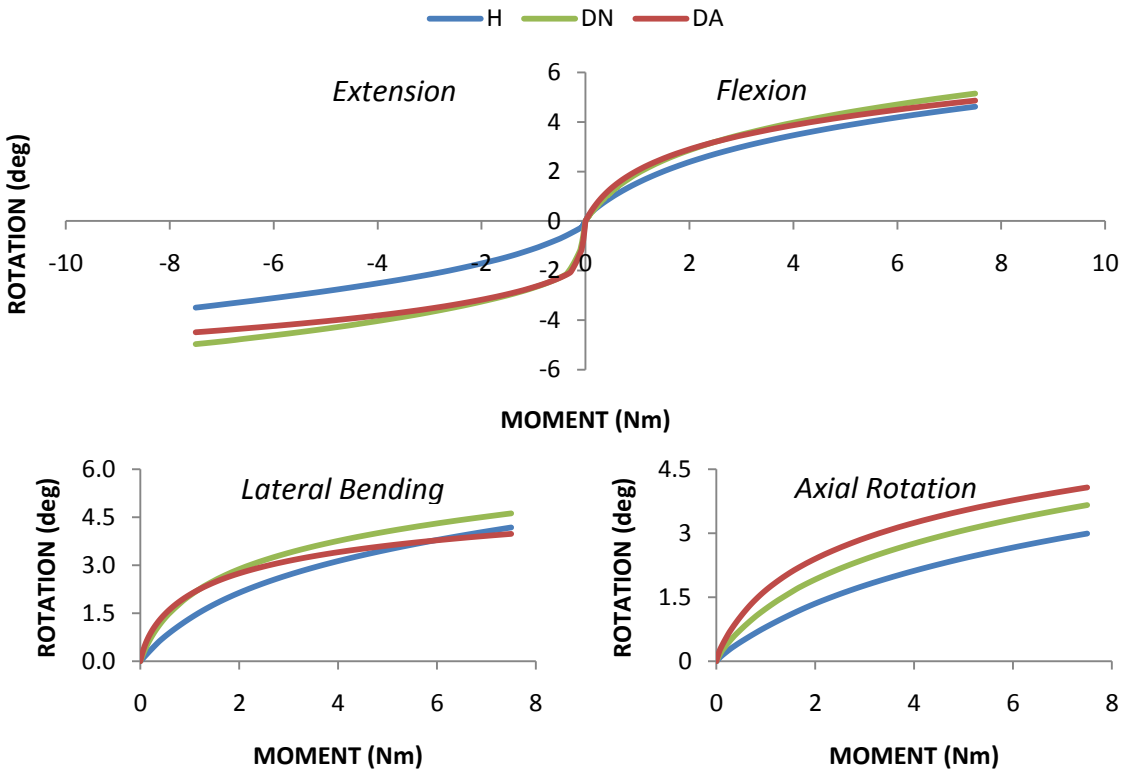

Figure 5.1: The range of motion predictions under pure-moment loading in all scenarios.

While the greatest ROM in extension was predicted for the DN case, the magnitude of stress predictions were reduced in the anterior region of the disc while they increased in the posterior region as the simulated degeneration progressed (Figure 5.2). In all cases, the highest

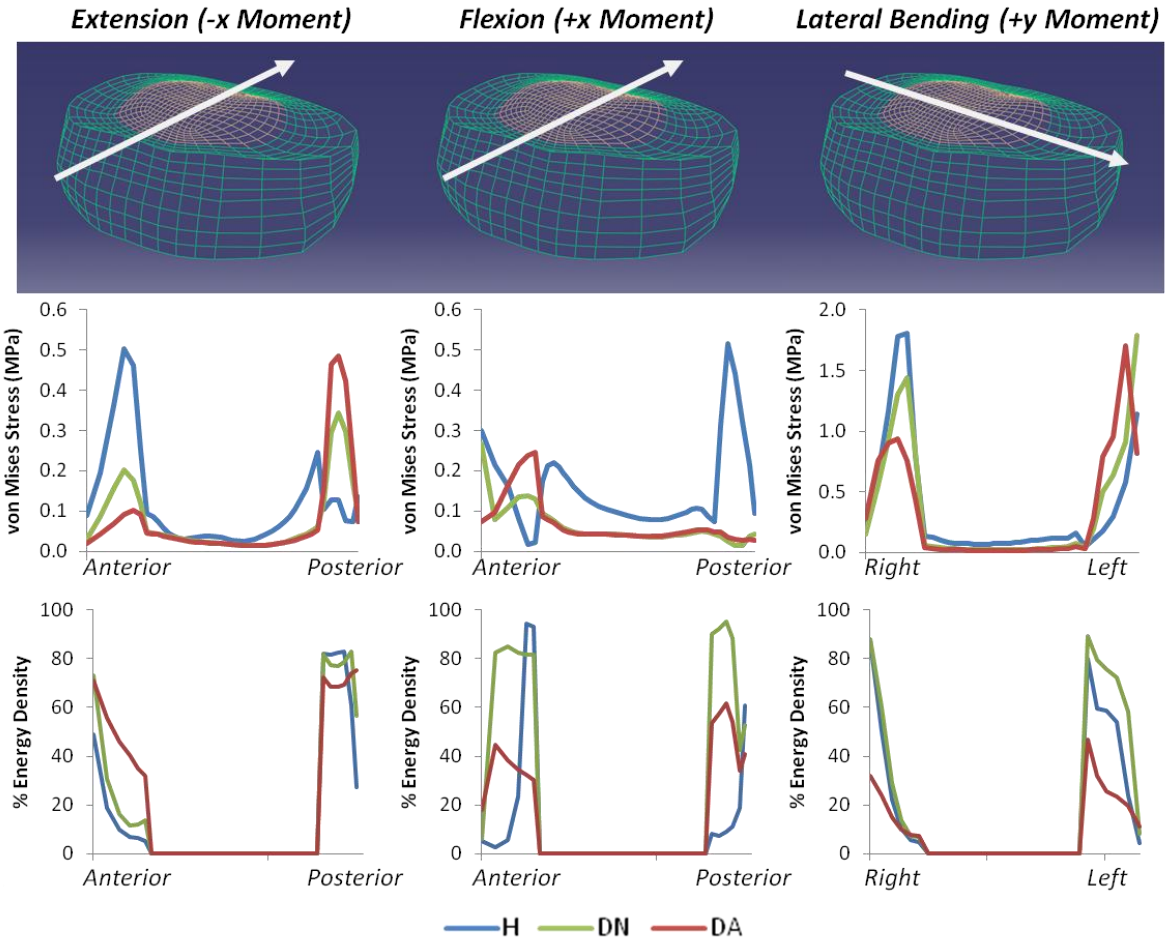

Figure 5.2: Local intradiscal von Mises stress predictions (middle row) and strain energy density percentage due to the matrix component (bottom row) in the annulus in the anteroposterior direction under extension (left) and flexion (middle) and in the medial-lateral direction under lateral bending (right). The white arrows indicate the positions of the nodes in the annulus corresponding to the horizontal axes of the charts below.

stresses were concentrated in the posterolateral region of the disc in extension loading. Similarly in lateral bending, the stress predictions in areas under tensile loads (right lateral region of the disc) were typically reduced, whereas the predictions in areas exposed to compressive loads (left lateral region of the disc) were increased as degeneration progressed.

The local predictions of energy and stress generation due to the fiber component of the annulus followed the same general patterns observed with respect to the von Mises stress parameter. Overall, the SED-based load sharing predictions between the matrix and fiber components of the healthy annulus fibrosus were in agreement with our earlier reports. The progression of degeneration initially increased the percentage load borne by the matrix in all loading cases in the DN scenario (most dramatically in flexion, from 15% to 49%), followed by a reduction in the DA scenario (Figure 5.3). The fiber component was predicted to carry the largest loads in axial rotation in all cases (91%, 84%, and 89% in H, DN, and DA, respectively). The local contribution of the matrix to the total energy prediction for the annulus increased at the anterior and posterior extremities both in flexion and extension (Figure 5.2). The pressure

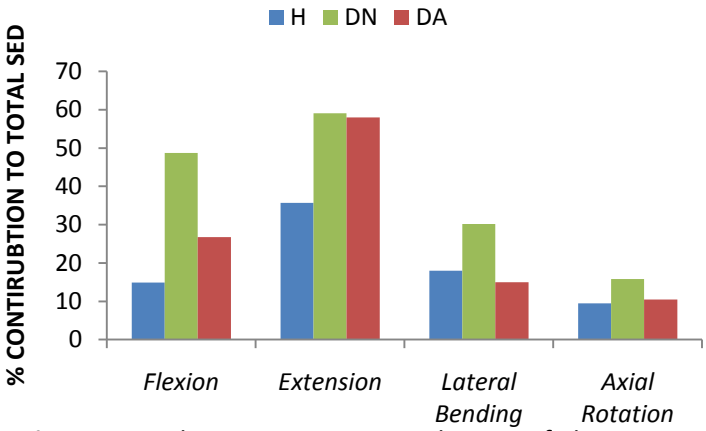

Figure 5.3: The percentage contribution of the matrix component to the average SED predictions in the annulus fibrosus.

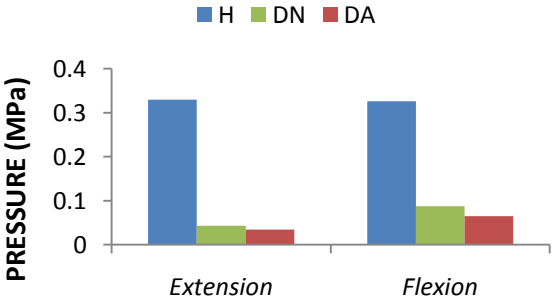

Figure 5.4: Mean intradiscal nuclear pressure predictions in extension and flexion loading.

predictions in the nucleus followed a decreasing pattern with the progression of degeneration, largely due to the removal swelling pressure in the simulations (Figure 5.4).

Changes in facet force transmission under extension loading followed a pattern similar to the ROM results, with the total forces being 81N, 105N and 106N in H, DN and DA cases, respectively (Figure 5.5). Contrary to the increasing trend in facet force transmission, the loads borne by the ligaments decreased in all loading scenarios due to degeneration (Figure 5.6). The greatest change relative to the healthy condition was predicted for lateral bending, with 16% and 19% reductions in the DN and DA cases, respectively. Among all ligaments, the anterior longitudinal ligament and facet capsules were identified as the major load bearing tissues. The highest ligament tension was generated in extension loading (295N, 275N and 288N in the H, DN and DA cases, respectively).

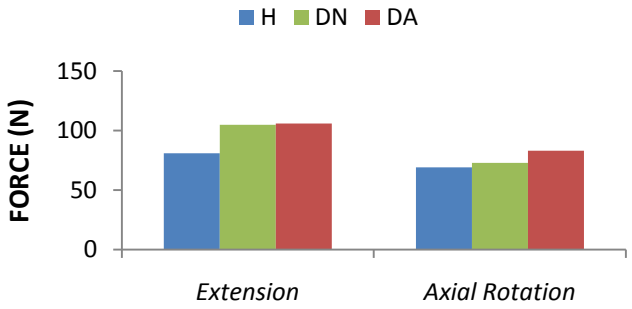

Figure 5.5: Facet force transmission under extension and axial rotation loading.

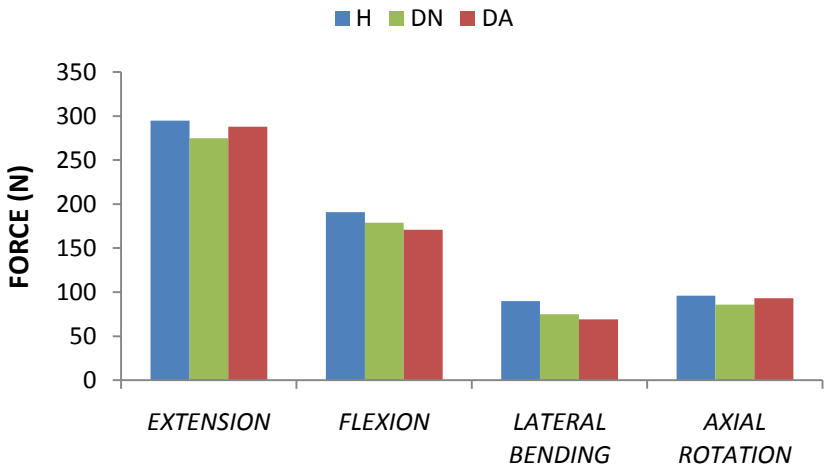

Figure 5.6: Total force predictions for the ligaments under all loading scenarios.

5.4 DISCUSSION

A unique degeneration model for the lumbar intervertebral disc, with tissue properties directly based on experimental data, was established in this study. A previously developed finite element model was modified by implementing material properties for the nucleus pulposus and orthotropic continuum models of annulus fibrosus. The predictions for the healthy condition were in good agreement with earlier results. Specifically, kinematics (leading to a less than 0.7° change in all loading directions) and load distribution patterns between the components of the annulus fibrosus were very similar.

Previously published *in vitro* experimental results indicate that the mobility of spinal segments typically increase at the earlier stages of degeneration, and tend to decrease as the disease becomes severe (Krismer, et al., 2000). This reduction is potentially due to the significant loss of disc height, formation of osteophytes around the rim of the endplate, and a large number of local defects in the annulus and nucleus. These conditions have not been simulated in this study, largely due to a lack of consistent pattern with respect to their formation. Instead, we implemented known (via experimentation and clinical observation) alterations in the mechanics of annulus and nucleus, in order to simulate a mild degeneration state that can potentially be treated upon devising a successful regenerative therapy. Nevertheless, our kinematic results are in agreement with the hypermobility findings in the literature. The most severe increase in ROM predictions was in extension, followed by changes in axial rotation (Figure 5.1). In flexion, extension and lateral bending, the mobility of the FSU increased with the removal of the simulated swelling pressure and alterations with respect to the nucleus pulposus properties. However, further degeneration of the annulus reversed this trend demonstrated by the decreasing ROM predictions. Consequently, this kinematic trend

may be interpreted as a stabilization effect (as the ROM is reported to be significantly reduced while the degeneration progresses), however, further data are necessary to reach a definitive conclusion.

Simulation of a depressurized nucleus (DN) resulted in a typical increase in ranges of motion, which was accompanied by an increase in facet force transmission and elevated load distribution patterns between the annular components. These results suggest that the reduction of pressure and degradation of the nucleus has a substantial effect on the internal biomechanics of the annulus, resulting in increased stress generation within the annular ground substance both locally (Figure 5.2) and globally (Figure 5.3). This may be one of the key mechanobiological alterations in the mechanics of the intervertebral disc that advances and accelerates the degenerative cascade (Roughley, 2004). On the other hand, the local stress predictions indicate a consistent change in von Mises stress distributions in the anteroposterior and mediolateral directions in flexion/extension and lateral bending loading, respectively (Figure 5.2). Despite the reduction in mobility with respect to the DN condition, stresses continue to increase with degeneration of the annulus. From a modeling perspective, this is most likely due to the altered mechanical properties of the annulus. However, the large change in the load borne by the ground substance, and the shifting of high stresses towards the posterior region of the disc in extension are consistent with the commonly seen annular tearing and herniation in the clinical setting.

As it is the case with any modeling endeavor, this study had a number of limitations. As explained in the Methods section in detail, only the alterations in tissue mechanics among the features of degenerative disc disease were modeled. Consequently, while this enabled the simulation of a consistent pattern for all disc constituents, spatial homogeneity of the annulus'

mechanical parameters (except for the lamellar variation in the collagen fiber orientation) throughout the disc geometry were assumed. The SED function coefficients for both healthy and degenerated annulus tissue were based on mechanical experiments conducted on specimens extracted from the anterior / anterolateral regions of the disc, and the same coefficients were assigned to the entire annulus fibrosus geometry. Degeneration was assumed to progress in an orderly fashion, such that the degenerative disease affected the annulus only after depressurization and degeneration of the nucleus. While this may not be the exact order of disease progression, the significant acceleration in annular aggrecan breakdown and change in dominant *in situ* loading mechanism (from tensile loads to compressive loads) due to loss of nucleus pressure (Lotz, et al., 2008) indicate that the effect of degenerative disease on annulus mechanics becomes more relevant following this aforementioned time point. All tissues were modeled as non-porous continua (with the implicit assumption of incompressibility). While the role of fluid flow in the degeneration cascade has not been explicitly determined, known (and sometimes conflicting) changes (Bernick, et al., 1982) (Rodriguez, et al., In Press) in the endplate and annulus permeability with age indicate that fluid flow may play an important part in this process. These alterations in the mechanical contribution of the fluid component as well as the interaction between the solid and fluid phases may potentially change the time-dependent behavior of the disc (such as relaxation or creep) (Iatridis, et al., 1997) (Boxberger, et al., 2009). Modeling of these phenomena would add substantial complexity to the model, and should be included in future work. Finally, a relatively simple SED function that did not include an explicit fiber-matrix interaction term was utilized in order to ensure computational stability, and consequently, solution convergence.

5.5 CONCLUSION

A unique degeneration model, with tissue properties based on direct experimental data, was established and the effects of degenerative disc disease on the biomechanics of spinal motion segments were assessed. An initial reduction in the nuclear swelling pressure and biomechanical degradation in nucleus pulposus substantially increased annular stresses, most notably on the ground substance. Further degeneration of the annulus reduced ROM in all loading directions except axial rotation. This finding is in agreement with the stiffening effect associated with severe degeneration that has been observed both *in vitro* and *in vivo.* Future work will include the utilization of this model in evaluation of contemporary surgical intervention techniques, such as disc arthroplasty (Chapter 6).

REFERENCES

Acaroglu, E., Iatridis, J., Setton, L., Foster, R., Mow, V., & Weidenbaum, M. (1995). Degeneration and aging affect the tensile behavior of human lumbar anulus fibrosus. *Spine* , 2690-2701.

Adams M, B. N. (2002). *The Biomechanics of Back Pain.* London: Churchill Livingstone.

Andersson, G. (1998). What are the age-related changes in the spine? *Baillieres Clin Rheumatol* , 161-173.

Antoniu, J., Steffen, T., & Nelson, F. (1996). The Human Intervertebral Disc: Evidence for Changes in the Biosynthesis and Denaturation of the Extracellular Matrix with Growth, Maturation, Ageing, and Degeneration. *J Clin Invest* , 996-1003.

Ayturk, U., Garcia, J., & Puttlitz, C. (2010). The Micromechanical Role of the Annulus Fibrosus Components Under Physiological Loading of the Lumbar Spine. *J Biomech Eng* , 132(6):061007.

Ayturk, U., Schuldt, D., Patel, V., & Puttlitz, C. (2011). Orthotropic Continuum Model Development for Healthy and Degenerated Annulus Fibrosus Based on a Biaxial Testing Protocol. *Transactions of the Annual Meeting of Orthopaedic Research Society.* Long Beach, CA.

Bernick, S., & Cailliet, R. (1982). Vertebral Endplate Changes with Aging of Human Vertebrae. *Spine* , 97-102.

Boxberger, J., Orlansky, A., Sen, S., & Elliott, D. (2009). Reduced nucleus pulposus glycosaminoglycan content alters intervertebral disc dynamic viscoelastic mechanics. *J Biomech* , 42(12):1941-6.

Fujita, Y., Duncan, N., & Lotz, J. (1997). Radial Tensile Properties of the Lumbar Annulus Fibrosus are Site and Degeneration Dependent. *J Orthop Res* , 814-819.

Fujiwara A, L. T. (2000). The effect of disc degeneration and facet joint osteoarthritis on the segmental flexibility of the lumbar spine. *Spine* , 3036-3044.

Guerin, H., & Elliott, D. (2006). Degeneration affects the fiber reorientation of human annulus fibrosus under tensile load. *Journal of Biomechanics* , 1410-1418.

Guerin, H., & Elliott, D. (2007). Quantifying the contributions of structure to annulus fibrosus mechanical function using a nonlinear, anisotropic, hyperelastic model. *Journal of Orthopaedic Research* , 508-516.

Guerin, H., & Elliott, D. (2006). Structure and properties of soft tissues in the spine. In E. A. Kurtz SM, *SPINE Technology Handbook* (pp. 35-62). London: Elsevier.

Holzapfel, G. (2000). *Nonliear Solid Mechanics.* Wiley.

Hsieh, A., Wagner, D., Cheng, L., & Lotz, J. (2005). Dependence of mechanical behavior of the murine tail disc on regional material properties: a parametric finite element study. *J Biomech Eng* , 127(7):1158-67.

Iatridis, J. (1999). Shear Mechanical Properties of Human Lumbar Annulus Fibrosus. *J Orthop Res* , 732-737.

Iatridis, J., & Gwynn, I. (2004). Mechanisms for Mechanical Damage in the Intervertebral Disc Annulus Fibrosus. *J Biomech* , 1165-1175.

Iatridis, J., Setton, L., Foster, R., Rawlins, B., Weidenbaum, M., & Mow, V. (1998). Degeneration affects the anisotropic and nonlinear behaviors of human anulus fibrosus in compression. *J Biomech* , 535-544.

Iatridis, J., Setton, L., Weidenbaum, M., & Mow, V. (1997). Alterations in the mechanical behavior of the human lumbar nucleus pulposus with degeneration and aging. *J Orthop Res* , 15(2):318-22.

Johannessen, W., & Elliott, D. (2005). Effects of degeneration on the biphasic material properties of human nucleus pulposus in confined compression. *Spine* , 30(24):E724-9.

Krismer, M., Haid, C., Behensky, H., Kapfinger, P., Landauer, F., & Rachbauer, F. (2000). Motion in lumbar functional spine units during side bending and axial rotation moments depending on the degree of degeneration. *Spine* , 2020-2027.

Lotz, J., Hadi, T., Bratton, C., Reiser, K., & Hsieh, A. (2008). Anulus fibrosus tension inhibits degenerative structural changes in lamellar collagen. *Eur Spine J* , 1149-1159.

Meakin, J., Redpath, T., & Hukins, D. (2001). The Effect of Partial Removal of the Nucleus Pulposus from the Intervertebral Disc on the Response of the Human Annulus Fibrosus to Compression. *Clinical Biomechanics* , 121-128.

Mimura M, P. M. (1994). Disc degeneration affects the multidirectional flexibility of the lumbar spine. *Spine* , 1371-80.

Natarajan, R., Williams, J., & Andersson, G. (2006). Modeling changes in intervertebral disc mechanics with degeneration. *Journal of Bone and Joint Surgery Supplement 2* , 36-40.

Niosi CA, O. T. (2004). Degenerative mechanics of the lumbar spine. *Spine J* , 202S-208S.

O'Connell, G., Guerin, H., & Elliott, D. (2009). Theoretical and uniaxial experimental evaluation of human annulus fibrosus degeneration. *J Biomech Eng* , 131(11):111007.

Rodriguez, A., Slichter, C., Acosta, F., Rodriguez-Soto, A., Burghardt, A., Majumdar, S., et al. (In Press). Human Disc Nucleus Properties and Vertebral Endplate Permeability. *Spine* , In Press.

Rohlmann, A., Zander, T., Schmidt, H., Wilke, H., & Bergmann, G. (2006). Analysis of the influence of disc degeneration on the mechanical behaviour of a lumbar motion segment using the finite element method. *J Biomech* , 2484-2490.

Roughley, P. (2004). Biology of Intervertebral Disc Aging and Degeneration. *Spine* , 29(23):2691-2699.

Ruberté, L., Natarajan, R., & Andersson, G. (2009). Influence of single-level lumbar degenerative disc disease on the behavior of the adjacent segments--a finite element model study. *J Biomech.* , 341-8.

Schmidt, H., Heuer, F., & Wilke, H. (2009). Dependency of disc degeneration on shear and tensile strains between annular fiber layers for complex loads. *Med Eng Phys* .

Schmidt, H., Heuer, F., Drumm, J., Klezl, Z., Claes, L., & Wilke, H. (2007). Application of a calibration method provides more realistic results for a finite element model of a lumbar spinal segment. *Clinical Biomechanics* , 377-84.

Schmidt, H., Kettler, A., Rohlmann, A., Claes, L., & Wilke, H. (2007). The risk of disc prolapses with complex loading in different degrees of disc degeneration - a finite element analysis. *Clin Biomech* , 988-998.

Setton, L., & Chen, J. (2006). Mechanobiology of the intervertebral disc and relevance to disc degeneration. *J Bone Joint Surg Am.* , 88 Suppl 2:52-7.

Spencer, A. (1984). Constitutive theory for strongly anisotropic solids. In Spencer, *Continuum Theory of the Mechanics of Fibre-Reinforced Composites* (pp. 1-32). New York: Springer Verlag.

Stokes, I., & Iatridis, J. (2005). Biomechanics of the Spine. In H. R. Mow VC, *Basic Orthopaedic Biomechanics and Mechano-Biology* (pp. 529-561). Philadelphia: Lippincott Williams & Wilkins.

Thompson, J., Pearce, R., Schechter, M., Adams, M., Tsang, I., & Bishop, P. (1990). Preliminary evaluation of a scheme for grading the gross morphology of the human intervertebral disc. *Spine* , 411-415.

Wagner, D., & Lotz, J. (2004). Theoretical model and experimental results for the nonlinear elastic behavior of human annulus fibrosus. *Journal of Orthopaedic Research* , 901-909.

Williams, J., Natarajan, R., & Andersson, G. (2007). Inclusion of regional poroelastic material properties better predicts biomechanical behavior of lumbar discs subjected to dynamic loading. *J Biomech* , 1981-7.

Zander, T., Rohlmann, A., Burra, N., & Bergmann, G. (2006). Effect of a posterior dynamic implant adjacent to a rigid spinal fixator. *Clin Biomech (Bristol, Avon)* , 767-74.

CHAPTER 6:

A Finite Element Study of One- and Two-Level Disc Replacement in the Lumbar Spine

6.1 INTRODUCTION

Disc arthroplasty has become an increasingly more common alternative to fusion, the current gold standard, for the treatment of disc degeneration. The goals associated with this technique are to restore the intact state biomechanics and prevent long-term adjacent segment degeneration by allowing motion at the treated level. The surgical procedure involves the removal of the anterior (ALL) and posterior (PLL) longitudinal ligaments, nucleus pulposus and cartilaginous endplate (Panjabi, et al., 2007) (Rundell, et al., 2008). The extent of annulus fibrosus resection remains an unknown surgical variable. Specifically, the most clinically important question focuses on if preservation of the annulus fibrosus tissue affects the acute biomechanical outcome of the treatment (Rohlmann, et al., 2005).

The most accurate indicators of implant performance in the short and long term periods following surgery are yet to be determined. X-ray radiography is the most commonly used modality to determine the mobility of spinal motion segments in the pre- and post-operative periods, providing a measure of stability in the clinical setting (Auerbach, et al., 2009) (Cakir, et al., 2009) (Käfer, et al., 2008). However, the biomechanical behavior of spine is rather complex (particularly due to its multi-joint structure involving interactions of several hard and soft tissues), and consequently treatment or disease-related alterations cannot be assessed based simply on kinematics (Crawford, 2005). Finite element models have the potential to provide further insight into the problem, with the condition that the predictions are extensively validated within the boundary conditions of interest (Zhang, et al., 2008) (Jones, et al., 2008).

In addition to the effects of single-level treatment and the associated surgical technique, the biomechanics of multi-level disc replacement remains to be fully assessed. The occurrence of degeneration in the lumbar discs is often not limited to a single level, and previous cadaveric

experimentation studies have evaluated the acute kinematic changes after two-level disc replacement (Panjabi, et al., 2007) (Cunningham, et al., 2009). To our knowledge, a detailed analysis of the associated biomechanical parameters has not been conducted, and one of the objectives of this study was to fill this knowledge gap.

The present study aimed to address these clinically relevant issues, and a comparative finite element analysis of the biomechanical behavior of the lumbar spine following disc replacement with the ProDisc-L (Synthes Spine, West Chester, PA, USA) was performed. The specific objectives of this study were to: (1) Determine if the extent of annulus preservation during implantation has a clinically meaningful effect on the resultant mechanics, and (2) what biomechanical effect one- and two-level disc replacement imparts on the spine within the framework of healthy and degenerated conditions of the intervertebral disc.

6.2 METHODS

6.2.1 Finite Element Model Development

A previously developed finite element model of the human lumbar spine (L1-L5) was utilized in this study. Briefly, the model geometry was based on a computed tomography (CT) scans of a cadaveric specimen, and meshing was performed with 8-noded hexagonal elements. Strain energy density (SED) based convergence resulted in a mesh with approximately 89,000 elements and 300,000 degrees of freedom. Model predictions of intersegmental range of motion, intradiscal nuclear pressure, facet force transmission, anterolateral cortical strain and anterior longitudinal ligament deformation were validated (see Chapter 3 for details). The healthy and degenerated discs were modeled based on experimentally derived material property data (see Chapter 4). The nuclei pulposi in the healthy discs were pressurized by isotropic volumetric expansion of the associated elements, while this pressurization was

excluded for the degenerated discs in addition to the alterations in the mechanical properties of the annulus and nucleus (Table 6.1).

Material	Elastic Modulus (MPa)	Poisson Ratio	Reference
Cortical Bone	E_{11} =8000	ν_{12} = 0.4	(Ueno and Liu, 1987)
	E_{22} = 8000	ν_{13} = 0.35	
	E_{33} = 12000	ν_{23} = 0.3	
Trabecular Bone	*Based on CT images*		(Crawford et al., 2003)
Posterior Elements	E = 3500	ν = 0.3	(Dooris et al., 2001)
Bony Endplates	E = 1000	ν = 0.3	(Whyne et al., 2001)
Facet Cartilage	Neo-Hookean, C_{10} = 2		(Noailly et al., 2005)
Annulus Fibrosus			
	Healthy	C_{10} = 0.0154, C_{20} = 0.0743, k_1 = 2.05, k_2 = 86.53, κ = 0.113	
	Degenerated	C_{10} = 0.01, C_{20} = 0.0695, k_1 = 3.12, k_2 = 179.42, κ = 0.245	
Nucleus Pulposus	Healthy	E = 1 ν = 0.49	(Johannessen, et al., 2005)
	Degenerated	E = 0.44 ν = 0.4	
Cartilaginous Endplate	E = 23.8	ν = 0.4	(Lu et al., 1995)
Ligaments	*Exponential force-displacement curves*		(Rohlmann et al., 2006)
CoCr	E = 210,000	ν = 0.3	(Chen, et al., 2009)
UHMWPE	E= 1018	ν = 0.46	

Table 6.1: Summary of the mechanical properties used in the model.

6.2.2 ProDisc-L Modeling

The ProDisc-L consists of three components: two cobalt-chromium (CoCr) endplates, positioned inferiorly and superiorly, with the superior plate articulating with an ultra-high-molecular-weight-polyethylene (UHMWPE) core fit inside the inferior plate. A computer-aided-design (CAD) geometry of the implant was meshed with 8-noded hexagonal elements (Figure 6.1). The total number of elements for the device was 65,000, and the total degrees of freedom of the model were increased to 535,000 upon simulation of the implantation. The material properties for CoCr and UHMWPE were obtained from the literature (Table 6.1). A complete representation of the complex geometry of the implant was only possible through the generation of a high resolution mesh. Due to the difference between the levels of refinement of the spinal and prosthetic models, a separate convergence study for the implant mesh was not

conducted. Implantation was simulated by assuming perfect osteo-integration of the implant with the native bone by rigidly tying the vertebral and prosthetic endplates. Finite sliding contact was simulated between the superior prosthetic endplate and the polyethylene core of the implant (static coefficient of friction: μ=0.02).

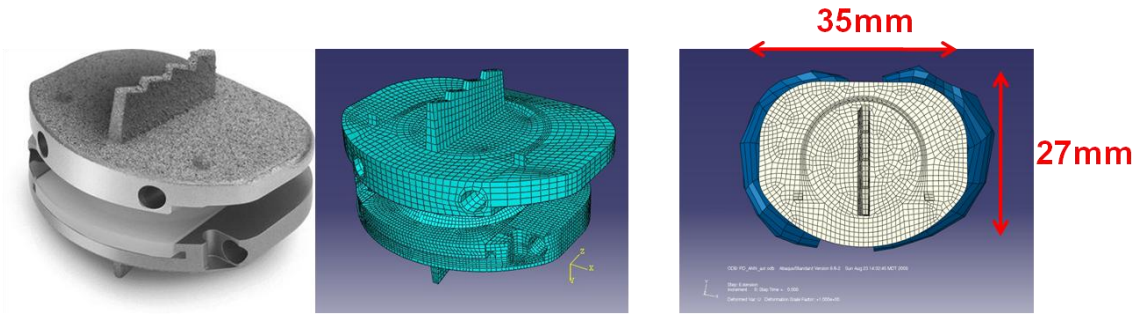

Figure 6.1: ProDisc (left) meshed with 8-noded hexagonal elements (middle). The implant was positioned approximately at the center of the endplate (right).

6.2.3 Implantation & Annular Resection

The ProDisc-L was implanted at the L3/L4 level of the model. Following the guidelines specified by the manufacturer, the anterior and posterior longitudinal ligaments, nucleus pulposus and cartilaginous endplates were removed. The effect of preservation the of annulus fibrosus was treated as a variable, and three implantation scenarios were simulated in order to determine the optimum surgical protocol: Complete annular wall resection (COMP), partial annular wall resection (PART) and minimal (MIN) resection of the annulus (implantation through a 12mm-wide anterior cavity) (Figure 6.2).

6.2.4 Bi-level Treatment

Once the appropriate annulus removal technique was determined, the same protocol was repeated in order to simulate an additional implantation at the L4/L5 level. Thus, single-level implantation (ONE, at L3/L4) and two-level implantation (TWO, at L3/L4 and L4/L5) were

modeled in addition to the healthy (INT) and degenerated (DEG, at L3/L4) conditions (Figure 6.2).

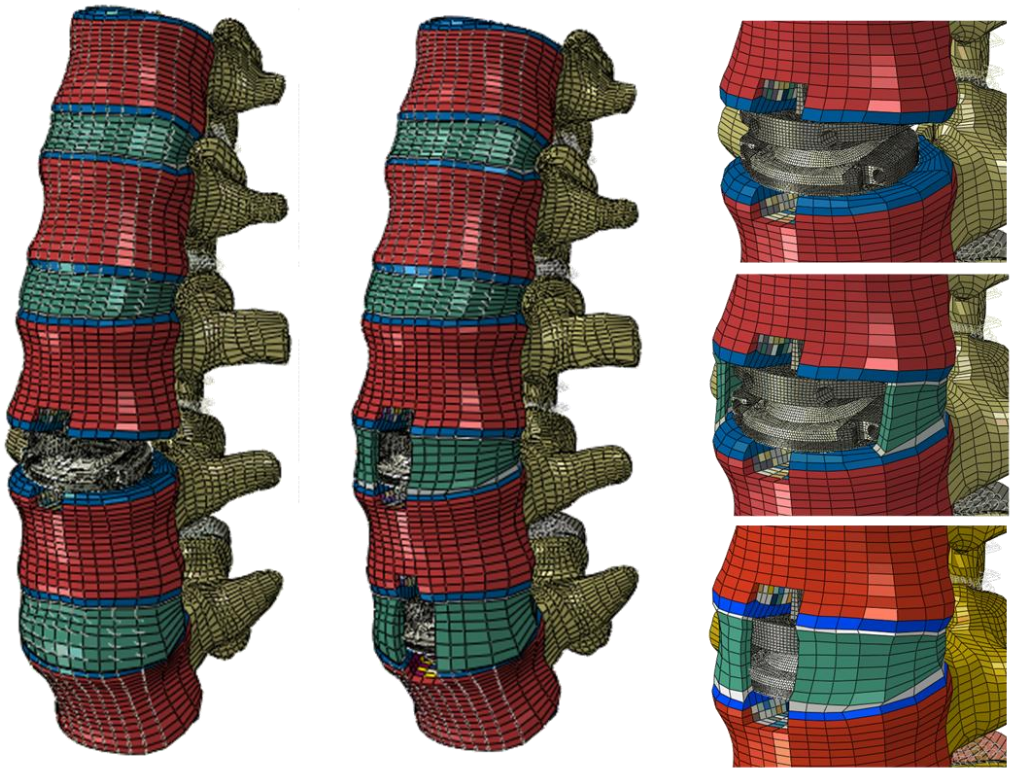

Figure 6.2: ProDisc implanted at the L3/L4 level alone (left) and at the L3/L4 and L4/L5 levels (middle). The implantation was simulated under three different degrees of annular resection: in the COMP (top right), PART (middle right) and MIN (bottom right) conditions.

6.2.5 Testing

All models were constrained at the inferior endplate of L5. Pure-moments up to 7.5 Nm were applied in the three principal loading directions (flexion/extension, lateral bending and axial rotation). All solutions were obtained using ABAQUS Standard (ver. 6.9, SIMULIA, Providence, RI) running on a high-performance workstation (Model: xw8400, Hewlett-Packard Company, Palo Alto, CA). A comparative assessment of all cases of interest was made based on range of motion, facet force transmission and nuclear pressure predictions.

6.3 RESULTS

6.3.1 Annular Resection

The COMP and PART scenarios led to the complete disarticulation of the implant in extension loading. MIN yielded the closest approximation of the INT case predictions in most of the loading conditions, both at the treated and adjacent levels (Figures 6.3-6.5). Consequently, this protocol was repeated in the simulation of the two-level disc replacement. While typical increases in ranges of motion were predicted in all treatment cases at the L3/L4 level (most notably in axial rotation: 11.3°, 3.6°, 2.5° and 2.3° in COMP, PART, MIN and INT cases, respectively (Figure 6.5)), mobility was reduced in flexion (from 5.2° in INT to 4.4°, 3.4° and 3.4° in COMP, PART and MIN cases, respectively (Figure 6.3)). On the other hand, the total range of motion in flexion and extension remained approximately the same for the MIN condition (7.63°) as compared to the INT condition (8.24°). Salvaging annular tissue had an increasing effect on the force transmission through the implant, and also reduced the facet force transmission in axial rotation (Figure 6.6).

6.3.2 Bi-level Treatment

The greatest kinematic effect of two-level disc replacement was predicted in extension at the L4/L5 level (Figure 6.7). However, the range of motion predictions in other loading conditions for all levels were close to the predictions of the one-level treatment and intact model simulations (Figures 6.7-6.9). The differences in total flexion/extension range of motion at the L3/L4 level (8.24° for INT) were not appreciable after the simulation of degeneration (8.62°) or application of either treatment (7.63° for ONE and 7.00° for TWO). Furthermore, both treatment scenarios yielded a consistent reduction in the nonlinearity of the moment-rotation curves at the treated levels.

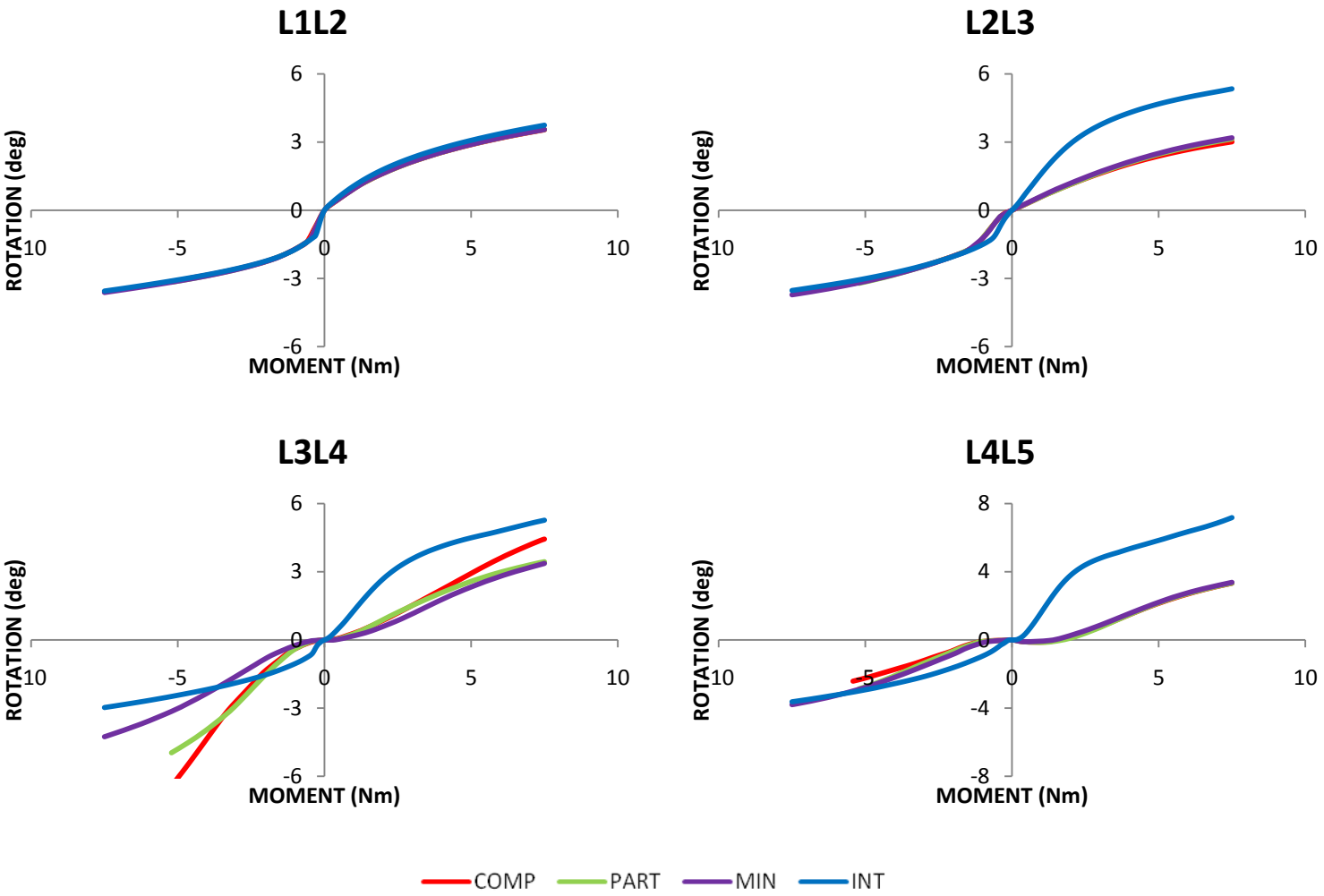

Figure 6.3: Intersegmental range of motion predictions for annular resection variants in flexion (+) and extension (-) with implantation at the L3/L4 level.

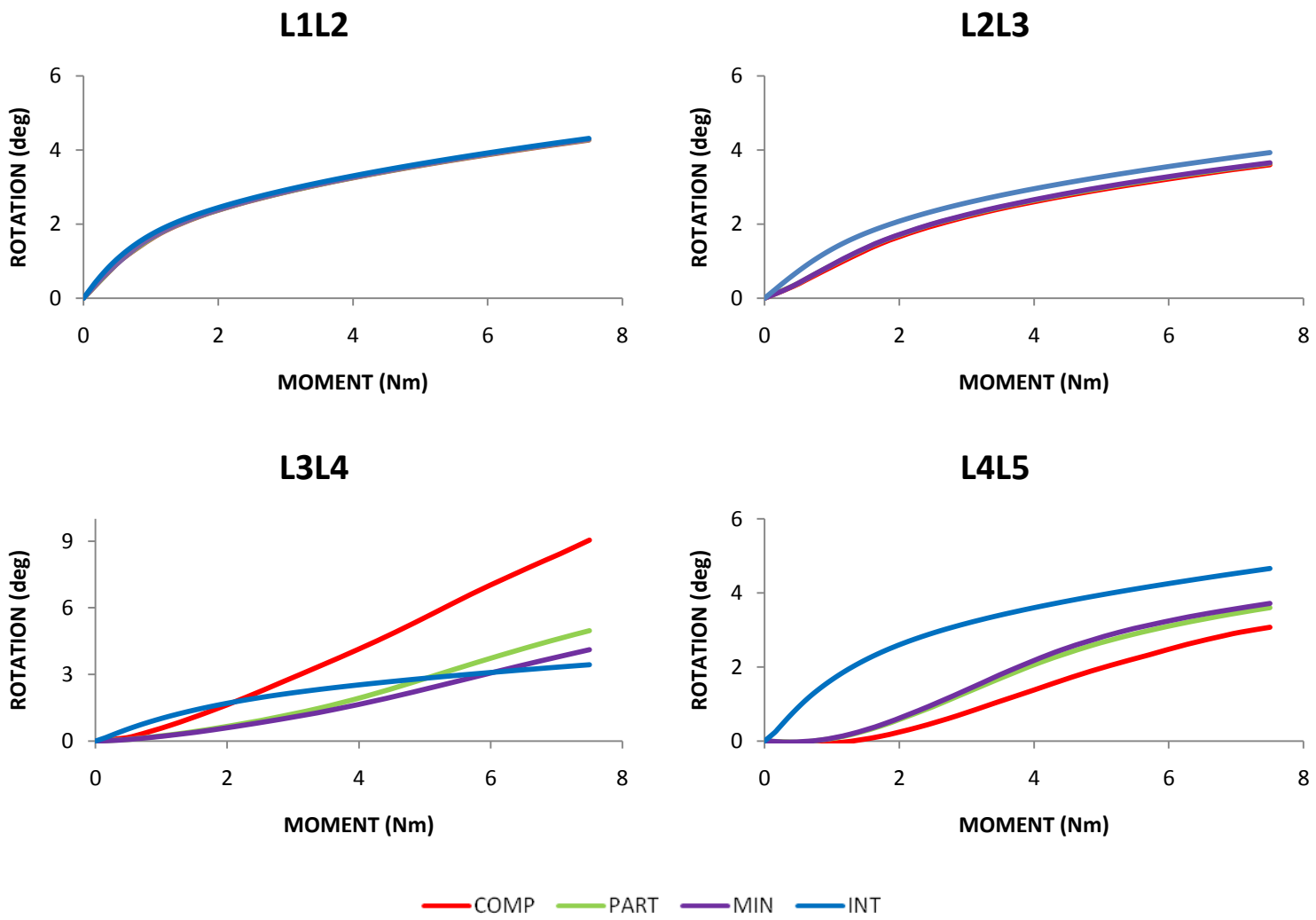

Figure 6.4: Intersegmental range of motion predictions for annular resection variants in unilateral bending with implantation at the L3/L4 level.

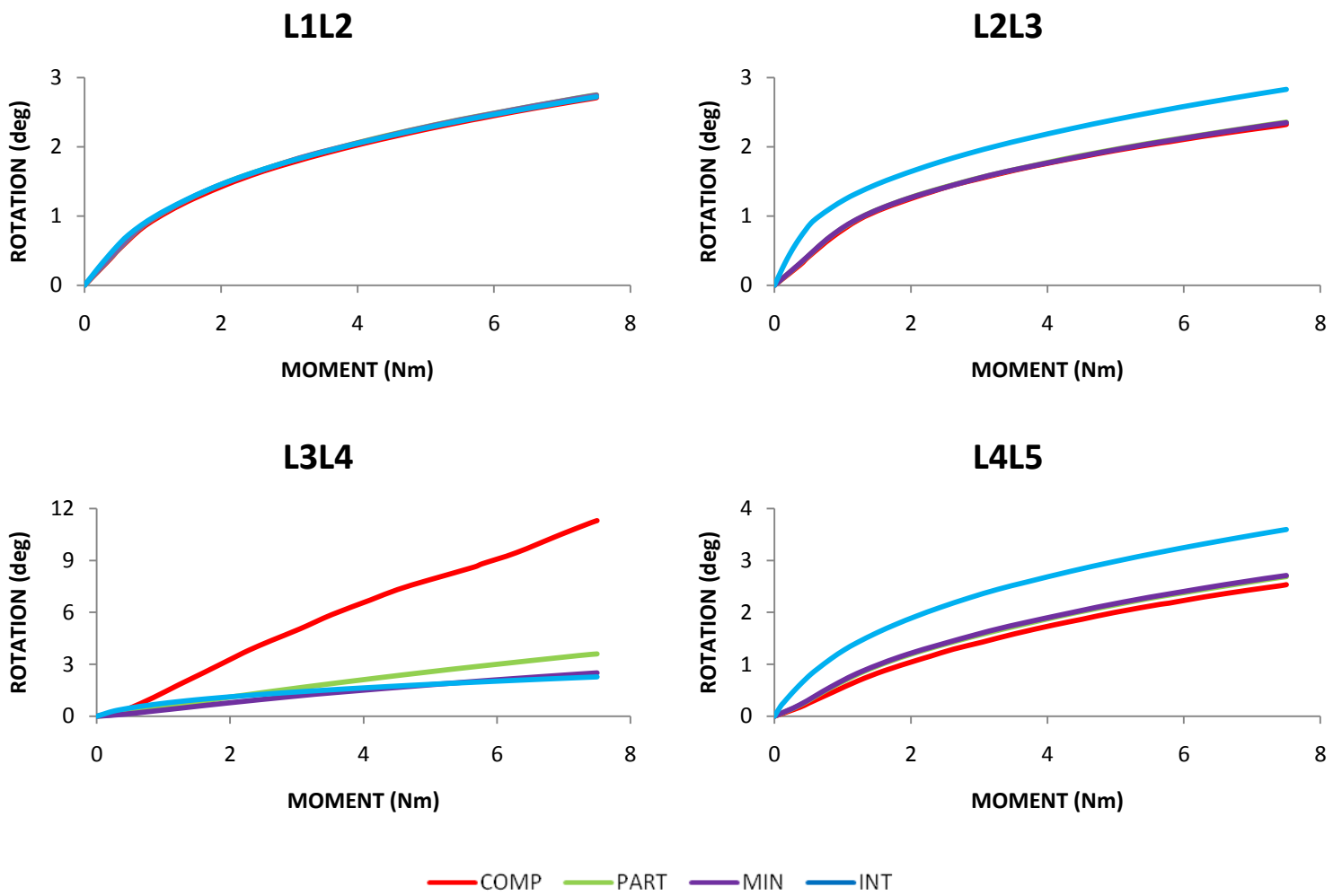

Figure 6.5: Intersegmental range of motion predictions for annular resection variants in uniaxial rotation with implantation at the L3/L4 level.

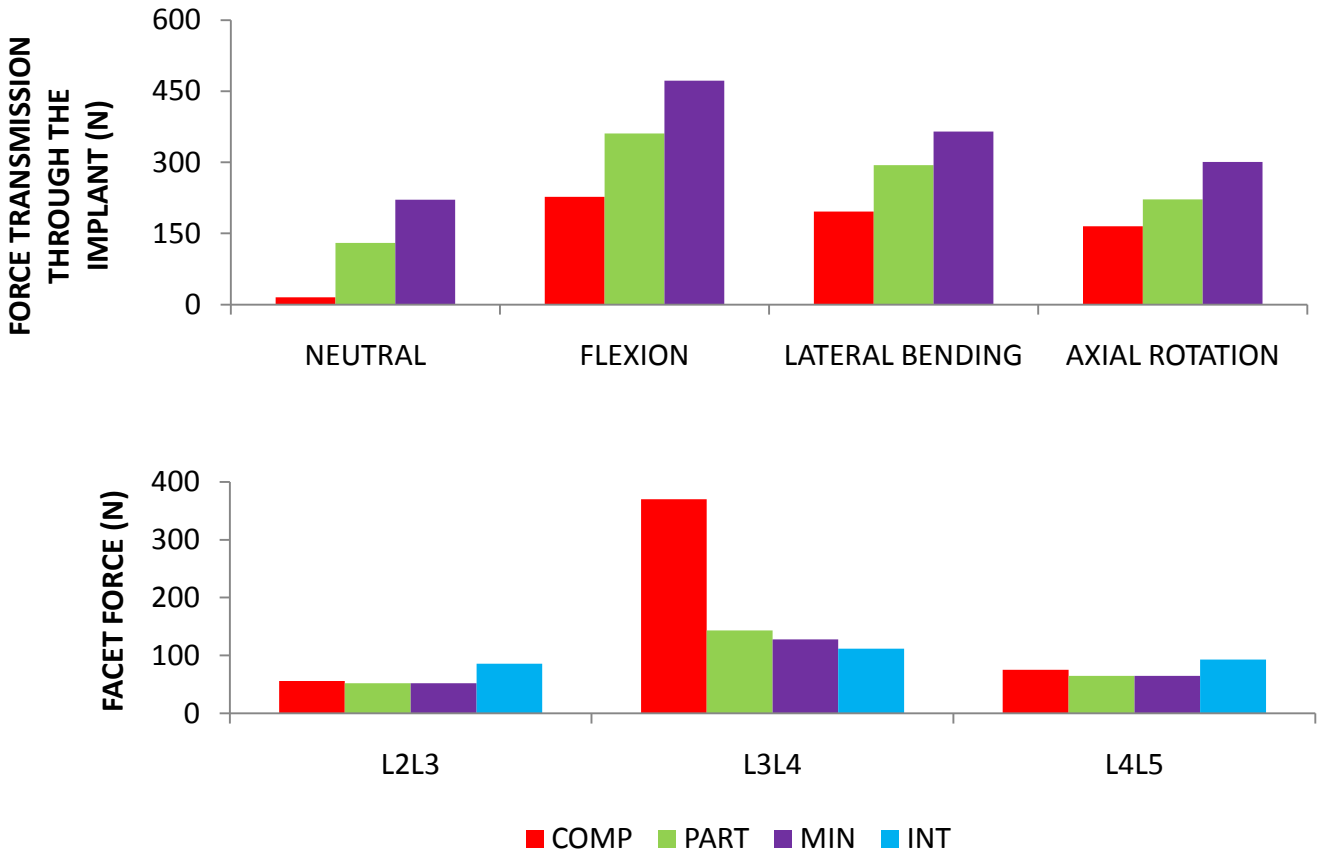

Figure 6.6: Force transmission through the implant under different loading conditions (top) and the facet force transmission predictions in axial rotation at the treated and adjacent levels (bottom).

Facet force transmission at the treated levels was predicted to increase substantially in extension (49N, 47N, 200N and 171N at L3/L4, and 84N, 83N, 88N and 232N at L4/L5 for INT, DEG, ONE, and TWO cases, respectively), which was consistent with the predicted increased ranges of motion (Figure 6.10). Changes in facet force transmission in axial rotation were not as dramatic, which also was consistent with the associated range of motion predictions. Neither of the treatment cases was predicted to have a great effect on the adjacent level nuclear pressures. The largest change in mean intradiscal pressure due to treatment was in flexion at the L2/L3 level, with a reduction from 717 KPa in the INT case to 528 KPa and 518 KPa in the ONE and TWO cases, respectively (Figure 6.10). The effect of degeneration on the adjacent level nuclear pressure predictions was minimal.

6.4 DISCUSSION

Using a previously developed finite element model, total disc replacement-related acute changes in the intersegmental kinematics and biomechanics of the human lumbar spine were evaluated. In addition to single- and two-level disc replacement cases, both the healthy condition and intervertebral disc degeneration cases were modeled. Predictions of spinal kinematics following the simulation of degeneration at the L3/L4 level were similar to those reported in the previous chapter. Specifically, the ranges of motion were increased in extension and axial rotation and reduced in lateral bending with respect to the healthy case. However, contrary to the previous predictions, there was a slight reduction in the mobility in flexion. This might be attributed to the differences in geometry, specifically disc height (which is lower at L3/L4), and the subsequent differences in the mechanics of the ligaments in the undeformed state. One of the notable features of the change in moment-rotation nonlinearity was the increased mobility under relatively low loads. Specifically, the range of motion in the -1/+1 Nm

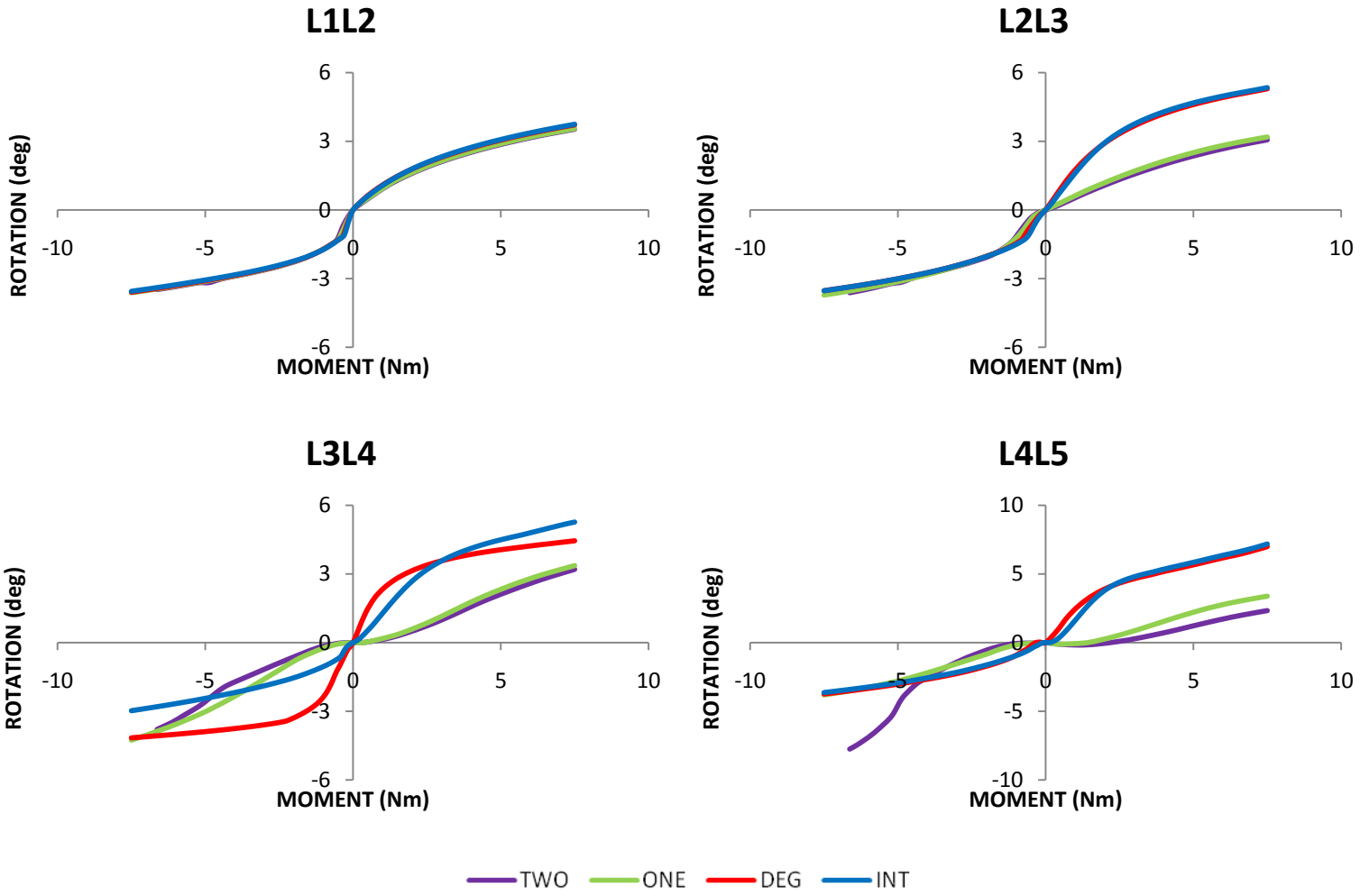

Figure 6.7: Intersegmental range of motion predictions for single (at the L3/L4 level) and bi-level (at the L3/L4 and L4/L5 levels) arthroplasty treatment in flexion (+) and extension (-).

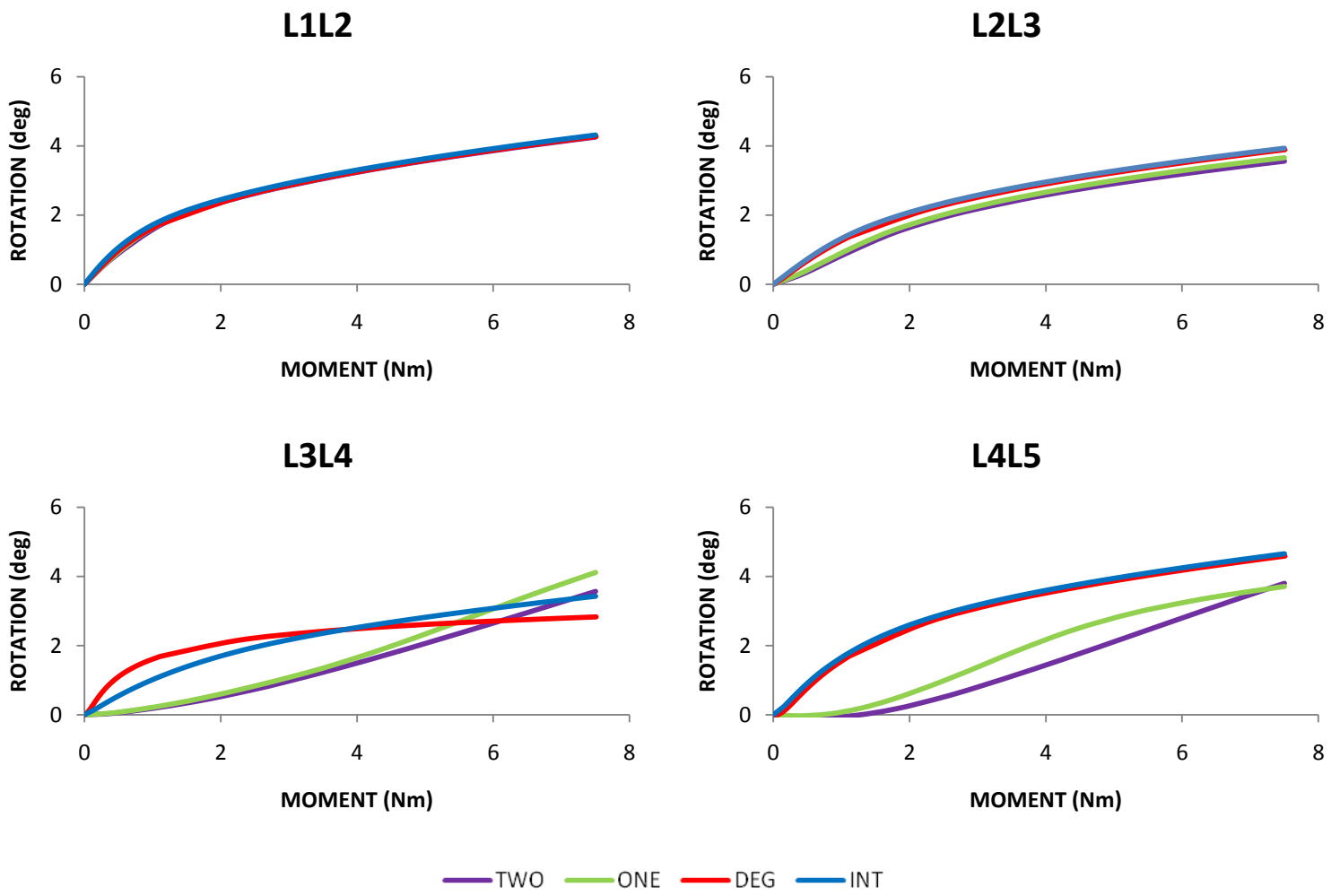

Figure 6.8: Intersegmental range of motion predictions for single (at the L3/L4 level) and bi-level (at the L3/L4 and L4/L5 levels) arthroplasty treatment in unilateral bending.

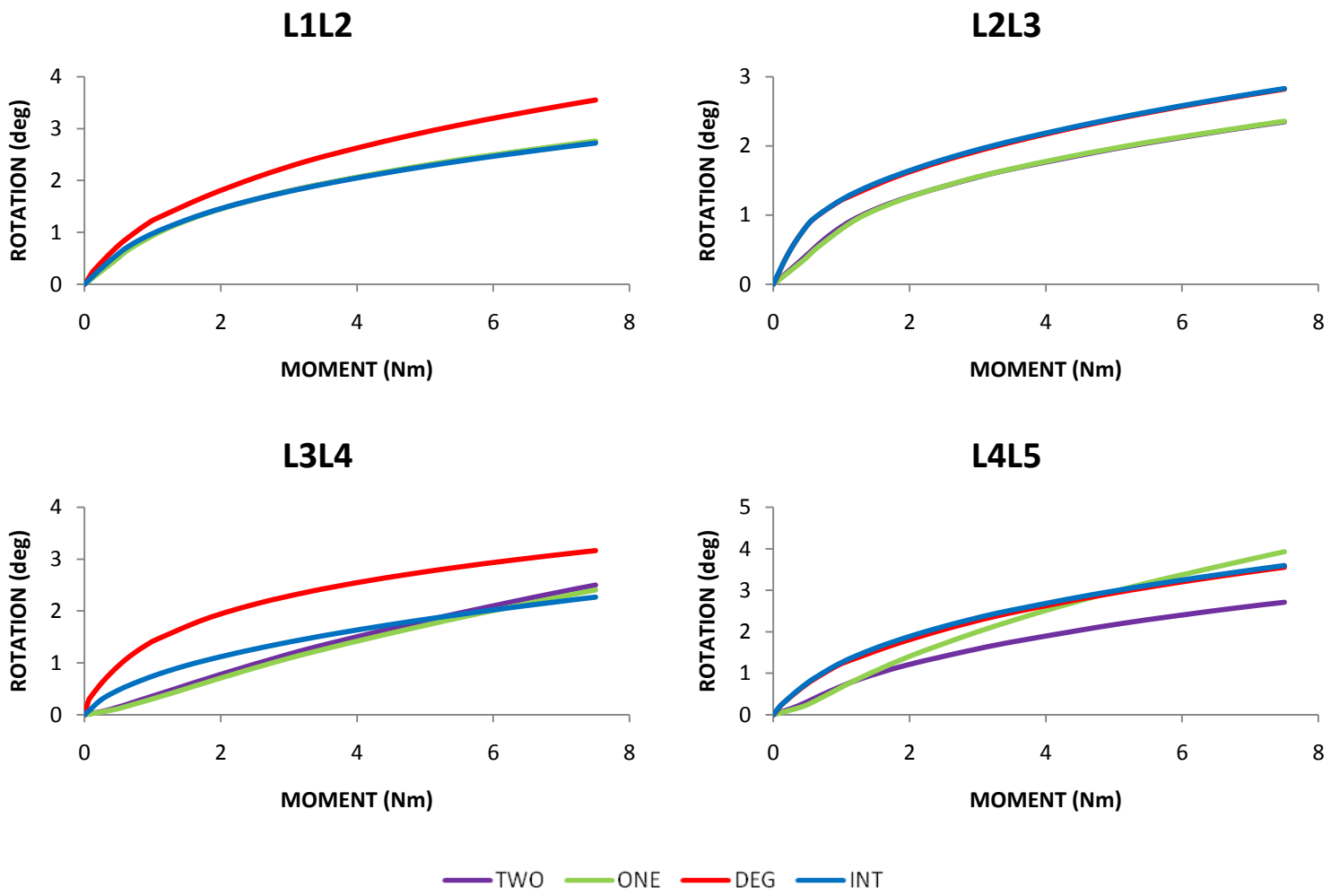

Figure 6.9: Intersegmental range of motion predictions for single (at the L3/L4 level) and bi-level arthroplasty (at the L3/L4 and L4/L5 levels) treatment in uniaxial rotation.

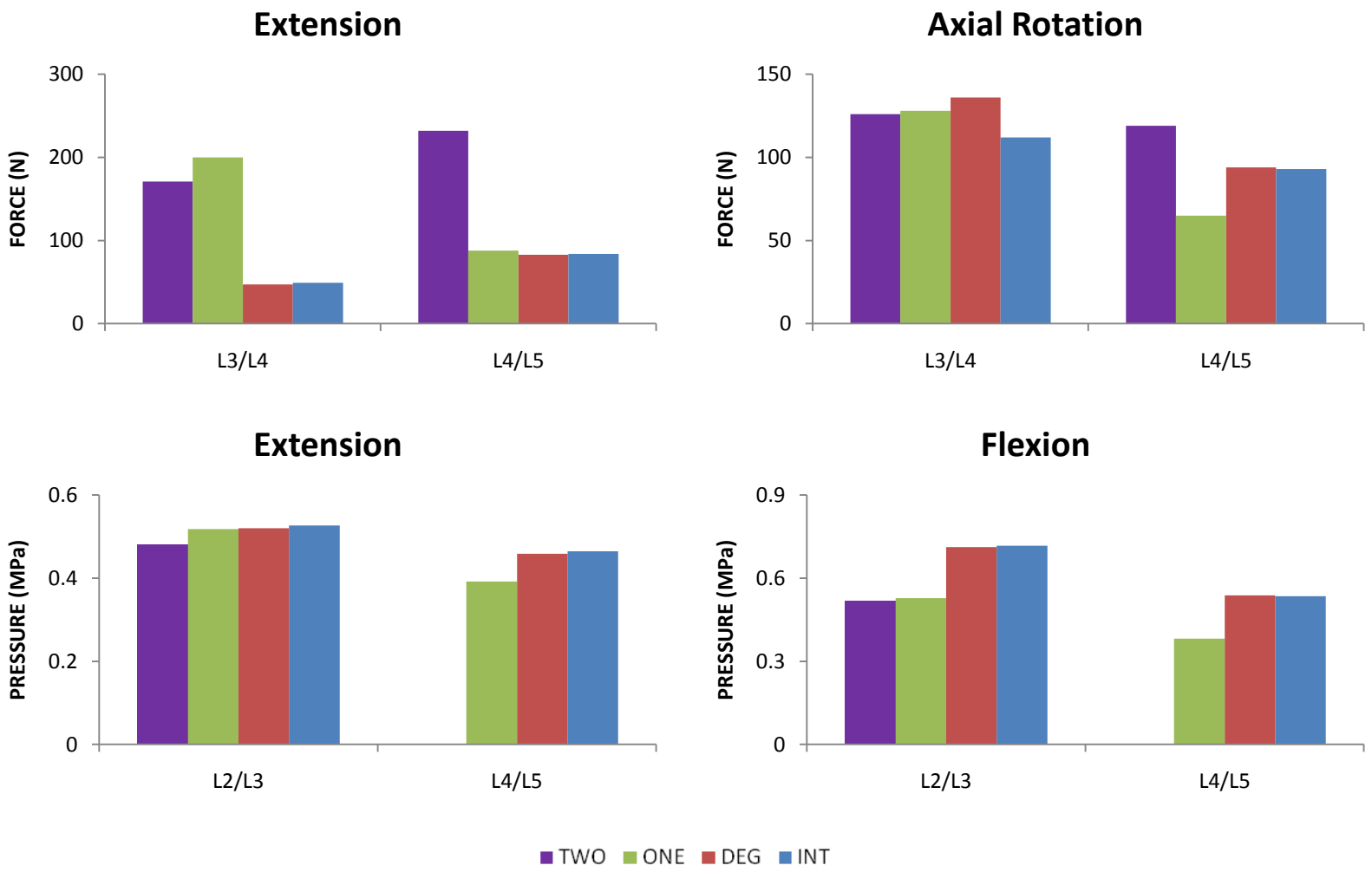

Figure 6.10: Facet force transmission predictions at the treated levels (top), and the mean intradiscal pressure predictions at the adjacent levels (bottom).

extension/flexion interval increased from 2.4° to 4.8°, indicating a substantial loss of stability in agreement with clinical “hypermobility” findings (Mimura M, 1994). There were no appreciable differences in the adjacent level kinematics due to degeneration. This trend was reflected in the biomechanical predictions as well, wherein the facet force transmission and nuclear pressure predictions remained approximately the same at the adjacent levels after the simulation of degeneration. Previous reports indicate that the subsequent initiation of degeneration at these levels is common (Waris, et al., 2007); however, our results suggest that the reasons behind this phenomenon are not of biomechanical nature.

Three different surgical scenarios were evaluated in order to determine the optimum annulus fibrosus resection methodology. Minimal resection of the annulus yielded the best outcome in terms of restoring the intact state biomechanics. This result was consistent with the manufacturer’s suggestions, as well as previously published model predictions (Rohlmann, et al., 2005). The drastic increases in the mobility of the treated level due to complete resection demonstrated the stabilizing effect of the annulus tissue. This was particularly evident in the case of axial rotation (in which the aforementioned treatment yielded a range of motion 9° greater than that in the intact case), since the ball-joint design of the implant did not provide a significant resistance to motion under this loading mechanism. The MIN and PART scenarios yielded similar kinematic results, except for the extension loading, which resulted in the complete disarticulation of the implant (Figure 6.3). The importance of the utilized surgical technique on stability was also demonstrated by the more specific, internal biomechanical parameters such as facet force transmission (wherein the MIN condition yielded the best result in comparison to the INT condition) and force transmission through the implant (Figure 6.6).

In both of the ONE and TWO scenarios, the moment-rotation responses of the treated segments were typically linearized (Figures 6.7-6.9). The load bearing roles of the soft tissue components such as the ligaments, the nucleus pulposus or and part of the annulus fibrosus were analyzed in detail in the previous chapters, and the removal of these highly nonlinear spinal components is likely the cause of the reduced nonlinearity. The alterations in the kinematic behavior of the treated (e.g. the reduction and increase in the ranges of motion in flexion and extension, respectively (Erkan, et al., 2009)) and adjacent levels are congruous with previous reports. Specifically, the "shifting" in the flexion/extension motion towards extension while preserving the total range of motion in the sagittal plane (Panjabi, et al., 2007) might have clinical significance in the long term (Bono, 2009), as it increases the facet force transmission predictions as well (Figure 6.10). On the other hand, previous work suggests that the high facet forces predicted for both treatment cases in extension loading may be alleviated by altering the position of the implant in the anteroposterior direction (Rohlmann, et al., 2005) (Rundell, et al., 2008). For the adjacent levels, the range of motion predictions indicate a general trend of reduction in mobility in all loading conditions except extension. The internal biomechanical parameters, such as the nuclear pressure, are also reduced at the adjacent levels due to treatment (Figure 6.10). Overall, the greatest impact of treatment on the superior levels was predicted to be the 40 % reduction (~2.2°) in range of motion in flexion, indicating that the application of higher loads would be necessary to restore the intact state kinematic behavior. However, no other distinct alterations in the biomechanics or kinematics of the adjacent segments that could potentially trigger degeneration were observed. There were no appreciable differences between the predictions of the ONE and TWO scenarios, in agreement with early clinical results (Bertagnoli, et al., 2005) (Hannibal, et al., 2007); however, the complete disarticulation of the implant at the L4/L5 level was predicted in extension. Nevertheless, this

was most likely due to the size of the implant and the exclusion of body weight compression, which did not induce the same degree of stability it did for the L3/L4 level.

The modeling effort presented herein involved a number of explicit and implicit assumptions. A single size implant was used by positioning the device approximately at the center of the vertebral endplate. Future work should assess the agreement between the implant and intervertebral disc height, as well as the effect of the positioning of the implant on the vertebral endplate. In addition to multi-level implantations, hybrid treatment techniques such as fusion & arthroplasty are common in the clinical setting, and the simulation of this condition in comparison to the cases presented in this study would generate valuable data. In all implantation simulations where a certain amount of the annulus was preserved, the remaining tissue was modeled as healthy. In order for the results to be more relevant to the clinical condition, the effect of degeneration on the preserved annulus tissue and the kinematic and biomechanical outcome should be assessed in comparison to the scenarios presented here. The pure-moment loading conditions are deemed sufficient for simulating the principal rotations of the spinal segments. However, more complex loading scenarios, such as the implementation of lumbar musculature as boundary conditions, have the potential to better approximate the *in vivo* biomechanical outcome. These conditions will be investigated as part of future work.

6.5 CONCLUSION

The biomechanical and kinematic effects of lumbar disc arthroplasty with the ProDisc-L implant were evaluated by the utilization of the finite element method. In agreement with previous reports and the manufacturer's directions, maximum preservation of the annulus fibrosus upon implantation of the prosthesis was determined as the best surgical protocol. Both one-level and two-level disc replacement resulted in increased facet forces and ranges of

motion at the treated levels in extension loading, while the changes were minimal in all other loading scenarios. Overall, multi-level treatment with the ProDisc-L was not predicted to yield undesirable changes in the biomechanics of lumbar spine as compared to one-level treatment.

REFERENCES

Auerbach, J., Jones, K., Milby, A., Anakwenze, O., & Balderston, R. (2009). Segmental contribution toward total lumbar range of motion in disc replacement and fusions: a comparison of operative and adjacent levels. *Spine* , 34(23):2510-7.

Bertagnoli, R., Yue, J., Shah, R., Nanieva, R., Pfeiffer, F., Fenk-Mayer, A., et al. (2005). The treatment of disabling multilevel lumbar discogenic low back pain with total disc arthroplasty utilizing the ProDisc prosthesis: a prospective study with 2-year minimum follow-up. *Spine* , 30(19):2192-9.

Bono, C. (2009). Hybrids: good for cars and the environment-are they good for the spine too? *Spine J* , 9(10):857-8.

Cakir, B., Schmidt, R., Mattes, T., Fraitzl, C., Reichel, H., & Käfer, W. (2009). Index level mobility after total lumbar disc replacement: is it beneficial or detrimental? *Spine* , 34(9):917-23.

Chen, S., Zhong, Z., Chen, C., Chen, W., & Hung, C. (2009). Biomechanical comparison between lumbar disc arthroplasty and fusion. *Med. Eng. Phys* , 31, 244-53.

Crawford, N. (2005). Biomechanics of lumbar arthroplasty. *Neurosurg Clin N Am* , 16(4):595-602.

Cunningham, B., Hu, N., Beatson, H., Serhan, H., Sefter, J., & McAfee, P. (2009). Revision strategies for single- and two-level total disc arthroplasty procedures: a biomechanical perspective. *Spine J* , 9(9):735-43.

Erkan, S., Rivera, Y., Wu, C., Mehbod, A., & Transfeldt, E. (2009). Biomechanical comparison of a two-level Maverick disc replacement with a hybrid one-level disc replacement and one-level anterior lumbar interbody fusion. *Spine J* , 9(10):830-5.

Hannibal, M., Thomas, D., Low, J., Hsu, K., & Zucherman, J. (2007). ProDisc-L total disc replacement: a comparison of 1-level versus 2-level arthroplasty patients with a minimum 2-year follow-up. *Spine* , 32(21):2322-6.

Johannessen, W., & Elliott, D. (2005). Effects of degeneration on the biphasic material properties of human nucleus pulposus in confined compression. *Spine* , 30(24):E724-9.

Jones, A., & Wilcox, R. (2008). Finite element analysis of the spine: towards a framework of verification, validation and sensitivity analysis. *Med Eng Phys* , 30:1287-304.

Käfer, W., Clessienne, C., Däxle, M., Kocak, T., Reichel, H., & Cakir, B. (2008). Posterior component impingement after lumbar total disc replacement: a radiographic analysis of 66 ProDisc-L prostheses in 56 patients. *Spine* , 33(22):2444-9.

Mimura M, P. M. (1994). Disc degeneration affects the multidirectional flexibility of the lumbar spine. *Spine* , 1371-80.

Mimura, M., Panjabi, M., Oxland, T., Crisco, J., Yamamoto, I., & Vasavada, A. (1994). Disc degeneration affects the multidirectional flexibility of the lumbar spine. *Spine* , 1371-80.

Panjabi, M., Henderson, G., Abjornson, C., & Yue, J. (2007). Multidirectional testing of one- and two-level ProDisc-L versus simulated fusions. *Spine* , 32(12):1311-9.

Rohlmann, A., Zander, T., & Bergmann, G. (2005). Effect of total disc replacement with ProDisc on intersegmental rotation of the lumbar spine. *Spine* , 30(7):738-43.

Rundell, S., Auerbach, J., Balderston, R., & Kurtz, S. (2008). Total disc replacement positioning affects facet contact forces and vertebral body strains. *Spine* , 33(23):2510-7.

Waris, E., Eskelin, M., Hermunen, H., & Kiviluoto, O. (2007). Disc degeneration in low back pain: a 17-year follow-up study using magnetic resonance imaging. *Spine* , 32 (6): 681–684.

Zhang, Q., & Teo, E. (2008). Finite element application in implant research for treatment of lumbar degenerative disc disease. *Med Eng Phys.* , 30(10):1246-56.

CHAPTER 7:

Conclusion

7.1 SUMMARY OF FINDINGS & FUTURE WORK

Disc degeneration-related alterations in the biomechanical behavior of the intervertebral disc and lumbar spinal segments were investigated in this study. The employed methodology was primarily based on (1*) in vitro* experimentation on cadaveric annulus fibrosus tissue in order to characterize its constitutive behavior in the healthy and diseased states, and (2) finite element modeling of the adult human lumbar spine (L1-L5) with the simulation of single-level disc degeneration and multi-level disc arthroplasty, in order to assess the acute biomechanical effects of surgical treatment.

In Chapter 2, the biomechanics of the healthy intervertebral disc and the annulus fibrosus in particular were evaluated in terms of their contributions to load bearing in the lumbar spine. The highly organized collagen fiber network was found to bear the majority of the load applied on the annulus during the principal rotation motions, and thus play a crucial role in the nonlinearity of spinal kinematics. The methodology described in Chapter 2 was extended to finite element modeling of the human lumbar spine (L1-L5) in Chapter 3. The detailed mesh convergence study revealed that global parameters like segmental kinematics or stiffness were unaffected by the mesh resolution, whereas the level of refinement had a great influence on the mechanics of the cartilaginous and bony endplates especially under shear loads. The predictive capability of the converged model was demonstrated with respect to the intersegmental ranges of motion, intradiscal nuclear pressure, facet force transmission, anterolateral cortical bone strain and ligament deformation predictions.

Chapter 4 outlined the biaxial and uniaxial tensile tests conducted on healthy and degenerated annulus fibrosus tissue. A nonlinear anisotropic strain energy function was developed, and the coefficients for each group were determined by fitting the model

predictions to the experimentally-derived stress-strain data. Degeneration was found to significantly increase the dispersion in the collagen fiber orientation and the nonlinearity of the fiber mechanical behavior. The previously determined coefficients were utilized in Chapter 5, in order to model disc degeneration at the motion segment level, through the implementation of the generated material models into the finite element model developed in Chapter 2. The simulated reduction in the nuclear swelling pressure and biomechanical degradation in nucleus pulposus substantially increased annular stresses while imposing higher loads on the annular ground substance. Degenerative changes increased the mobility of the motion segment in all loading scenarios except for lateral bending. The kinematic and biomechanical changes were greatest in extension loading, and these findings mirror the common clinical findings of herniation and annular failure.

Finally in Chapter 6, the simulation of one- and two-level disc arthroplasty was documented. The degree of annular tissue preservation during implantation of the prosthetic device was found to have a critical effect on the stability of the treated motion segment. These model predictions agree with previous clinical studies and the suggested manufacturer's implant protocol. For both treatment cases, alterations in the treated or adjacent level biomechanics were found to be relatively minor as compared to the healthy case, although particular shifts and linearization were predicted in flexion/extension moment-rotation behavior. The outcome of this section and the previous chapters indicate that the annulus fibrosus is of critical importance in the functioning of lumbar spinal segments in their healthy, diseased and treated conditions. Furthermore, its significance is largely due to the presence of the highly organized collagen fiber network embedded in its ground substance. Specifically, the kinematic and mechanical data (local energy and stress predictions in particular) presented in Chapters 2 and 5

support our initial hypothesis by demonstrating critical changes in the load-sharing mechanism within the intervertebral disc.

While the results reported in this dissertation work are encouraging for the continued utilization of disc arthroplasty in the treatment of degenerative disease, further investigations are warranted. The results predicted for the pure-moment loading scenarios were in good agreement with *in vivo* kinematic measurements; however more complex loading cases that incorporate lumbar muscular activity would yield valuable data in the assessment of implant performance. These efforts should be part of future intervertebral disc replacement modeling work.